REMOTE SENSING AND GEOSPATIAL MODELING

OF WILDLAND FIREFIGHTER SAFETY

by

Michael James Campbell

A dissertation submitted to the faculty of
The University of Utah
in partial fulfillment of the requirements for the degree of

Doctor of Philosophy

Department of Geography

The University of Utah

May 2018

The University of Utah Graduate School

STATEMENT OF DISSERTATION APPROVAL

The dissertation of **Michael James Campbell**

has been approved by the following supervisory committee members:

Philip Dennison	, Chair	**11/14/2017** Date Approved
Thomas Cova	, Member	**11/29/2017** Date Approved
S. McKenzie Skiles	, Member	**11/29/2017** Date Approved
Bret Butler	, Member	**11/14/2017** Date Approved
Andrew Hudak	, Member	**11/16/2017** Date Approved

and by **Andrea Brunelle**, Chair/Dean of

the Department/College/School of **Geography**

and by David B. Kieda, Dean of The Graduate School.

ABSTRACT

With increasing wildfire activity throughout the western United States comes an increased need for wildland firefighters to protect civilians, structures, and public resources. In order to mitigate threats to their safety, firefighters employ the use of safety zones (SZ: areas where firefighters are free from harm) and escape routes (ER: pathways for accessing SZ). Currently, SZ and ER are designated by firefighters based on ground-level information, the interpretation of which can be error-prone. This research aims to provide robust methods to assist in the ER and SZ evaluation processes, using remote sensing and geospatial modeling. In particular, I investigate the degree to which lidar can be used to characterize the landscape conditions that directly affect SZ and ER quality. I present a new metric and lidar-based algorithm for evaluating SZ based on zone geometry, surrounding vegetation height, and number of firefighters present. The resulting map contains a depiction of potential SZ throughout Tahoe National Forest, each of which has a value that indicates its wind- and slope-dependent suitability. I then inquire into the effects of three landscape conditions on travel rates for the purpose of developing a geospatial ER optimization model. I compare experimentally-derived travel rates to lidar-derived estimates of slope, vegetation density, and ground surface roughness, finding that vegetation density had the strongest negative effect. Relative travel impedances are then mapped throughout Levan Wildlife Management Area and combined with a route-finding algorithm, enabling the identification of maximally-

efficient escape routes between any two known locations. Lastly, I explore a number of variables that can affect the accurate characterization of understory vegetation density, finding lidar pulse density, overstory vegetation density, and canopy height all had significant effects. In addition, I compare two widely-used metrics for understory density estimation, overall relative point density and normalized relative point density, finding that the latter possessed far superior predictive power. This research provides novel insight into the potential use of lidar in wildland firefighter safety planning. There are a number of constraints to widespread implementation, some of which are temporary, such as the current lack of nationwide lidar data, and some of which require continued study, such as refining our ability to characterize understory vegetation conditions. However, this research is an important step forward in a direction that has potential to greatly improve the safety of those who put themselves at risk to ensure the safety of life and property.

TABLE OF CONTENTS

ABSTRACT..... iii

LIST OF TABLES.....vii

LIST OF FIGURES.....viii

ACKNOWLEDGEMENTS.....xi

INTRODUCTION..... 1

References.....7

Chapters

1 SAFE SEPARATION DISTANCE SCORE: A NEW METRIC FOR EVALUATING WILDLAND FIREFIGHTER SAFETY ZONES USING LIDAR.....14

1.1 Abstract.....14
1.2 Introduction.....15
1.3 Methods.....18
1.4 Results.....26
1.5 Discussion and conclusions..... 28
1.6 Acknowledgements.....33
1.7 References.....46

2 A LIDAR-BASED ANALYSIS OF THE EFFECTS OF SLOPE, VEGETATION DENSITY, AND GROUND SURFACE ROUGHNESS ON TRAVEL RATES FOR WILDLAND FIREFIGHTER ESCAPE ROUTE MAPPING..... 50

2.1 Abstract.....50
2.2 Introduction.....51
2.3 Methods.....55
2.4 Results.....60
2.5 Discussion.....63
2.6 Conclusions.....70
2.7 Acknowledgements.....71
2.8 References.....89

3 QUANTIFYING UNDERSTORY VEGETATION DENSITY USING SMALL FOOTPRINT AIRBORNE LIDAR....93

3.1 Abstract....93
3.2 Introduction....94
3.3 Background....97
3.4 Methods....107
3.5 Results....114
3.6 Discussion....116
3.7 Conclusions....120
3.8 References....135

CONCLUSIONS....144

References....151

LIST OF TABLES

Table

1.1. Slope-wind factor safe separation distance matrix from Butler (2015).....34

1.2. Number of suitable safety zones in each combination of wind speed and slope according to SSDS values.....35

1.3. Percent of study area within distance and travel time of safety zones with different SSDS thresholds..... 36

2.1. Study participant summary..... 72

2.2. Transect landscape parameter mean values..... 73

2.3. Results from regression analyses to determine optimal light detection and ranging (LiDAR) normalized relative point density (NRD) height range for predicting travel rate along slopes of less than 5°.....74

2.4. Fixed effects for model predicting travel rates. Probabilities are significant at: ***, α = 0.001. Residual degrees of freedom = 1269..... 75

2.5. Resulting travel distances, times and rates for simulated escape routes.....76

3.1. Spectral variables used in stepwise logistic regression to classify board vs. non-board on cover board photos.....121

3.2. Stepwise logistic regression model results for cover board photo classification. Null deviance = 6131.12 on 4799 degrees of freedom. Residual deviance = 658.92 on 4791 degrees of freedom.....122

3.3. Cover board photo classification accuracy assessment..... 123

3.4. Results of multiple regression analysis between bootstrapped R^2 values and pulse density, overstory density, and canopy height ($R^2 = 0.104$, $p < 0.001$).....124

LIST OF FIGURES

Figure

1.1. Wildland firefighter fatalities by type (BEBA = burnover, entrapment, burns, and asphyxiation; VHA = vehicle, helicopter, aircraft; HA = heart attack; OM = other medical; TS = tree, snag) (National Interagency Fire Center 2016).....37

1.2. Basic safety zone example diagram (after Dennison *et al.* 2014).....38

1.3. Study area map.....39

1.4. Model workflow from canopy height model (a) to clearing classification (b), surrounding tree crown delineation and height calculation (c), segment-based mean surrounding vegetation height calculation (d), pixel-based SSDS calculation and safety zone placement (e), and safety zone SSDS result (f).....40

1.5. Tree crown delineation method..... 41

1.6. Potential safety zones with associated safe separation distance score values throughout the study area. The area burned by the 1994 Cottonwood fire is outlined in red..... 42

1.7. Scatterplots of safety zone SSDS values compared to slopes broken down by wind speed category. The blue and red regions represent areas of suitability and unsuitability, respectively, according to slope and wind conditions as defined by the slope-wind factor matrix (Table 1.1)..... 43

1.8. Euclidean distance and estimated travel time to nearest potential safety zone at a range of SSDS thresholds throughout the study area.....44

1.9. Linear regression between safety zone SSDS and clearing area in which the safety zone fell.....45

2.1. Study area map, with background imagery care of ESRI (ESRI Inc., Redlands, CA, USA, www.esri.com).....77

2.2. Roughness calculation; digital terrain model (DTM) elevation values exaggerated 3x to highlight texture.....78

2.3. Example transect with associated light detection and ranging (LiDAR) point cloud cross-section and example height range (0.15–2.75 m); heights scaled for clarity, with background imagery care of ESRI (ESRI Inc., Redlands, CA, USA, www.esri.com).....79

2.4. Landscape parameters with transects.....80

2.5. Power of light detection and ranging (LiDAR) normalized relative point density (NRD) height ranges from 0 to 5 m for predicting travel rates along slopes of <5° as approximated by Nakagawa and Schielzeth (2013)'s measure for marginal R^2 (R^2_m) compared with average study subject height. Best interval (0.15–2.75 m) shown.....81

2.6. Effect of density, as approximated by the optimal light detection and ranging (LiDAR) normalized relative point density (NRD) height range (0.15–2.75 m), on travel rates along slopes less than 5°.....82

2.7. Predicted results of linear mixed effects regression (LMER) for each landscape condition within the range of values found on transects throughout the study area, assuming a median value of the other two conditions.....83

2.8. Two simulated escape routes representing the least-cost paths between points *a* and *b* in both directions; background imagery: ESRI (ESRI Inc., Redlands, CA, USA, www.esri.com).....84

2.9. Results of least-cost routes between 1000 randomly generated point location pairs throughout the study area with route overlap displayed against landscape parameters.....85

2.10. Density plot of light detection and ranging (LiDAR) point return heights, measured as a proportion of all returns, for a transect with dense juniper.....86

2.11. How each study participant's travel rates ranked among all participants for each transect.....87

2.12. Comparison of model results (calculated assuming zero vegetation density and zero ground surface roughness) to three well-established models used to estimate the effects of slope on travel rate. Davey *et al.* (1994)'s model was calibrated to match our model's 0° slope travel rate.....88

3.1. Three-dimensional lidar point cloud example of a multi-aged lodgepole pine (*Pinus contorta*) forest stand containing both a dense overstory and understory. The yellow circles represent simulated lidar point returns. The dotted lines distinguish between vertical strata representing ground returns (< 0.25 m), understory returns (0.25 – 2 m), and overstory returns (> 2 m)..... 125

3.2. The relationship between tree height and theoretical tree separation distance under which individual lidar pulses could interact with multiple trees at various scan angles..... 126

3.3. Study area map. Monroe Mountain area of Fishlake National Forest outlined in black.....127

3.4. Cover board photo setup..... 128

3.5. Transect layout.....129

3.6. Cover board photo classification example results. In the lower two panels, white indicates pixels classified as “board” and black indicates pixels classified as “non-board”.....130

3.7. Comparison between ordinary least squares regression models predicting cover board density using lidar-based understory overall relative point density (ORD) (a) and normalized relative point density (NRD) (b)..... 131

3.8. The bootstrapped effect of lidar pulse density (a), overstory canopy density (as approximated by lidar overall relative point density of all points higher than 1.85 m) (b), and canopy height (as approximated by 95th percentile of lidar point return height) (c) on the ability of lidar to model understory cover (as approximated by the amount of variance in cover board cover explained by lidar understory normalized relative point density)..... 132

3.9. Photo-by-photo cover estimates for an example transect that demonstrate the effect that a single tree can have on overall, transect-level cover estimates.....133

3.10. The effect of understory complexity, as approximated by the standard deviation of cover derived from individual photo cover estimates, on the ability to characterize understory density using lidar NRD..... 134

ACKNOWLEDGEMENTS

I would like to thank Philip Dennison, my committee chair and advisor, whose unparalleled mentorship has been fundamental to my success as a graduate student and beyond. I would also like to express immense gratitude to each of my committee members, past and present, including Bret Butler, Andrew Hudak, Thomas Cova, McKenzie Skiles, and Ran Wei, each of whom have contributed significantly to my PhD experience. I would like to thank Phoebe McNeally, who facilitated my life as a graduate student and researcher in innumerable and invaluable ways. I would also like to thank Andrea Brunelle, who was instrumental in the success of my field experiment. Countless thanks to Pamela Mitchell and Lisa Clayton, whose tireless efforts form the glue that held together my graduate school experience and that of so many others. In addition, I would like to recognize the many individuals whose help in the field or exchange of ideas have greatly facilitated my research, including Simon Brewer, Vachel Carter, Daniel Maynard, Austin Coates, Timothy Berggren, and Sandra Miller. I would like to thank my friends and family, who enhance and improve my life every single day. Lastly, and most importantly, I would like to thank my wife, Lucy Parham, for her endless love and support throughout this entire, amazing experience.

Funding for this research was provided by the US Forest Service National Fire Plan through the Office of Research, the National Wildfire Coordinating Group Fire Behavior Subcommittee, and the Wildland Fire Management Research Development &

Application Program, Cooperative Agreements 14JV11221637123 and 15CR11221637105.

INTRODUCTION

Wildfire activity has been on the rise throughout much of the western US in recent decades (Dennison et al., 2014a; Jolly et al., 2015; Westerling et al., 2006). A century of fire suppression causing a buildup of fuels coupled with temperature increases and earlier spring snowmelt have resulted in longer fire seasons, with larger, more intense and severe fires (Dennison et al., 2014a; Flannigan et al., 2009; Jolly et al., 2015; Miller et al., 2009; Westerling et al., 2006; Westerling, 2016). Based on current projections of global climate change, these trends are likely to continue, and perhaps even worsen in the future (Abatzoglou and Williams, 2016; IPCC, 2013; Liu et al., 2010; Parks et al., 2016). Increased wildfire activity is particularly problematic in the wildland-urban interface, where rapid development has encroached into fire-prone areas of the western US, increasing the risk to civilian lives and properties (Cohen, 2000; Hammer et al., 2009; Liu et al., 2015; Martinuzzi et al., 2015; Mell et al., 2017; Radeloff et al., 2005). This increased risk, combined with the inherent complexity of fuelbed structure within the wildland-urban interface, has resulted in significant increases in fire suppression costs in recent decades (Calkin et al., 2014; Gude et al., 2013; Mell et al., 2017). Among the many resources available to fire management agencies for fire control, wildland firefighters are the most fundamental and important (Pyne, 1996). Thus, with increased fire activity, more firefighters are being deployed to protect the lives and assets of civilians in the wildland-urban interface and beyond.

Wildland firefighting is an arduous profession fraught with complexity and risk. Firefighters are tasked with working long hours (up to 24-hour shifts), often in rugged terrain, at high altitudes and in hot temperatures (Ruby et al., 2002). The primary task in firefighting is to construct a fire line – a continuous strip of land where flammable material is removed to expose mineral soil in order to contain and prevent the spread of a wildfire (National Wildfire Coordinating Group, 2016). This frequently necessitates working in close proximity to the edge of a fire, particularly when engaging in direct and parallel attack containment strategies (Cheney et al., 2001). In doing so, firefighters are putting themselves at risk of injury or fatality from convective and radiant heat exposure and smoke inhalation. Between 1910 and 2015, there were 1099 documented wildland firefighter fatalities in the United States (National Interagency Fire Center, 2016). In accordance with the highly varied wildland firefighting environment, the causes of death are wide-ranging, but the largest fatality category is that of burnovers, entrapments, burns, and asphyxiation (BEBA), with 501 total fatalities in that same time frame (46% of all fatalities) (National Interagency Fire Center, 2016). Whereas many fatality types occur in isolation, such as heart attacks, vehicular accidents, or getting hit by a falling tree or snag, BEBA can sometimes occur in large-scale multiple-fatality events. The average number of fatalities per BEBA event is 2.73, as compared to, for example, aircraft fatalities (1.87) and vehicle fatalities (1.26). Between 1910 and 2015, there were 10 individual events in which over 10 firefighters perished due to BEBA, including major historical fires such as the Great Fire of 1910 (78 fatalities), the Mann Gulch fire of 1949 (13 fatalities) and the more recent South Canyon fire of 1994 (14 fatalities) and Yarnell Hill fire of 2013 (19 fatalities). Burnovers and entrapments are events in which a fire

overtakes firefighting personnel due to unforeseen changes in fire behavior and an associated inability to utilize suitable safety zones and escape routes (National Wildfire Coordinating Group, 2016). As this definition suggests, safety zones and escape routes are two critical components of wildland firefighter safety (Alexander et al., 2005; Beighley, 1995; Butler, 2014; Butler et al., 2000; Butler and Cohen, 1998; Campbell et al., 2017a, 2017b; Dennison et al., 2014b; Fryer et al., 2013; Gleason, 1991; National Wildfire Coordinating Group, 2014; Page and Butler, 2017; Rossi et al., 2011; Ruby et al., 2003; Zárate et al., 2008).

A safety zone (SZ) is an area devoid of flammable material where firefighters can reterat to in dangerous situations to avoid danger, risk, or injury (Beighley, 1995; National Wildfire Coordinating Group, 2016). An effective SZ is one in which firefighters within can remain uninjured, regardless of nearby or surrounding fire conditions. This differs from deployment zones and survival zones, which are used in the absence of suitable SZ as a method of last resort to avoid fatality, but are likely to cause injury (National Wildfire Coordinating Group, 2016; Page and Butler, 2017). The conditions that control SZ effectiveness have been fairly well defined throughout the literature (Butler, 2014; Butler and Cohen, 1998; Campbell et al., 2017b; Dennison et al., 2014b; Gleason, 1991; Page and Butler, 2017). SZ should be cleared of vegetation (naturally, mechanically, or burned out) (National Wildfire Coordinating Group, 2016, 2014), large enough to accommodate the fire crew and equipment (Dennison et al., 2014b), maintain safe separation distance from surrounding fuels on all sides (Butler and Cohen, 1998), and not be upslope or downwind of flames in order to avoid the effects of convective heat (Butler, 2014; National Wildfire Coordinating Group, 2014; Zárate et al.,

2008). At present, SZ are evaluated on the ground in advance of firefighting as a part of daily fire management activities, and continually re-evaluated throughout the day as crew location and fire conditions change (National Fire Protection Association, 2017). Accordingly, this necessitates a ground-level interpretation of fuel/vegetation conditions both within and surrounding the SZ (e.g. fuel loading, vegetation height) and estimation of SZ size and geometry by firefighters, which can potentially be subject to errors.

Even the best SZ, however, is of little use unless it is accessible by the fire crew. Accordingly, once an SZ has been defined, the fire crew must then identify a suitable escape route (ER). An ER is a pre-planned and understood route firefighters take to move from the fire line to a safety zone or other low-risk area (National Wildfire Coordinating Group, 2016). ER effectiveness can be defined in terms of the margin of safety (MOS) they provide. Beighley (1995) defined a MOS as "a cushion of time in excess of the time needed by the firefighters to get to the safety zone before the fire gets to them". As this definition alludes to, there are two primary variables of concern: the time it takes for the firefighters to reach the safety zone (T_1) and the time it takes for the fire to spread to them (T_2). Thus, an equation for MOS can be represented as $MOS = T_1 - T_2$ (Beighley, 1995). If, according to this equation, MOS is calculated to be positive, the firefighters will be safe; if MOS is negative, the firefighters will not. The estimation of T_2 has received much attention in the fire science literature, with a number of well-established tools having been developed for the prediction of fire behavior, such as FARSITE, FlamMap, and BehavePlus (Andrews et al., 2005; Finney, 2006, 2004). Despite its equal importance for calculating MOS, the studies attempting to estimate T_1 have been relatively few and far between (Alexander et al., 2005; Butler et al., 2000; Ruby et al., 2003). What limited

research there is suggests that there are both external and internal factors that control ER effectiveness. External factors include landscape parameters such as slope, vegetation density, and ground surface conditions, whereas internal factors primarily relate to fitness and experience levels of individual firefighters (Alexander et al., 2005; Anguelova et al., 2010; Butler et al., 2000; Pandolf et al., 1977; Ruby et al., 2003; Tobler, 1993; Wood and Schmidtlein, 2012). The Incident Response Pocket Guide makes mention of all of these variables, but provides no quantitative basis for implementation (National Wildfire Coordinating Group, 2014). Thus, in the absence of robust, quantitative evidence, firefighters are left to not only interpret the external, landscape conditions that lie between the crew and the SZ, but also estimate the degree to which they will affect their travel rates.

In order to enhance and improve wildland firefighter safety planning processes, it would be highly advantageous to be able to provide firefighters with objective measures of SZ and ER quality. One possible approach to doing just that would be the utilization of remote sensing and geospatial technology. Lidar remote sensing, in particular, has been shown to be capable of assessing those conditions that define SZ and ER suitability with a high degree of spatial precision, including terrain elevation and slope (Clark et al., 2004; Hodgson et al., 2005; Hodgson and Bresnahan, 2004; Hopkinson et al., 2005; Reutebuch et al., 2003; Su and Bork, 2006; Wang and Glenn, 2009), vegetation height (Andersen et al., 2006; Ben-Arie et al., 2009; Clark et al., 2004; Falkowski et al., 2006; Holmgren et al., 2003; Hopkinson et al., 2006, 2005; Khosravipour et al., 2015; Nelson, 1997; Popescu et al., 2002; Streutker and Glenn, 2006), understory vegetation structure (Goodwin et al., 2007; Hudak et al., 2008; Kramer et al., 2016; Maltamo et al., 2005;

Martinuzzi et al., 2009; Mutlu et al., 2008; Riaño et al., 2003; Seielstad and Queen, 2003; Singh et al., 2015; Skowronski et al., 2007; Su and Bork, 2007; Wing et al., 2012), and ground surface roughness (Frankel and Dolan, 2007; Glenn et al., 2006; Sagy et al., 2007; Sankey et al., 2010). Despite the vast potential for applying lidar to wildland firefighter safety, prior to the work presented in this dissertation, only one work to date had done so (Dennison et al., 2014b). Although highly capable, lidar is not without its limitations. Particularly when attempting to characterize understory conditions for ER suitability assessment, there are a number of variables that can affect the modeled accuracy thereof, including the field methods used for model training and validation, the selection of appropriate predictive lidar metrics, lidar pulse density, overstory vegetation density, and canopy height.

The work described herein aims to inquire into the potential use of lidar remote sensing and geospatial modeling for SZ and ER identification and evaluation. The specific objectives of this research are to (1) develop a new metric and lidar-based algorithm for identifying and evaluating wildland firefighter SZ on a broad scale; (2) determine the effects that landscape conditions including slope, understory vegetation density, and ground surface roughness have on travel rates in order to develop a geospatial model for ER optimization; and (3) determine the optimal methods for modeling understory vegetation density and assess the degree to which factors such as pulse density, overstory vegetation density, and canopy height affect model accuracy. This dissertation is presented in three chapters, each of which addresses one of the study objectives defined above, in order, followed by a summary of the major conclusions gleaned from the research as a whole.

References

Abatzoglou, J.T., Williams, A.P., 2016. Impact of anthropogenic climate change on wildfire across western US forests. Proceedings of the National Academy of Sciences 113, 11770–11775.

Alexander, M.E., Baxter, G.J., Dakin, G.R., 2005. Travel rates of Alberta wildland firefighters using escape routes, in: Butler, B.W., Alexander, M. E. (Eds.), Human Factors - 10 Years Later. Presented at the Eighth International Wildland Fire Safety Summit, International Association of Wildland Fire, Missoula, MT.

Andersen, H.-E., Reutebuch, S.E., McGaughey, R.J., 2006. A rigorous assessment of tree height measurements obtained using airborne lidar and conventional field methods. Canadian Journal of Remote Sensing 32, 355–366.

Andrews, P.L., Bevins, C.D., Seli, R.C., 2005. BehavePlus fire modeling system, version 4.0: User's guide.

Anguelova, Z., Stow, D.A., Kaiser, J., Dennison, P.E., Cova, T., 2010. Integrating fire behavior and pedestrian mobility models to assess potential risk to humans from wildfires within the U.S.–Mexico border zone. The Professional Geographer 62, 230–247.

Beighley, M., 1995. Beyond the safety zone: Creating a margin of safety. Fire Management Notes 55, 21–24.

Ben-Arie, J.R., Hay, G.J., Powers, R.P., Castilla, G., St-Onge, B., 2009. Development of a pit filling algorithm for LiDAR canopy height models. Computers & Geosciences 35, 1940–1949.

Butler, B.W., 2014. Wildland firefighter safety zones: A review of past science and summary of future needs. International Journal of Wildland Fire 23, 295–308.

Butler, B.W., Cohen, J.D., 1998. Firefighter safety zones: A theoretical model based on radiative heating. International Journal of Wildland Fire 8, 73–77.

Butler, B.W., Cohen, J.D., Putnam, T., Bartlette, R.A., Bradshaw, L.S., 2000. A method for evaluating the effectiveness of firefighter escape routes. 4th International Wildland Fire Safety Summit 10–12.

Calkin, D.E., Cohen, J.D., Finney, M.A., Thompson, M.P., 2014. How risk management can prevent future wildfire disasters in the wildland-urban interface. Proceedings of the National Academy of Sciences 111, 746–751.

Campbell, M.J., Dennison, P.E., Butler, B.W., 2017a. A LiDAR-based analysis of the effects of slope, vegetation density, and ground surface roughness on travel rates for wildland firefighter escape route mapping. International Journal of Wildland Fire 26, 884–895.

Campbell, M.J., Dennison, P.E., Butler, B.W., 2017b. Safe separation distance score: A new metric for evaluating wildland firefighter safety zones using lidar. International Journal of Geographical Information Science 31, 1448–1466.

Cheney, P., Gould, J., McCaw, L., 2001. The dead-man zone—A neglected area of firefighter safety. Australian Forestry 64, 45–50.

Clark, M.L., Clark, D.B., Roberts, D.A., 2004. Small-footprint lidar estimation of sub-canopy elevation and tree height in a tropical rain forest landscape. Remote Sensing of Environment 91, 68–89.

Cohen, J.D., 2000. Preventing Disaster: Home ignitability in the wildland-urban interface. Journal of Forestry 98, 15–21.

Dennison, P.E., Brewer, S.C., Arnold, J.D., Moritz, M.A., 2014a. Large wildfire trends in the western United States, 1984–2011. Geophysical Research Letters 41, 2014GL059576.

Dennison, P.E., Fryer, G.K., Cova, T.J., 2014b. Identification of firefighter safety zones using lidar. Environmental Modeling & Software 59, 91–97.

Falkowski, M.J., Smith, A.M.., Hudak, A.T., Gessler, P.E., Vierling, L.A., Crookston, N.L., 2006. Automated estimation of individual conifer tree height and crown diameter via two-dimensional spatial wavelet analysis of lidar data. Canadian Journal of Remote Sensing 32, 153–161.

Finney, M.A., 2006. An Overview of FlamMap fire modeling capabilities, in: Fuels management -- How to measure success: Conference proceedings. USDA Forest Service, Rocky Mountain Research Station, Portland, OR, pp. 213–220.

Finney, M.A., 2004. FARSITE: Fire area simulator: model development and evaluation (Research Paper No. RMRS-RP-4). USDA Forest Service, Rocky Mountain Research Station Ogden, UT.

Flannigan, M.D., Krawchuk, M.A., Groot, W.J. de, Wotton, B.M., Gowman, L.M., 2009. Implications of changing climate for global wildland fire. International Journal of Wildland Fire 18, 483–507.

Frankel, K.L., Dolan, J.F., 2007. Characterizing arid region alluvial fan surface roughness with airborne laser swath mapping digital topographic data. Journal of Geophysical Research 112, F02025.

Fryer, G.K., Dennison, P.E., Cova, T.J., 2013. Wildland firefighter entrapment avoidance: modeling evacuation triggers. International Journal of Wildland Fire 22, 883–893.

Gleason, P., 1991. Lookouts, communications, escape routes, and safety zones [WWW Document]. Wildland Fire Leadership. URL

https://www.fireleadership.gov/toolbox/documents/lces_gleason.html (accessed 2.17.17).

Glenn, N.F., Streutker, D.R., Chadwick, D.J., Thackray, G.D., Dorsch, S.J., 2006. Analysis of LiDAR-derived topographic information for characterizing and differentiating landslide morphology and activity. Geomorphology 73, 131–148.

Goodwin, N.R., Coops, N.C., Bater, C., Gergel, S.E., 2007. Assessment of sub-canopy structure in a complex coniferous forest, in: Proceedings of the ISPR Workshop "Laser Scanning 2007 and SilviLaser 2007", Espoo, September 12–14, 2007, Finland. pp. 169–172.

Gude, P.H., Jones, K., Rasker, R., Greenwood, M.C., 2013. Evidence for the effect of homes on wildfire suppression costs. International Journal of Wildland Fire 22, 537.

Hammer, R.B., Stewart, S.I., Radeloff, V.C., 2009. Demographic trends, the wildland–urban interface, and wildfire management. Society & Natural Resources 22, 777–782.

Hodgson, M.E., Bresnahan, P., 2004. Accuracy of airborne lidar-derived Elevation. Photogrammetric Engineering & Remote Sensing 70, 331–339.

Hodgson, M.E., Jensen, J., Raber, G., Tullis, J., Davis, B.A., Thompson, G., Schuckman, K., 2005. An evaluation of lidar-derived elevation and terrain slope in leaf-off conditions. Photogrammetric Engineering & Remote Sensing 71, 817–823.

Holmgren, J., Nilsson, M., Olsson, H., 2003. Simulating the effects of lidar scanning angle for estimation of mean tree height and canopy closure. Canadian Journal of Remote Sensing 29, 623–632.

Hopkinson, C., Chasmer, L., Lim, K., Treitz, P., Creed, I., 2006. Towards a universal lidar canopy height indicator. Canadian Journal of Remote Sensing 32, 139–152.

Hopkinson, C., Chasmer, L.E., Sass, G., Creed, I.F., Sitar, M., Kalbfleisch, W., Treitz, P., 2005. Vegetation class dependent errors in lidar ground elevation and canopy height estimates in a boreal wetland environment. Canadian Journal of Remote Sensing 31, 191–206.

Hudak, A.T., Crookston, N.L., Evans, J.S., Hall, D.E., Falkowski, M.J., 2008. Nearest neighbor imputation of species-level, plot-scale forest structure attributes from LiDAR data. Remote Sensing of Environment, Earth Observations for Terrestrial Biodiversity and Ecosystems Special Issue 112, 2232–2245.

IPCC, 2013. Summary for policymakers, in: Stocker, T.F., Qin, D., Plattner, G.-K., Tignor, S.K., Allen, J., Boschung, A., Nauels, Y., Xia, Y., Bex, V., Midgley, P.M. (Eds.), Climate change 2013: The physical science basis. Contribution of the working group I to the fifth assessment report of the Intergovernmental Panel on

Climate Change. Cambridge University Press, Cambridge, UK and New York, NY, USA.

Jolly, W.M., Cochrane, M.A., Freeborn, P.H., Holden, Z.A., Brown, T.J., Williamson, G.J., Bowman, D.M.J.S., 2015. Climate-induced variations in global wildfire danger from 1979 to 2013. Nature Communications 6, 7537.

Khosravipour, A., Skidmore, A.K., Wang, T., Isenburg, M., Khoshelham, K., 2015. Effect of slope on treetop detection using a LiDAR canopy height model. ISPRS Journal of Photogrammetry and Remote Sensing 104, 44–52.

Kramer, H.A., Collins, B.M., Lake, F.K., Jakubowski, M.K., Stephens, S.L., Kelly, M., 2016. Estimating ladder fuels: A new approach combining field photography with LiDAR. Remote Sensing 8, 766.

Liu, Y., Stanturf, J., Goodrick, S., 2010. Trends in global wildfire potential in a changing climate. Forest Ecology and Management, Adaptation of Forests and Forest Management to Changing Climate 259, 685–697.

Liu, Z., Wimberly, M.C., Lamsal, A., Sohl, T.L., Hawbaker, T.J., 2015. Climate change and wildfire risk in an expanding wildland–urban interface: A case study from the Colorado Front Range Corridor. Landscape Ecology 30, 1943–1957.

Maltamo, M., Packalén, P., Yu, X., Eerikäinen, K., Hyyppä, J., Pitkänen, J., 2005. Identifying and quantifying structural characteristics of heterogeneous boreal forests using laser scanner data. Forest Ecology and Management 216, 41–50.

Martinuzzi, S., Stewart, S.I., Mockrin, M.H., Hammer, R.B., Radeloff, V.C., 2015. The 2010 wildland-urban interface of the conterminous United States.

Martinuzzi, S., Vierling, L.A., Gould, W.A., Falkowski, M.J., Evans, J.S., Hudak, A.T., Vierling, K.T., 2009. Mapping snags and understory shrubs for a LiDAR-based assessment of wildlife habitat suitability. Remote Sensing of Environment 113, 2533–2546.

Mell, W.E., Manzello, S.L., Maranghides, A., Butry, D., Rehm, R.G., 2010. The wildland-urban interface problem – Current approaches and research needs. International Journal of Wildland Fire 19, 238–251.

Miller, J.D., Safford, H.D., Crimmins, M., Thode, A.E., 2009. Quantitative evidence for increasing forest fire severity in the Sierra Nevada and Southern Cascade Mountains, California and Nevada, USA. Ecosystems 12, 16–32.

Mutlu, M., Popescu, S.C., Stripling, C., Spencer, T., 2008. Mapping surface fuel models using lidar and multispectral data fusion for fire behavior. Remote Sensing of Environment 112, 274–285.

National Fire Protection Association, 2017. NFPA - Wildfires [WWW Document]. URL http://www.nfpa.org/public-education/by-topic/wildfire-and-seasonal-fires/wildland-fires (accessed 2.19.17).

National Interagency Fire Center, 2016. Wildland fire fatalities by year [WWW Document]. URL https://www.nifc.gov/safety/safety_documents/Fatalities-by-Year.pdf (accessed 2.17.17).

National Wildfire Coordinating Group, 2016. Glossary A-Z | NWCG [WWW Document]. URL https://www.nwcg.gov/glossary/a-z (accessed 2.17.17).

National Wildfire Coordinating Group, 2014. Incident Response Pocket Guide.

Nelson, R., 1997. Modeling forest canopy heights: The effects of canopy shape. Remote Sensing of Environment 60, 327–334.

Page, W.G., Butler, B.W., 2017. An empirically based approach to defining wildland firefighter safety and survival zone separation distances. International Journal of Wildland Fire 26, 655–667.

Pandolf, K.B., Givoni, B., Goldman, R.F., 1977. Predicting energy expenditure with loads while standing or walking very slowly. Journal of Applied Physiology: Respiratory, Environmental and Exercise Physiology 43, 577–581.

Parks, S.A., Miller, C., Abatzoglou, J.T., Holsinger, L.M., Parisien, M.-A., Dobrowski, S.Z., 2016. How will climate change affect wildland fire severity in the western US? Environmental Research Letters 11, 035002.

Popescu, S.C., Wynne, R.H., Nelson, R.F., 2002. Estimating plot-level tree heights with lidar: local filtering with a canopy-height based variable window size. Computers and Electronics in Agriculture 37, 71–95.

Pyne, S.J., 1996. Introduction to Wildland Fire, 2nd ed. Wiley, New York.

Radeloff, V.C., Hammer, R.B., Stewart, S.I., Fried, J.S., Holcomb, S.S., McKeefry, J.F., 2005. The wildland–urban interface in the United States. Ecological Applications 15, 799–805.

Reutebuch, S.E., McGaughey, R.J., Andersen, H.-E., Carson, W.W., 2003. Accuracy of a high-resolution lidar terrain model under a conifer forest canopy. Canadian Journal of Remote Sensing 29, 527–535.

Riaño, D., Meier, E., Allgower, B., Chuvieco, E., Ustin, S.L., 2003. Modeling airborne laser scanning data for the spatial generation of critical forest parameters in fire behavior modeling. Remote Sensing of Environment 86, 177–186.

Rossi, J.L., Simeoni, A., Moretti, B., Leroy-Cancellieri, V., 2011. An analytical model based on radiative heating for the determination of safety distances for wildland fires. Fire Safety Journal 46, 520–527.

Ruby, B.C., Iii, G.W.L., Armstrong, D.W., Gaskill, S.E., 2003. Wildland firefighter load carriage: effects on transit time and physiological responses during simulated escape to safety zone. International Journal of Wildland Fire 12, 111–116.

Ruby, B.C., Shriver, T.C., Zderic, T.W., Sharkey, B.J., Burks, C., Tysk, S., 2002. Total energy expenditure during arduous wildfire suppression. Medicine and Science in Sports and Exercise 34, 1048–1054.

Sagy, A., Brodsky, E.E., Axen, G.J., 2007. Evolution of fault-surface roughness with slip. Geology 35, 283–286.

Sankey, J.B., Glenn, N.F., Germino, M.J., Gironella, A.I.N., Thackray, G.D., 2010. Relationships of aeolian erosion and deposition with LiDAR-derived landscape surface roughness following wildfire. Geomorphology 119, 135–145.

Seielstad, C.A., Queen, L.P., 2003. Using airborne laser altimetry to determine fuel models for estimating fire behavior. Journal of Forestry 101, 10–15.

Singh, K.K., Davis, A.J., Meentemeyer, R.K., 2015. Detecting understory plant invasion in urban forests using LiDAR. International Journal of Applied Earth Observation and Geoinformation 38, 267–279.

Skowronski, N., Clark, K., Nelson, R., Hom, J., Patterson, M., 2007. Remotely sensed measurements of forest structure and fuel loads in the Pinelands of New Jersey. Remote Sensing of Environment, The Application of Remote Sensing to Fire Research in the Eastern United States 108, 123–129.

Streutker, D.R., Glenn, N.F., 2006. LiDAR measurement of sagebrush steppe vegetation heights. Remote Sensing of Environment 102, 135–145.

Su, J.G., Bork, E.W., 2007. Characterization of diverse plant communities in Aspen Parkland rangeland using LiDAR data. Applied Vegetation Science 10, 407–416.

Su, J.G., Bork, E.W., 2006. Influence of vegetation, slope, and lidar sampling angle on DEM accuracy. Photogrammetric Engineering & Remote Sensing 72, 1265–1274.

Tobler, W.R., 1993. Three presentations on geographical analysis and modeling (No. 93–1). National Center for Geographic Information and Analysis, University of California at Santa Barbara.

Wang, C., Glenn, N.F., 2009. Integrating LiDAR intensity and elevation data for terrain characterization in a forested area. IEEE Geoscience and Remote Sensing Letters 6, 463–466.

Westerling, A.L., 2016. Increasing western US forest wildfire activity: Sensitivity to changes in the timing of spring. Philosophical Transactions of the Royal Society B 371, 20150178.

Westerling, A.L., Hidalgo, H.G., Cayan, D.R., Swetnam, T.W., 2006. Warming and earlier spring increase Western U.S. forest wildfire activity. Science 313, 940–943.

Wing, B.M., Ritchie, M.W., Boston, K., Cohen, W.B., Gitelman, A., Olsen, M.J., 2012. Prediction of understory vegetation cover with airborne lidar in an interior ponderosa pine forest. Remote Sensing of Environment 124, 730–741.

Wood, N.J., Schmidtlein, M.C., 2012. Anisotropic path modeling to assess pedestrian-evacuation potential from Cascadia-related tsunamis in the US Pacific Northwest. Natural Hazards 62, 275–300.

Zárate, L., Arnaldos, J., Casal, J., 2008. Establishing safety distances for wildland fires. Fire Safety Journal 43, 565–575.

CHAPTER 1[1]

SAFE SEPARATION DISTANCE SCORE: A NEW METRIC FOR EVALUATING WILDLAND FIREFIGHTER SAFETY ZONES USING LIDAR

1.1 Abstract

Safety zones are areas where firefighters can retreat to in order to avoid bodily harm when threatened by burnover or entrapment from wildland fire. At present, safety zones are primarily designated by firefighting personnel as part of daily fire management activities. Though critical to safety zone assessment, the effectiveness of this approach is inherently limited by the individual firefighter's or crew boss's ability to accurately and consistently interpret vegetation conditions, topography, and spatial characteristics of potential safety zones (e.g. area and geometry of a forest clearing). In order to facilitate the safety zone identification and characterization process, this study introduces a new metric for safety zone evaluation: the Safe Separation Distance Score (SSDS). The SSDS is a numerical representation of the relative suitability of a given area as a safety zone according to its size, geometry, and surrounding vegetation height. This paper describes an algorithm for calculating pixel-based and polygon-based SSDS from lidar data. SSDS is calculated for every potential safety zone within a lidar dataset covering Tahoe

[1] Reprinted with permission from Campbell, M.C., Dennison, P.E., Butler, B.W., 2017. Safe separation distance score: A new metric for evaluating wildland firefighter safety zones using lidar. International Journal of Geographical Information Science 31, 1448-1466.

National Forest, California, USA. A total of 2367 potential safety zones with an SSDS ≥1 were mapped, representing areas that are suitable for fires burning in low wind and low slope conditions. The highest SSDS calculated within the study area was 9.65, a score that represents suitability in the highest wind-steepest slope conditions. Potential safety zones were clustered in space, with areas in the northern and eastern portions of the National Forest containing an abundance of safety zones while areas to the south and west were completely devoid of them. SSDS can be calculated for potential safety zones in advance of firefighting, and can allow firefighters to carefully compare and select safety zones based on their location, terrain, and wind conditions. This technique shows promise as a standard method for objectively identifying and ranking safety zones on a spatial basis.

1.2 Introduction

Between 1910 and 2015, there were 1087 documented wildland firefighter fatalities in the United States (National Interagency Fire Center 2016). The causes of fatalities vary greatly (Figure 1.1), but the leading causes fall into the category of burnovers, entrapments, burns and asphyxiation (BEBA). BEBA are the direct result of fatal exposure to excessive heat, fire, and/or smoke and comprise 45% of the total fatalities from 1910 to 2015. Burnover results from fire rapidly overtaking firefighting personnel before they can move to a safe area, and entrapment indicates that firefighters' ability to move to a safe area is compromised. Though BEBA have declined as a percentage of total fatalities in recent decades (Figure 1.1), burnover and entrapment have been implicated in recent tragic incidents involving multiple fatalities, including 14 firefighters in the 1994 South Canyon fire in Colorado and 19 firefighters in the 2013

Yarnell Hill fire in Arizona (Arizona State Forestry Division 2013, Butler *et al.* 1998). These events are not limited to the United States. For example, in 2010, 44 police and firefighters were entrapped and ultimately perished in the 2010 Mount Carmel Fire in Israel (United Nations Office for the Coordination of Humanitarian Affairs 2010).

Gleason (1991) proposed a system of interdependent safety measures to reduce firefighter risk of burnover and entrapment: lookouts, communications, escape routes, and safety zones (LCES). Safety zones are a critical component of this system, essentially areas large enough to allow firefighters to escape the harmful effects of fire (Beighley 1995). According to the US National Wildfire Coordinating Group (NWCG) Incident Response Pocket Guide (IRPG), LCES should be established and known to all members of a fire crew before it is needed (National Wildfire Coordinating Group 2014). The IRPG indicates that safety zones can be areas that have already burned, can be natural (rock areas, water, meadows) or constructed (clear-cuts, roads, helicopter landing zones), and should be scouted for size and hazards. If they are upslope of flames, downwind of flames, or adjacent to particularly heavy fuels, a larger safety zone is needed (National Wildfire Coordinating Group 2014).

Safety zones must be large enough to hold firefighting personnel and equipment, and should provide a safe separation distance (SSD) between vegetation and these assets (Figure 1.2). The SSD must be large enough that heat from the wildfire is reduced to the point that a fire shelter is not necessary to prevent firefighter injury. The current NWCG guideline for estimating SSD comes from Butler and Cohen (1998), who determined, based on radiant heat modeling, that SSD should be equal to or greater than four times flame height. This guideline assumes flat terrain and does not account for convective heat

transfer, which can strongly contribute to firefighter heat exposure (Butler *et al.* 2015, Butler 2014).

Relatively few studies have attempted to characterize convective heat flux in a wildland fire environment, due to its inherent complexity and measurement difficulty. Frankman *et al.* (2013) demonstrated the varied but significant effects of convective energy flux (both heating and cooling), which were heavily influenced by fuel, wind, and terrain conditions. Zárate *et al.* (2008) suggested adding a 20% increase in SSD to account for the additional convective heat flux. Butler *et al.* (2015) point out that exposure to high winds and adjacency to steep slopes has the potential to transfer convective heat as far as two to three flame lengths ahead of the fire front. To account for convective heat flux, Butler (2015) proposed that the SSD calculation can be adjusted using a 'slope-wind factor' (Δ):

$$SSD = 8 \times H_v \times \Delta, \quad (1.1)$$

where H_v is vegetation height. For flat terrain and low wind speeds, SSD is simply eight times vegetation height, identical to the current NWCG guideline (assuming flame height is equal to two times the vegetation height). Although flame height will not always be equal to twice the vegetation height, it is a useful approximation for crown fire conditions, enabling a broad-scale pre-fire assessment of SSD based on existing vegetation conditions, rather than requiring that firefighters predict flame heights. As slope and wind speed increase, the slope-wind factor increases to provide a larger SSD value. Examples of slope-wind factors from Butler (2015) are shown in Table 1.1. Based on the slope-wind factor, a potential safety zone sufficient for flat terrain and moderate

wind speed (SSD = 8 × H_v × 1.5) could be too small for flat terrain and strong wind speed (SSD = 8 × H_v × 3).

Field estimates of safety zone geometry and surrounding vegetation height, which are used to calculate SSD, are prone to large errors (Bechtold *et al.* 1998, Steele 2000). This study demonstrates a method for identifying, evaluating and mapping the relative suitability of all potential safety zones throughout a given area in order to improve the process of safety zone designation. Specifically, the objectives of this study are (1) to introduce a new metric for evaluating potential safety zones, based on safety zone geometry, area, surrounding vegetation height, and number of firefighting personnel present: the Safe Separation Distance Score (SSDS), (2) to develop an algorithm to map SSDS using lidar data, and (3) to test the implementation of the algorithm on a lidar dataset from Tahoe National Forest.

1.3 Methods

1.3.1 Data and study area

Lidar is a type of active remote-sensing system that enables the generation of very high spatial resolution three-dimensional models of terrain and above-ground structure (vegetation, buildings, etc.) (Lefsky *et al.* 2002). Discrete return lidar instruments, which are typically mounted on an aircraft, emit hundreds of thousands of individual pulses of laser light to the ground every second. The light in each pulse interacts with features on the ground and reflects back to the sensor. Extremely accurate measurement of the elapsed time between light transmission and reception enables calculation of a precise elevation of the reflective object (Lefsky *et al.* 2002). The result of such data collection is typically a point cloud comprised of millions of points, each with an associated *x*, *y*, and *z*

value. In order to be able to extract useful information from a lidar point cloud, points are generally classified into ground and non-ground (e.g. vegetation and buildings) (Meng *et al.* 2010). Many methods exist for ground point classification, the accuracies of which vary significantly according to the method used, the terrain conditions and the degree to which surface features obscure the ground surface (Reutebuch *et al.* 2003). Discrete ground points can be interpolated into digital terrain models (DTMs), which are continuous raster representations of the ground surface (Kraus and Pfeifer 2001). In the presence of vegetation, lidar pulses typically interact with several surfaces prior to reaching the ground surface. In these cases, the 'last return' can often, though not always, represent the ground surface, while the 'first return' represents the elevation of the highest reflective surface. First return points can be interpolated to generate a digital surface model (DSM). In the absence of above-ground objects (e.g. bare soil), surface and terrain model pixel values should be equal. Vegetation height can be computed by subtracting terrain elevations from surface elevations (Dubayah and Drake 2000, Popescu *et al.* 2002). Dennison *et al.* (2014) used lidar to map safety zones for different expected flame heights, but did not directly utilize variable vegetation height information provided by lidar data.

SSDS were calculated for potential safety zones within Tahoe National Forest, California, USA. A lidar-derived DTM and DSM, each with a spatial resolution of 1.0 m, were obtained from the US Forest Service (Figure 1.3). The raw point cloud data from which these datasets were derived were collected between 2013 and 2014 with an average pulse density of 8 pulses/m^2.

The study area encompasses 5335 km^2, 4549 km^2 (85%) of which is within the Tahoe National Forest administrative boundary. There is a wide range of elevations throughout the study area, from 268 m at its lowest point to 2813 m at the highest with a mean elevation of 1686 m. The land cover is primarily composed of conifer forest (77%), shrubland (8%), riparian vegetation (4%), sparse vegetation (3%), hardwood forest (2%), and grassland (1%), with the remaining area being a combination of a variety of rarer cover types, including developed land (LANDFIRE 2012). Within the dominant conifer class, the distribution of forest types is as follows: Douglas-fir (*Pseudostuga menziesii*)/grand fir (*Abies grandis*)/white fir (*Abies concolor*) mix (34%), red fir (*Abies magnifica*) (28%), Douglas-fir (*Pseudotsuga menziesii*)/ponderosa pine (*Pinus ponderosa*)/lodgepole pine (*Pinus contorta*) mix (21%), ponderosa pine (*Pinus ponderosa*) (15%), and other conifer (2%).

1.3.2 Safety zone model

SSDS is a unitless value that is attributed to a forest clearing that provides firefighting personnel with an estimate of the relative suitability of that clearing as a safety zone according to its area, geometry, surrounding vegetation height, and number of firefighting personnel and equipment present. SSDS can be compared directly to the slope-wind factor for expected wind speed and slope (Table 1.1) to determine whether a specific safety zone is adequate for expected conditions. Using lidar data, an SSDS can be calculated for all potential safety zones within an area. Multiple geospatial data processing steps are required to calculate SSDS from a lidar-derived terrain and surface models. An automated model was developed in Python using primarily ESRI ArcGIS tools to facilitate the safety zone analysis across a relatively large study area with many

forest clearings varying in size, shape, and surrounding vegetation conditions. This section describes, in detail, the model workflow.

In order to be able to assess vegetation height, a canopy height model (CHM) was generated by subtracting the terrain elevation from the surface elevation for each pixel (x,y), such that:

$$CHM_{(x,y)} = DSM_{(x,y)} - DTM_{(x,y)}, \quad (1.2)$$

where DSM is the digital surface model and DTM is the digital terrain model. The resulting raster dataset contained a pixel-based representation of height, in meters, above the ground surface (Figure 1.4(a)). In order to locate forest clearings, a tree/non-tree map was generated using a simple height threshold classification, wherein all CHM values less than 1 m in height were classified as 'non-tree' and all CHM values equal to or greater than 1 m in height were classified as 'tree'. A kernel filtering process was then applied to the tree/non-tree classification to eliminate small and/or isolated trees that would be unlikely, in a wildfire setting, to have sufficient connectivity to surrounding fuels to negatively affect the quality of an otherwise open area as a safety zone (Dennison *et al.* 2014). A 10% threshold within a circular kernel 30 m in diameter was used for filtering. If the area classified as 'tree' was less than 10% of the 30 m kernel, it was reclassified to 'non-tree'. Both the diameter of the kernel and the percent threshold are important parameters of the model that have direct impacts on the resultant classification of clearings versus treed areas, but for the purposes of this study, no sensitivity tests were performed to determine their relative effects on resulting safety zone maps.

Clearings were located by buffering the ‘tree’ pixels by 8 m and identifying those areas remaining beyond the extent of the buffers. Eight meters was used because in a best-case scenario (low wind, low slope, 1 m tall surrounding trees), the safe separation distance would be 8 m (8 × 1 m × 1). Clearings were then buffered back to the forest edge by 8 m, in order to represent the full extent of the clearing. Figure 1.4(b) illustrates one such clearing, though it should be noted that Figure 1.4, as a whole, illustrates a single example of processes performed on nearly 86,000 clearings throughout the study area.

For each individual clearing, the following steps were performed. In the interest of assessing the vegetation immediately surrounding the clearing, a 10 m buffer was created around it. The CHM was then clipped to the extent of this buffer area and surrounding tree crowns were delineated individually using a watershed segmentation technique first introduced by Wang *et al.* (2004). Figure 1.5 graphically depicts this technique. Beginning with a CHM, all non-tree pixels (height <1 m) were removed and the resulting raster was inverted (multiplied by −1) to create tree ‘basins’ out of what were previously tree peaks. A ‘flow direction’ image was then generated which simulates the flow of water within each of these tree basins. Because these basins all drain internally (because, in reality, each tree comes to an individual peak), we then delineate individual basins, or watersheds, which generate a raster approximation of individual tree crowns. These tree crowns are then converted to a vector polygon for further analysis.

Tree crown polygons were used to calculate individual tree heights by computing a within-polygon maximum CHM value. As Figure 1.4(c) highlights, the result of this process was an array of polygons surrounding the clearing, each of which has an associated height. However, to analyze the effect of each individual tree height on SSD

would be extremely processing-intensive, rendering an algorithm such as this ineffective for application on a broad scale. On the other hand, to compute a single mean surrounding vegetation height for an entire clearing would be an over-generalization, particularly for large clearings where surrounding vegetation heights can vary significantly from one portion of their perimeter to another. This variability in vegetation height is important to capture, as it will have direct impacts on where the safety zone should be located within a clearing (further from areas with taller vegetation, closer to areas with shorter vegetation). Thus, mean surrounding vegetation height was calculated within each of a series of buffer segments, each 10 m wide and roughly 100 m in length, surrounding each clearing (Figure 1.4(d)). Mean tree height was weighted by tree crown area to avoid the downward-bias resulting from the likely presence of a greater number of smaller (and shorter) trees than larger (and taller) trees, such that:

$$H_v = \frac{\sum_{i=1}^{n} a_i \times h_i}{\sum_{i=1}^{n} a_i}, \tag{1.3}$$

where *a* is crown area and *h* is height for each individual tree crown *i*. For each linear buffer, Euclidean distance from surrounding vegetation was then calculated on a continuous pixel basis within the clearing. Using mean vegetation height and distance from surrounding vegetation for each pixel (*x*,*y*) within the clearing, a pixel-based SSDS(*x*,*y*) was calculated, such that:

$$SSDS_{(x,y)} = \frac{ED_{(x,y)}}{(8 \times H_v)}, \tag{1.4}$$

where ED(x,y) is the Euclidean distance from vegetation raster data for each pixel (x,y). This SSDS calculation is essentially a transformation of the proposed SSD equation (Equation (1.1)), substituting the Euclidean distance raster data for SSD and solving for Δ on a pixel-by-pixel basis, thus making SSDS and Δ directly comparable values. As a result of this calculation, each clearing had a series of individual SSDS raster layers, each associated with one of the linear buffers surrounding the clearing. A single clearing-wide SSDS raster is then generated by computing a pixel-by-pixel minimum SSDS value among each of the contributing SSDS rasters.

Most often the clearings that emerged from this mapping process were irregularly-shaped, unlike the simplified case illustrated in (Figure 1.2). Figure 1.4 highlights one such irregular clearing. Though it maintained non-tree connectivity throughout the clearing, its large size and irregular shape could enable the placement of multiple safety zones within. From a geospatial standpoint, one can clearly see in Figure 1.4(e) how there are several local maxima of SSDS within the clearing due to the effects of clearing geometry and variable surrounding vegetation height. In order to address this we employed another watershed-based approach for locating safety zones within the clearing. This involved taking the inverse of the SSDS raster (multiplying SSDS by −1 to form SSDS 'basins'), calculating 'flow direction', and locating 'sinks', or areas of internal drainage, the results of which represent the points of local maximum SSDS, or the safest points within each distinct portion of the clearing (Figure 1.4(e)).

The last critical variable addressed in this model is firefighter crew size. Safety zones need to be large enough to accommodate both personnel and equipment (e.g. engines). Andrews *et al.* (2005) suggests 4.6 m^2 (50 ft^2) is required for each crew member

and 27.9 m^2 (300 ft^2) is required for each engine. For the purpose of this study, an assumed crew size of 20 firefighters and 2 engines was used, requiring a minimum safety zone area of 148.6 m^2. Circular areas of this size, representing potential safety zones where firefighters and equipment would assemble, were centered on the points of local maximum SSDS (Figure 1.4(e)). Rather than use this highest SSDS to represent the entire safety zone, however, the lowest within-safety zone SSDS is used, because this represents the relative safety of the zone on its outside edge. Again, because SSDS values are directly comparable to Δ values, we can determine that, because the lowest possible Δ is 1, then any safety zone with an SSDS <1 will be unsuitable in any wind and terrain conditions. Thus, all potential safety zones with an SSDS much less than 1 are eliminated from consideration. However, given the continuous nature of SSDS, one could still identify perhaps sub-optimal but still viable safety zones with SSDS of 0.9 or 0.95, if these are the only options available to a fire crew, as seen in (Figure 1.4(f)).

Finally, a slope raster dataset is calculated throughout the entire study area using the lidar-derived DTM. Mean slope is then computed within each safety zone. The resulting safety zone polygons each have an associated SSDS and slope written to the attribute table. Since SSDS is derived directly from the proposed SSD equation, SSDS values can then be queried and compared to the Δ values in the slope-wind factor matrix to determine the relative suitability of that clearing as a potential safety zone. For example, if a safety zone has an SSDS of 1.5, it is suitable in all conditions where a Δ of 1.5 or less is required.

1.4 Results

The resulting map of potential safety zones with associated SSDS values (greater than 1) throughout the study area can be seen in Figure 1.6. As the map highlights, there are relatively few safety zones that have an SSDS of 1 or greater, which is to say that at the time of lidar acquisition, the vegetation conditions found within the study area would offer relatively few potential safety zones that are sufficiently large in even the best-case (low wind and low slope) scenarios. Clustering of potential safety zones is clearly evident, particularly in the northeastern portion of the study area. Much of the vegetation in this area was burned in the high severity Cottonwood fire in 1994. Although roughly 20 years passed between the Cottonwood fire and the lidar data acquisition, the subsequent slow regeneration of vegetation in certain areas of the fire lends itself well to use as potential safety zones, according to the results of our model. Potential safety zones are particularly sparse in the southern and western portions of the study area, where continuous swaths of forest 400 km^2 or greater in area, are entirely devoid of potential safety zones even at the lowest recommended SSDS of 1. It should be noted that many of the largest safety zones with the highest SSDS values are lakes. While lakes may seem like an ideal safety zone (no slope, vegetation, or possibility of burning), they present their own set of risks, such as drowning or hypothermia (Butler 2014). The resulting safety zones were compared to the USGS National Hydrography Dataset, and all of those that fell within a waterbody were removed.

Table 1.2 provides a tabular account of the number of potentially viable safety zones in each combination of wind speed and slope according to resulting SSDS. It stands to reason that there are many more potential safety zones with low SSDS, suitable

in low wind-flat slope conditions, than high SSDSs, suitable in high wind-steep slope conditions, simply because there are many more small forest clearings than large. With that said, there are still only a total of 2367 potential safety zones with scores of greater than or equal to 1 throughout the entire study area. When comparing SSDS values to the slope-wind factor matrix, we see that a safety zone with an SSDS of 1 would be suitable in the lowest wind and slope conditions (<3 ms^{-1} and <30%, respectively). However, as wind speeds and slopes increase, higher SSDS values are needed to render a safety zone viable. For example, if wind speeds are slightly higher (4–7 ms^{-1}), and slopes remain less than 30%, an SSDS of at least 2 is needed, of which there are a total of 352. The highest SSDS value found throughout the study area was 9.65, which would be suitable for any combination of wind speed and slope. Given that slope is a static landscape variable, SSDS can be compared to slope in order to determine the wind speed conditions in which a given safety zone would be viable. When comparing safety zone slopes to SSDS values, we see that even at the lowest wind speed category (<3 ms^{-1}), there are only 1547 potentially suitable safety zones (Figure 1.7). As wind speed increases to 4–7, 8–13, and greater than 13 ms^{-1}, the number of safety zones drops to 500, 79, and 14, respectively.

Perhaps equally important to the number of potential safety zones is their spatial distribution, which directly impacts accessibility. As stated earlier, there is a clearly non-random distribution of safety zones throughout the study area, leaving vast tracts of forested land without any viable safety zones, particularly in the southwest. Figure 1.8 depicts distance intervals and associated approximate travel times to safety zones with varying SSDS thresholds. Travel rates were assumed to be 1.4 ms^{-1}, an empirically derived average hiking rate along flat slopes from Tobler (1993). Table 1.3 highlights the

proportions of the study area that fall within these same distance and time intervals from safety zones. In low wind-low slope scenarios, where an SSDS of at least 1 is needed, roughly 8% of the study area is within a 5-minute hike to the nearest safety zone, 17% within 10 min, 41% within 30 min, and 64% within an hour (Figure 1.8, Table 1.3). Conversely, with high-SSDS safety zones being so sparse throughout the study area, only 1% of the area is within an hour of the nearest safety zone with SSDS ≥7.

Clearing area is the best predictor of SSDS. Given that most forest clearings contain several potential safety zones, we performed a linear regression between the SSDS of the highest-rated safety zone within each clearing and the clearing area. As the data were heavily right-skewed, we used a reciprocal-square transformation for the SSDS data and a log transformation for the area data (Figure 1.9). The relatively low predictive power that emerged ($r^2 = 0.38$) is due to the fact that clearing geometry and surrounding vegetation height also have significant impacts on a given safety zone's SSDS. Additional geometric parameters such as clearing perimeter and area-to-perimeter ratio were also tested for statistical relationships, but their predictive powers were lower ($r^2 = 0.32$ and $r^2 = 0.28$, respectively).

1.5 Discussion and conclusions

This study introduced a new metric and geospatial model for identifying and evaluating potential wildland firefighter safety zones using lidar data. Lidar proves to be an excellent resource for assessing many of the most important predictors of safety zone quality: clearing size and geometry, within- and surrounding-clearing vegetation height, and slope. However, at present, safety zones are evaluated and designated on the ground by firefighting personnel with limited influence of geospatial information. The use of a

standardized metric (SSDS) evaluated through a robust, automated computer model, such as was introduced in this study, stands to greatly increase the reliability and consistency with which safety zones are evaluated. Instead of relying on visual interpretation of safety zone area, geometry and surrounding vegetation height for each individual potential safety zone visited on the ground, the SSDS model provides firefighters with a map of all of the potential safety zones in the surrounding area, each of which is attributed with a value that can be used to determine the wind and terrain conditions in which a given safety zone will be suitable. It should be clearly noted, however, that this methodology is not a replacement of ground-based safety zone evaluation. Like any model-based remote-sensing analysis, ground verification is essential. Unlike most other remote-sensing analyses, ground verification is particularly important in this study, given the potentially dangerous and even fatal consequences of utilizing an unsuitable safety zone. However, whereas under the existing protocol for safety zone identification, all potential safety zones must be visited and verified, the method we have presented will enable a more targeted approach, eliminating the need to visit areas the model has determined that no viable safety zones exist, according to surrounding vegetation, clearing geometry, slope, wind, and crew size. This will greatly increase the efficiency of safety zone selection and minimize potential for selecting unsuitable sites.

The results of the model implementation in Tahoe National Forest highlight a relative sparseness of suitable safety zones, especially for high winds and steep slopes. Particularly in the western and southern portions of the study area, if a wildfire were to occur, safety zones (at least those composed of existing forest clearings) are few and far between. However, knowing where safety zones are not may be just as useful as knowing

where safety zones are. In the event of a wildfire in an area devoid of natural safety zones, this model can be used to highlight areas where safety zones could be created through the use of controlled burning, timber harvesting or other manipulation of existing fuels, or through the utilization of recently burned areas in a wildfire. If creation or enlargement of safety zones in not feasible then fire management tactics should be modified to reduce firefighter risk, such as standing down until conditions change or the fire moves to a more suitable location. Similarly, if an area has an existing potential safety zone, but the SSDS is too low for the slope and wind conditions, it could provide an impetus to expand the safety zone to a suitable size and/or geometry.

One of the most important parameters not addressed by this model is fuel type, both within and surrounding the potential safety zone. The model, in its present form, makes a key assumption that vegetation less than 1 m in height is 'non-tree', and therefore eligible to become a safety zone, provided other conditions are met. While the 1 m threshold is a model parameter that can be manipulated, regardless of vegetation height, certain fuel types are undesirable for safety zones. For example, shrubs may be short in stature but highly flammable and might not provide a viable safety zone without treatment. Although we are only taking advantage of lidar's ability to characterize vegetation height in this study, lidar can be further exploited for the estimation of other fuel parameters, such as crown bulk density and canopy base height (Andersen *et al.* 2005). Another potential solution to this issue is incorporation with additional remote-sensing data. The use of hyperspectral imagery, for example, could be used to characterize within-safety zone fuel conditions through the spectral unmixing of green vegetation, non-photosynthetic vegetation and soils (Roberts *et al.* 2006). Alternatively,

in the absence of hyperspectral image availability, tools such as LANDFIRE can provide critical fuel information such as vegetation type, height and cover, and fire behavior fuel models, albeit at a coarser level of thematic precision and with limited accuracy (Rollins 2009). Additionally, it is understood that fuel type and condition of the vegetation surrounding the safety zone will impact the relative flammability of this vegetation, potential for crown fire, and fire intensity. In order to eventually incorporate such information into SSDS, more detailed studies on the specific relationships between fuel and fire parameters are needed.

Another key variable not assessed in the implementation of this algorithm is safety zone accessibility. A large safety zone completely devoid of flammable vegetation may be evaluated as having a very high SSDS, suggesting suitability in a wide range of wind and terrain conditions, but if it is not accessible by a fire crew, it is not a viable option. Escape routes are a critical component of fire safety, representing pre-defined pathways for accessing safety zones (National Wildfire Coordinating Group 2016). Given the similarities between the conditions that define the relative suitability of escape routes and safety zones (low slope, low vegetation cover), similar lidar-based approaches can be used in the future for determining optimal escape routes from fire crew location to a safety zone.

A key limitation to the practical application of this study and widespread use of the proposed model for safety zone evaluation, at present, is the lack of lidar data availability throughout most of the United States. In order to obtain a reliable picture of safety zones on a broad scale, there needs to be a similarly reliable lidar dataset extending into all areas where wildfires can occur. With the USGS 3D Elevation Program underway

(Snyder 2012), a nationwide map of safety zones could be generated and provided to land management and firefighting agencies. However, at the time of writing, with the expected completion of a nationwide lidar dataset still several years in the future, a more targeted approach to lidar data collection in fire-prone areas can provide critical information for supporting firefighter safety operations in the interim. Alternatively, in the absence of lidar data there are other options that could prove viable, such as stereo imagery-based pseudo-point cloud extraction. However, a key limitation with stereo imagery methods is the absence of a reliable ground surface model in areas with dense tree canopies, thus limiting the ability to extract tree heights which are a critical parameter in safety zone analysis (St-Onge *et al.* 2008). Another related limitation is the fact that lidar represents a single snapshot in time. Particularly in fire-prone areas, vegetation is a dynamic entity that changes with the presence of disturbance events including wildfire, timber harvesting, insect and disease outbreaks, major wind events, and, over a much longer timescale, climate change. By one account (National Fire Protection Association 2011), as much as 90% of safety zones are designated 'in the black'– in already-burned areas. These areas would obviously not be depicted in a safety zone map created using lidar data flown prior to the wildfire event. One possible solution to this is the incorporation of unmanned aerial vehicular technology. The model as it is being presented in this study is intended to be a tool for pre-fire planning (O'Connor *et al.* 2016), though it is conceivable that this methodology could be adapted to a rapid response tool used for a more targeted approach for safety zone identification and evaluation. Alternatively, the use of predictive vegetation growth models and fuel accumulation curves could be used to estimate vegetation conditions following disturbance events to fill in temporal gaps in

lidar data collections and/or to highlight areas to target repeat lidar data collection efforts.

Finally, it is worth noting that the scientific basis of convective and radiant heat transfer modeling upon which Δ and, as a result, SSDS are based, still requires further study (Finney *et al.* 2013, 2015). As stated earlier, particularly convective heat transfer is a tremendously challenging physical phenomenon to model in a controlled environment. While the data used in this study are based on recent findings in the research of radiant and convective heat transfer in wildfires and their effects on humans, more research is needed. Specifically, a more nuanced understanding of the effects of specific vegetation types and fuel conditions, which can both be approximated with remote sensing, on heat transfer would greatly improve the effectiveness of implementing our algorithm. That being said, even if the specific Δ and SSDS numbers were to be updated with newer science, the core methodology presented in this study would remain a viable option for increasing firefighter safety.

1.6 Acknowledgements

Funding for this research was provided by the US Forest Service National Fire Plan through the Office of Research, the NWCG Fire Behavior Subcommittee, and the Wildland Fire Management Research Development & Application Program, Cooperative Agreements 14JV11221637123 and 15CR11221637105. We would like to thank the Forest Service Region 5 Remote Sensing Lab, Carlos Ramirez, Scott Conway, and Kirk Evans for providing lidar products for Tahoe National Forest. Finally, we would like to thank the anonymous reviewers, whose thoughtful questions and comments helped to improve this paper.

Table 1.1. Slope-wind factor safe separation distance matrix from Butler (2015).

Slope-Wind Factor (Δ)				
	Slope (%)			
Wind Speed (ms^{-1})	Flat (<20%)	21–30%	31–50%	>50%
Light (0–3)	1	1	3	5
Moderate (4–7)	1.5	2	4	6
Strong (8–13)	3	3	6	7.5
Very Strong (>13)	4.5	5	7	9

Table 1.2. Number of suitable safety zones in each combination of wind speed and slope according to SSDS values.

	Slope (%)			
Wind Speed (ms^{-1})	Flat (<20%)	21–30%	31–50%	>50%
Light (0–3)	2367	2367	99	15
Moderate (4–7)	881	352	30	7
Strong (8–13)	99	99	7	2
Very Strong (>13)	19	15	2	2

Table 1.3. Percent of study area within distance and travel time of safety zones with different SSDS thresholds.

Distance:	0-420 m	420-840 m	840-2520 m	2520-5040 m	> 5040 m
Time:	0-5 min	5-10 min	10-30 min	30-60 min	> 60 min
SSDS ≥ 1	8.11%	8.69%	23.94%	23.65%	35.61%
SSDS ≥ 2	1.84%	2.57%	9.57%	18.06%	67.95%
SSDS ≥ 3	0.67%	1.07%	3.53%	7.71%	87.02%
SSDS ≥ 4	0.25%	0.48%	2.28%	5.82%	91.17%
SSDS ≥ 5	0.13%	0.31%	1.28%	3.34%	94.94%
SSDS ≥ 6	0.06%	0.17%	0.94%	2.29%	96.54%
SSDS ≥ 7	0.01%	0.04%	0.29%	0.85%	98.80%
SSDS ≥ 8	0.01%	0.04%	0.29%	0.85%	98.80%
SSDS ≥ 9	0.01%	0.04%	0.29%	0.85%	98.80%

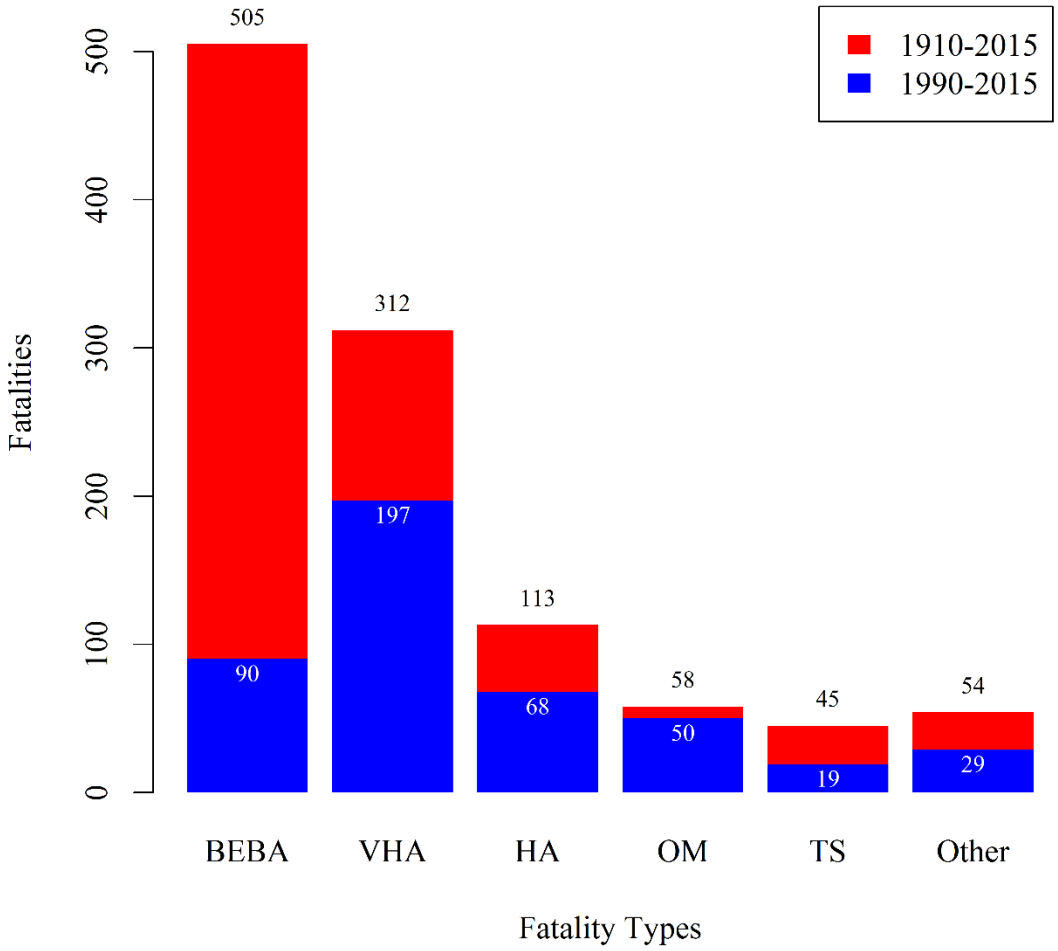

Figure 1.1. Wildland firefighter fatalities by type (BEBA = burnover, entrapment, burns, and asphyxiation; VHA = vehicle, helicopter, aircraft; HA = heart attack; OM = other medical; TS = tree, snag) (National Interagency Fire Center 2016).

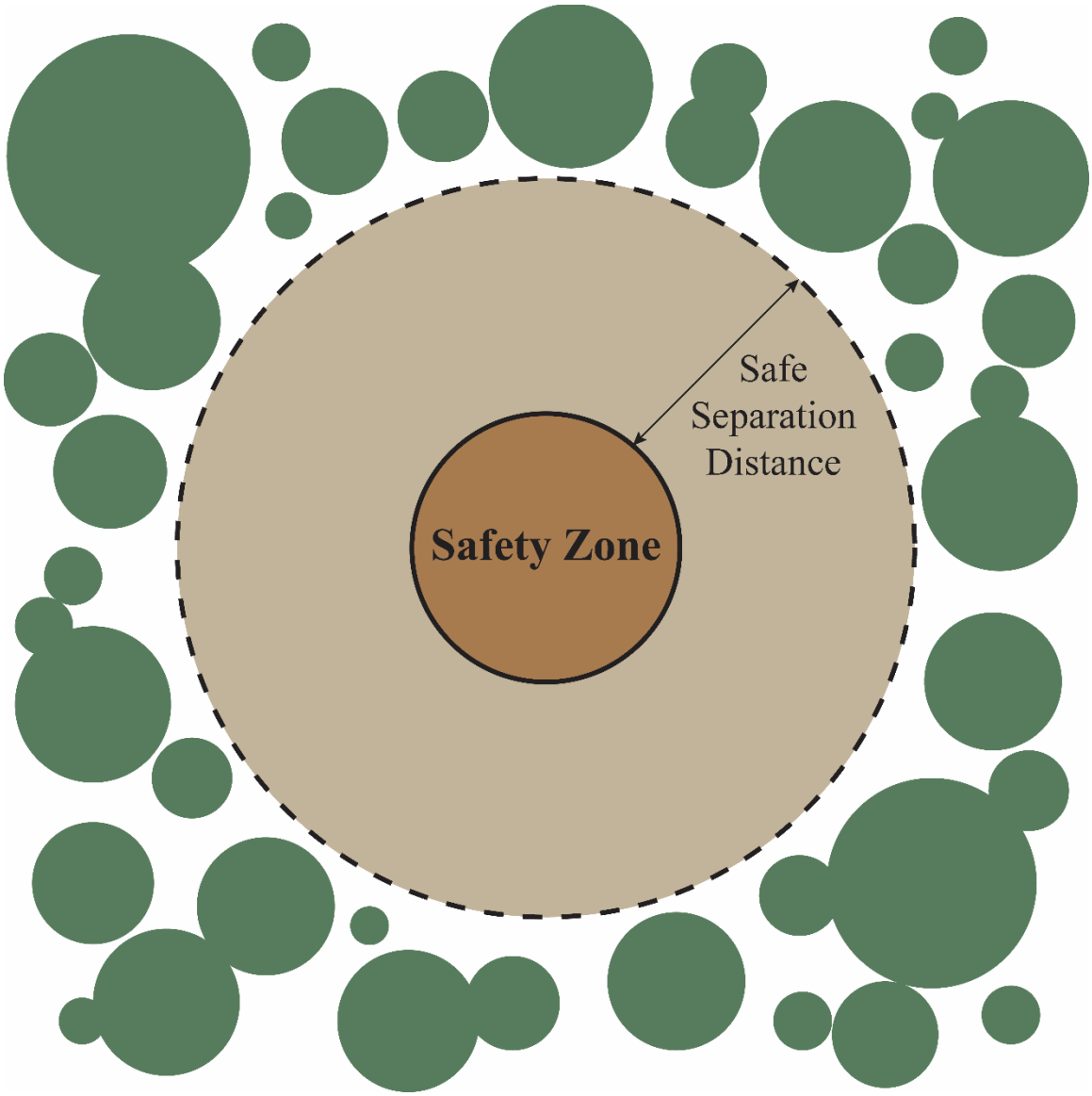

Figure 1.2. Basic safety zone example diagram (after Dennison *et al.* (2014)).

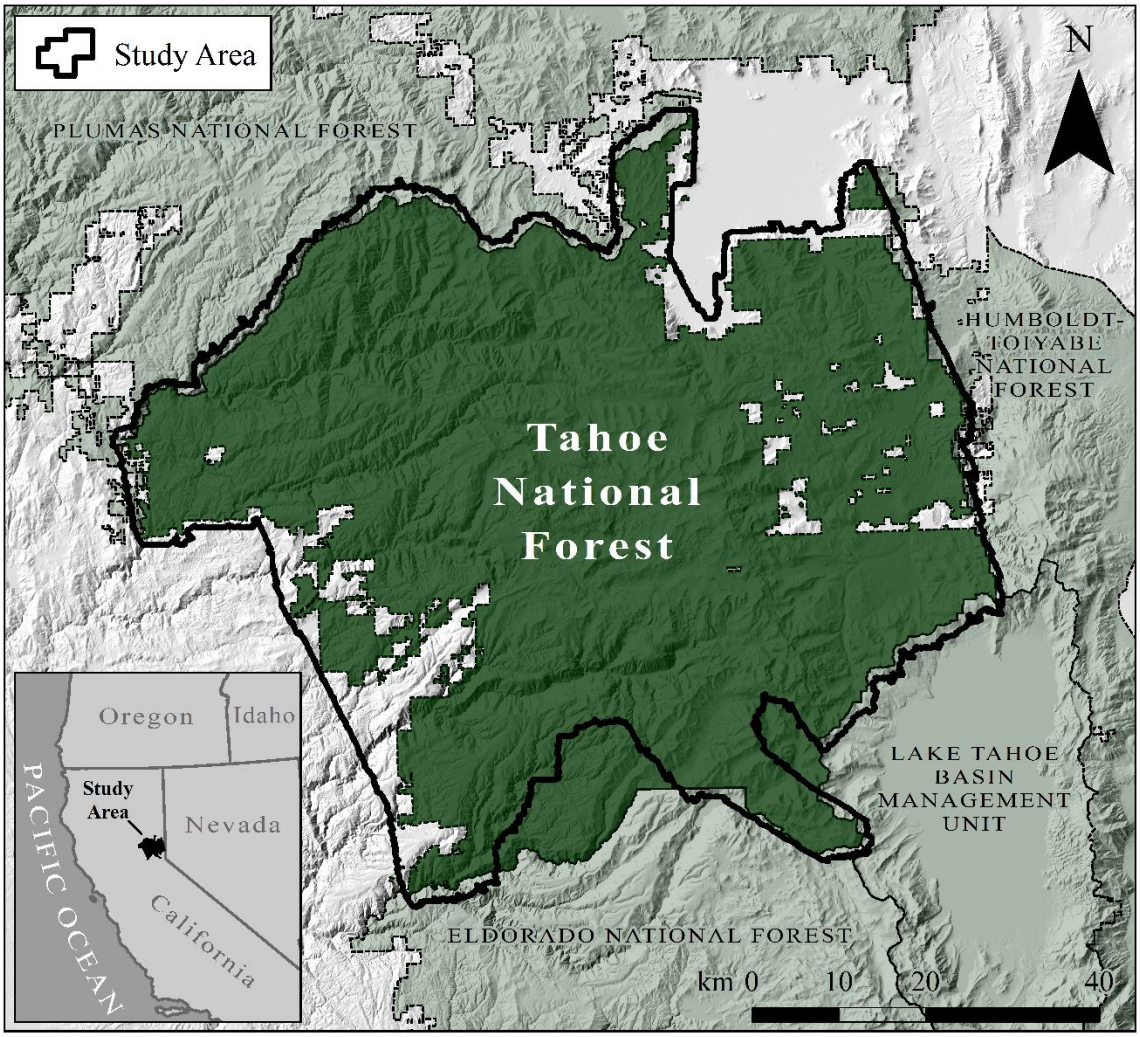

Figure 1.3. Study area map.

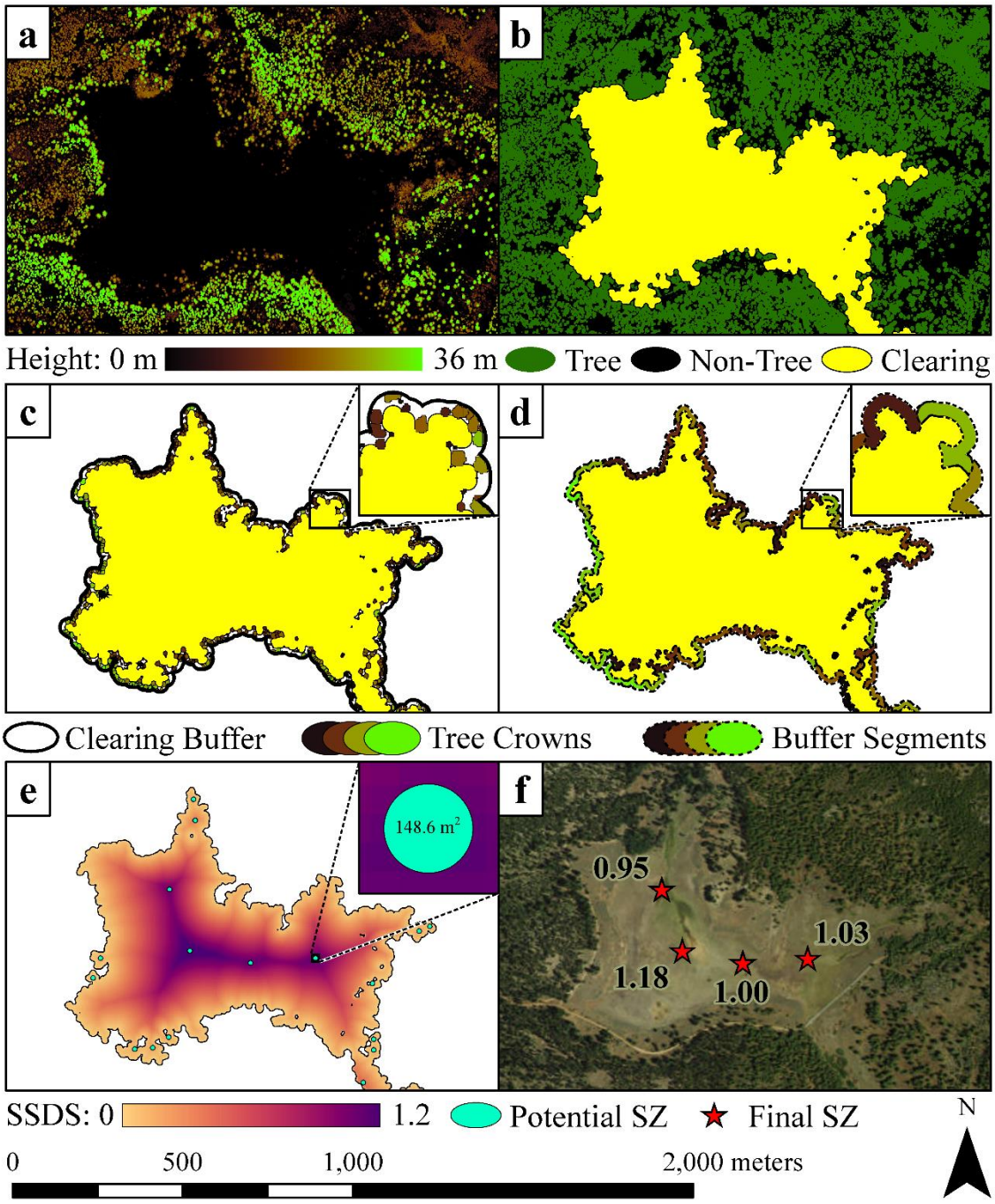

Figure 1.4. Model workflow from canopy height model (a) to clearing classification (b), surrounding tree crown delineation and height calculation (c), segment-based mean surrounding vegetation height calculation (d), pixel-based SSDS calculation and safety zone placement (e), and safety zone SSDS result (f).

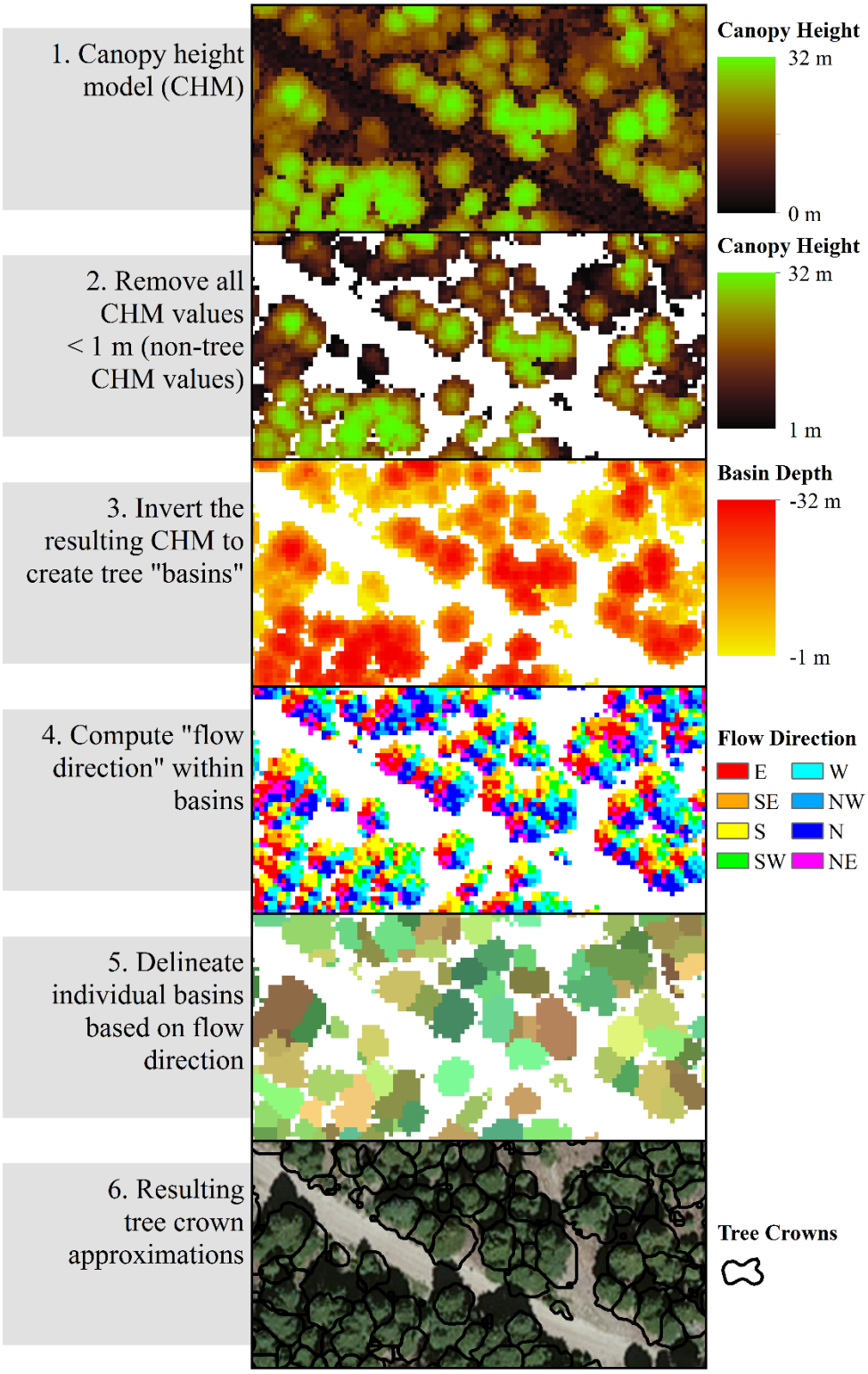

Figure 1.5. Tree crown delineation method.

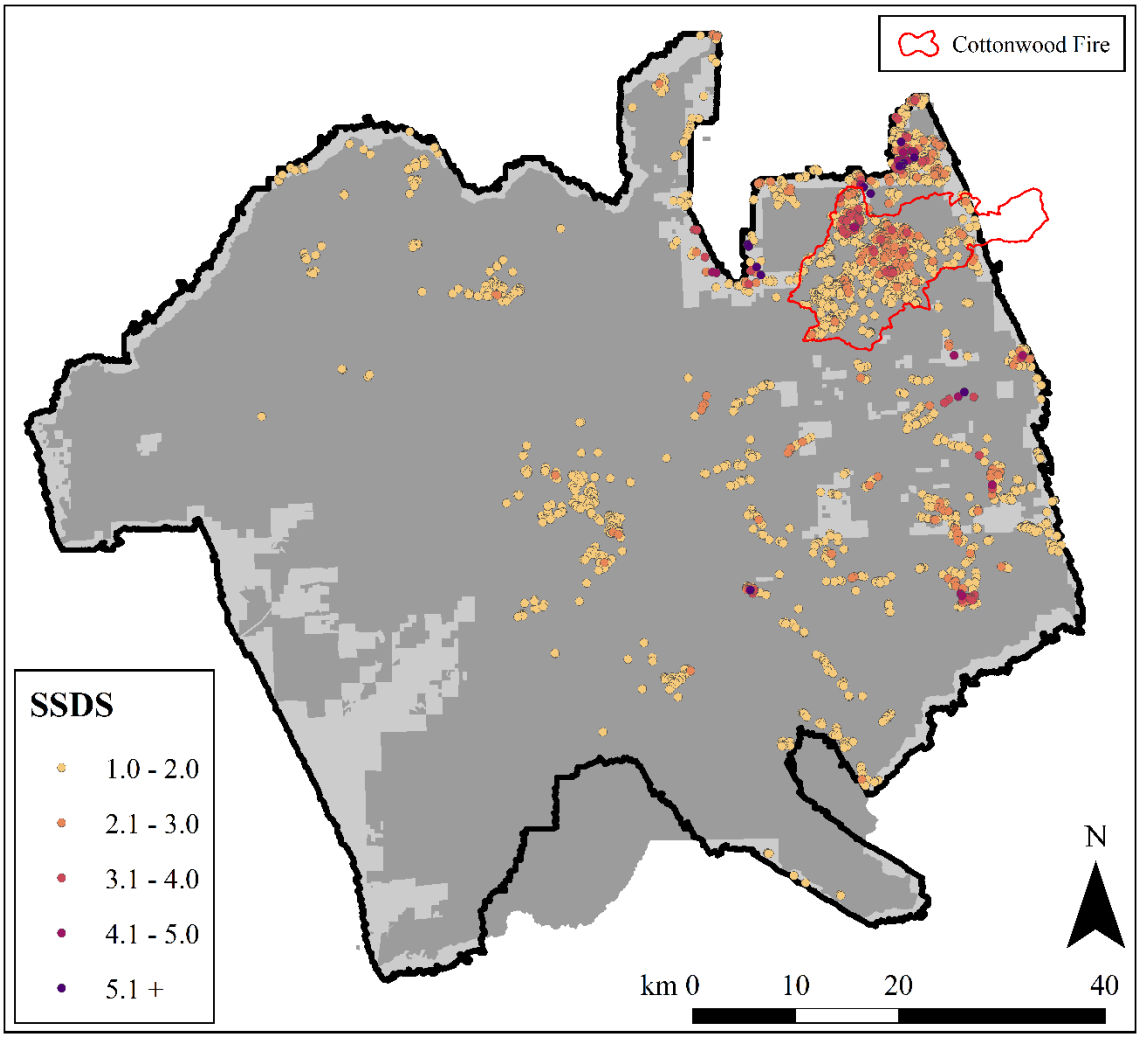

Figure 1.6. Potential safety zones with associated safe separation distance score values throughout the study area. The area burned by the 1994 Cottonwood fire is outlined in red.

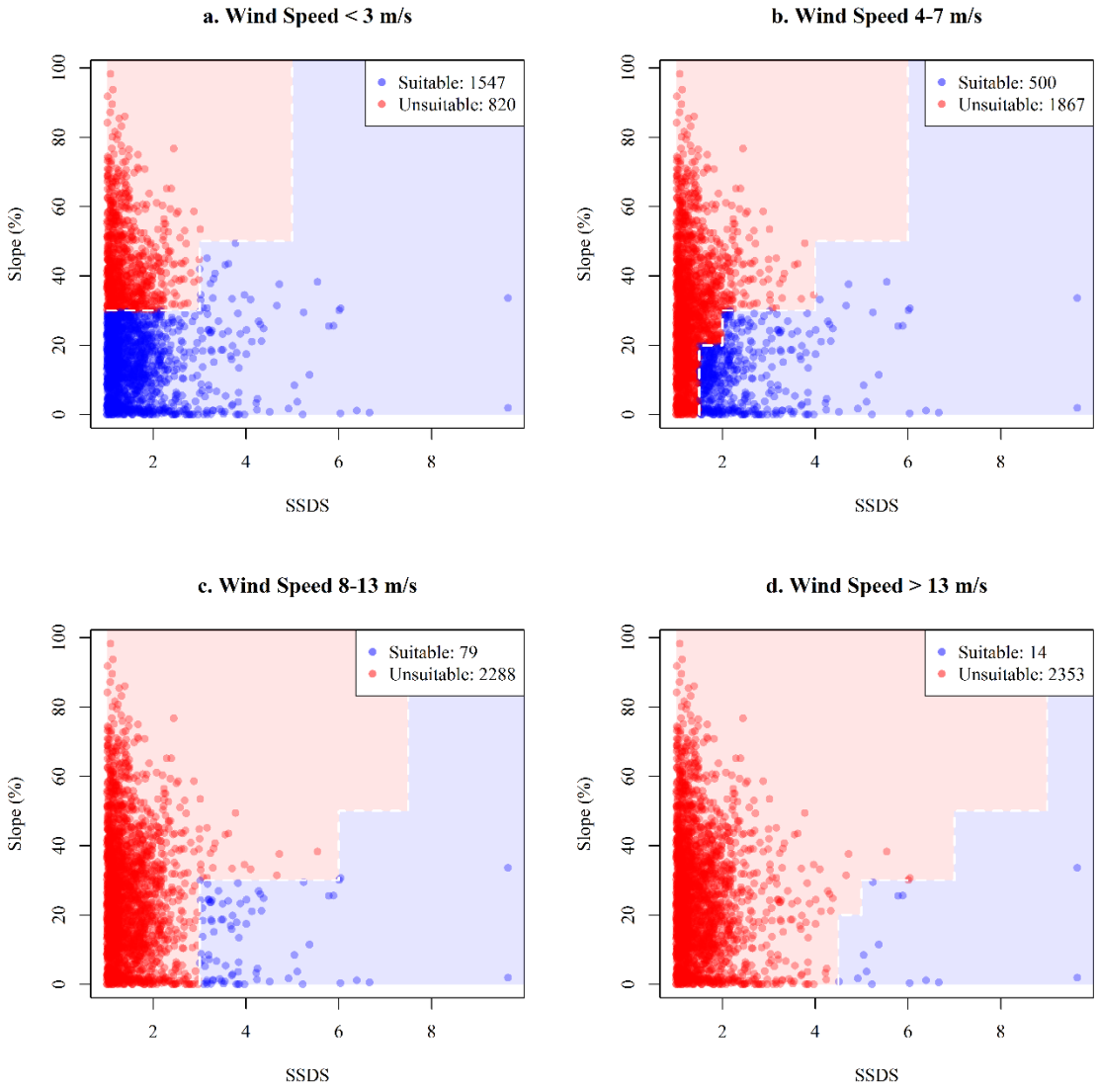

Figure 1.7. Scatterplots of safety zone SSDS values compared to slopes broken down by wind speed category. The blue and red regions represent areas of suitability and unsuitability, respectively, according to slope and wind conditions as defined by the slope-wind factor matrix (Table 1.1).

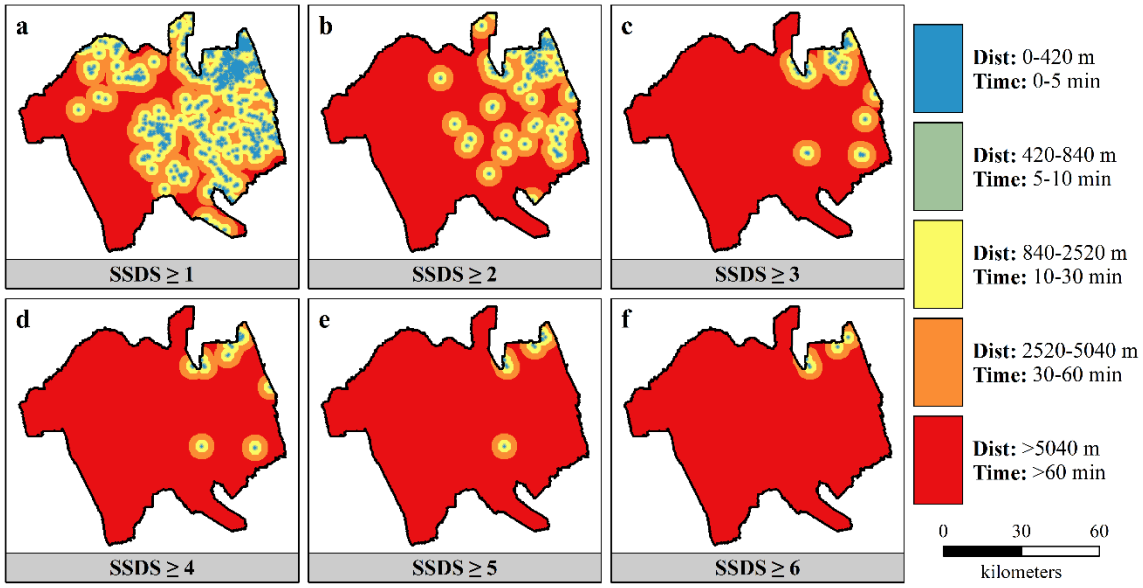

Figure 1.8. Euclidean distance and estimated travel time to nearest potential safety zone at a range of SSDS thresholds throughout the study area.

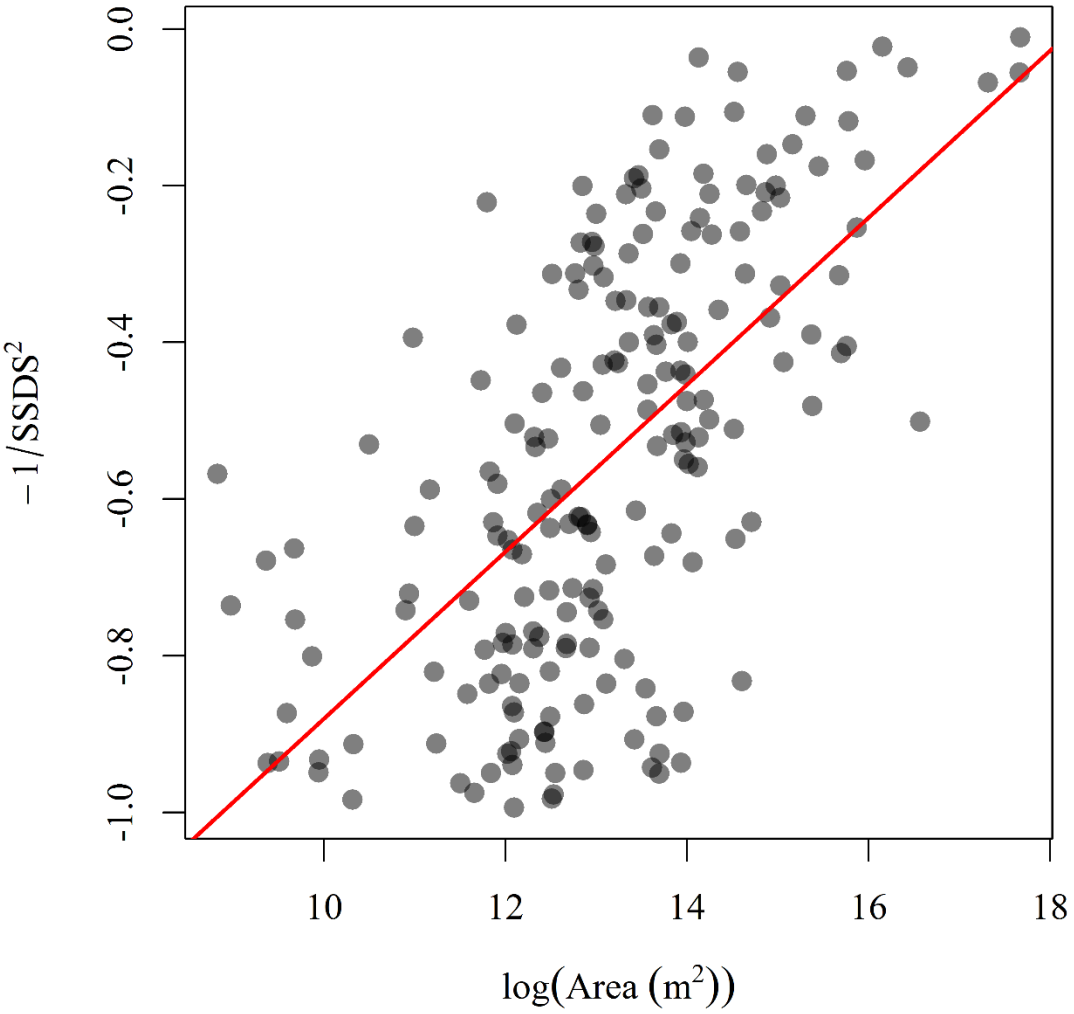

Figure 1.9. Linear regression between safety zone SSDS and clearing area in which the safety zone fell.

1.7 References

Andersen, H.-E., McGaughey, R.J., and Reutebuch, S.E., 2005. Estimating forest canopy fuel parameters using LIDAR data. *Remote Sensing of Environment*, 94, 441–449. doi:10.1016/j. rse.2004.10.013

Andrews, P.L., 2009. BehavePlus fire modeling system, version 5.0: variables. *General technical report RMRS-GTR-213WWW revised*. Department of Agriculture, Forest Service, Rocky Mountain Research Station, Fort Collins, CO.

Arizona State Forestry Division. *Yarnell hill fire: serious accident investigation report.* 23 September 2013 [online]. Available from: http://wildfiretoday.com/documents/Yarnell_Hill_Fire_report.pdf [Accessed 10 July 2016].

Bechtold, W.A., Zarnoch, S.J., and Burkman, W.G., 1998. Comparisons of modeled height predictions to ocular height estimates. *Southern Journal of Applied Forestry*, 22 (4), 216–221.

Beighley, M., 1995. Beyond the safety zone: creating a margin of safety. *Fire Management Notes*, 55 (4), 22–24.

Butler, B.W., et al., 1998. Fire behavior associated with the 1994 South Canyon fire on storm king mountain, CO. *USDA forest service research paper RMRSRP-9*. Rocky Mountain Research Station, Fort Collins, CO.

Butler, B.W., 2014. Wildland firefighter safety zones: a review of past science and summary of future needs. *International Journal of Wildland Fire*, 23, 295–308. doi:10.1071/WF13021

Butler, B.W., 2015. Firefighter safety zones [online]. *Fire, fuel, and smoke science program, USDA forest service rocky mountain research station*. Available from: http://www.firelab.org/project/ firefighter-safety-zones [Accessed 30 July 2016].

Butler, B.W. and Cohen, J.D., 1998a. Firefighter safety zones: a theoretical model based on radiative heating. *International Journal of Wildland Fire*, 8 (2), 73–77. doi:10.1071/WF9980073

Butler, B.W. and Cohen, J.D., 1998b. Firefighter safety zones: how big is big enough? *Fire Management Notes*, 58, 13–16.

Butler, B.W., Parsons, R., and Mell, W., 2015. *Recent findings relating to firefighter safety zones*. Missoula: U.S. Department of Agriculture, Forest Service, Rocky Mountain Research Station, 30–34.

Dennison, P.E., Fryer, G.K., and Cova, T.J., 2014. Identification of firefighter safety zones using lidar. *Environmental Modelling & Software*, 59, 91–97. doi:10.1016/j.envsoft.2014.05.017

Dubayah, R.O. and Drake, J.B., 2000. Lidar remote sensing for forestry. *Journal of Forestry*, 98 (6), 44–46.

Finney, M.A., et al., 2013. On the need for a theory of wildland fire spread. *International Journal of Wildland Fire*, 22, 25–36. doi:10.1071/WF11117

Finney, M.A., et al., 2015. Role of buoyant flame dynamics in wildfire spread. *Proceedings of the National Academy of Sciences*, 112 (32), 9833–9838. doi:10.1073/pnas.1504498112

Frankman, D., et al., 2013. Measurements of convective and radiative heating in wildland fires. *International Journal of Wildland Fire*, 22 (2), 157–167. doi:10.1071/WF11097

Gleason, P., 1991. LCES – a key to safety in the wildland fire environment. *Fire Management Notes*, 52 (4), 9.

Kraus, K. and Pfeifer, N., 2001. Advanced DTM generation from lidar data. *International Archives of Photogrammetry Remote Sensing and Spatial Information Sciences*, 34 (3/W4), 23–30.

LANDFIRE, 2012. Existing vegetation type layer, LANDFIRE 1.3.0 [online]. *US department of the interior, geological survey*. Available from: http://landfire.cr.usgs.gov/viewer/[Accessed 10 July 2016].

Lefsky, M.A., et al., 2002. Lidar remote sensing for ecosystem studies lidar, an emerging remote sensing technology that directly measures the three-dimensional distribution of plant canopies, can accurately estimate vegetation structural attributes and should be of particular interest to forest, landscape, and global ecologists. *BioScience*, 52 (1), 19–30.

Meng, X., Currit, N., and Zhao, K., 2010. Ground filtering algorithms for airborne lidar data: a review of critical issues. *Remote Sensing*, 2 (3), 833–860. doi:10.3390/rs2030833

National Fire Protection Agency, 2011. *Firewise communities: firefighter safety in the WUI [online]*. Available from: http://learningcenter.firewise.org/Firefighter-Safety/3-4.ph. [Accessed 4 January 2016].

National Interagency Fire Center, 2016. *Wildland fire fatalities by year [online]*. Available from: https://www.nifc.gov/safety/safety_documents/Fatalities-by-Year.pdf [Accessed 4 January 2016].

National Wildfire Coordinating Group, 2014. *Incident response pocket guide [online]*. Available from: http://www.nwcg.gov/sites/default/files/products/pms461.pdf [Accessed 4 January 2016].

National Wildfire Coordinating Group, 2016. *Glossary A-Z [online]*. Available from: http://www. nwcg.gov/glossary/a-z [Accessed 4 January 2016].

O'Connor, C.D., *et al.*, 2016. Getting ahead of the wildfire problem: quantifying and mapping management challenges and opportunities. *Geosciences*, 6 (35), 1–18. doi:10.3390/ geosciences6030035

Popescu, S.C., Wynne, R.H., and Nelson, R.F., 2002. Estimating plot-level tree heights with lidar: local filtering with a canopy-height based variable window size. *Computers and Electronics in Agriculture*, 37, 71–95. doi:10.1016/S0168-1699(02)00121-7

Reutebuch, S.E., et al., 2003. Accuracy of a high-resolution lidar terrain model under a conifer forest canopy. *Canadian Journal of Remote Sensing*, 29 (5), 527–535. doi:10.5589/m03-022

Roberts, D.A., et al., 2006. Evaluation of Airborne Visible/Infrared imaging Spectrometer (AVIRIS) and Moderate Resolution Imaging Spectrometer (MODIS) measures of live fuel moisture and fuel condition in a shrubland ecosystem in southern California. *Journal of Geophysical Research*, 111, 1–16. doi:10.1029/2005JG000113

Rollins, M.G., 2009. LANDFIRE: a nationally consistent vegetation, wildland fire, and fuel assessment. *International Journal of Wildland Fire*, 18 (3), 235–249. doi:10.1071/WF08088

Snyder, G.I., 2012. *The 3D elevation program: summary of program direction [online]*. US Department of the Interior, US Geological Survey. Available from: https://pubs.usgs.gov/fs/ 2012/3089/pdf/fs2012-3089.pdf [Accessed 14 December 2016].

Steele, J., 2000. Effective firefighter safety zone size: a perception of firefighter safety. *4th International wildland fire safety summit*, Edmonton, AB, CA: International Association of Wildland Fire, 171–177.

St-Onge, B., et al., 2008. Mapping canopy height using a combination of digital stereo-photogrammetry and lidar. *International Journal of Remote Sensing*, 29 (11), 3343–3364. doi:10.1080/ 01431160701469040

Tobler, W., 1993. *Three presentations on geographical analysis and modeling, Technical Report 93-1*. Santa Barbara: National Center for Geographic Information and Analysis, University of California.

United National Office for the Coordination of Humanitarian Affairs. *Israel Carmel fire situation report #2.* 6 December 2010 [online]. Available from: http://reliefweb.int/sites/reliefweb.int/files/ resources/DD3E82B287DB17CD852577F1006E883B-Full_Report.pdf [Accessed 10 July 2016].

Wang, L., Gong, P., and Biging, G.S., 2004. Individual tree-crown delineation and treetop detection in high-spatial-resolution aerial imagery. *Photogrammetric Engineering & Remote Sensing*, 70 (3), 351–357. doi:10.14358/PERS.70.3.351

Zarate, L., Arnaldos, J., and Casal, J., 2008. Establishing safety distances for wildland fires. *Fire Safety Journal*, 43 (8), 565–575. doi:10.1016/j.firesaf.2008.01.001

CHAPTER 2[2]

A LIDAR-BASED ANALYSIS OF THE EFFECTS OF SLOPE, VEGETATION DENSITY, AND GROUND SURFACE ROUGHNESS ON TRAVEL RATES FOR WILDLAND FIREFIGHTER ESCAPE ROUTE MAPPING

2.1 Abstract

Escape routes are essential components of wildland firefighter safety, providing pre-defined pathways to a safety zone. Among the many factors that affect travel rates along an escape route, landscape conditions such as slope, low-lying vegetation density, and ground surface roughness are particularly influential, and can be measured using airborne light detection and ranging (LiDAR) data. In order to develop a robust, quantitative understanding of the effects of these landscape conditions on travel rates, we performed an experiment wherein study participants were timed while walking along a series of transects within a study area dominated by grasses, sagebrush and juniper. We compared resultant travel rates to LiDAR-derived estimates of slope, vegetation density and ground surface roughness using linear mixed effects modeling to quantify the relationships between these landscape conditions and travel rates. The best-fit model

[2] Reprinted with permission from Campbell, M.C., Dennison, P.E., Butler, B.W., 2017. A LiDAR-based analysis of the effects of slope, vegetation density, and ground surface roughness on travel rates for wildland firefighter escape route mapping. International Journal of Wildland Fire 26, 884-895.

revealed significant negative relationships between travel rates and each of the three landscape conditions, suggesting that, in order of decreasing magnitude, as density, slope and roughness increase, travel rates decrease. Model coefficients were used to map travel impedance within the study area using LiDAR data, which enabled mapping the most efficient routes from fire crew locations to safety zones and provided an estimate of travel time.

2.2 Introduction

Wildland firefighter escape routes are pre-planned routes firefighters take to move to a safety zone or other low-risk area (National Wildfire Coordinating Group 2016). Escape routes are an essential component of the Lookouts, Communications, Escape Routes, and Safety Zones (LCES) system and 10 standard firefighting orders for firefighter safety planning (Gleason 1991; Ziegler 2007). They should be established in advance of firefighting, known to all members of a fire crew, and re-evaluated as conditions change throughout the day (National Fire Protection Association 2011). The goal in selecting escape routes is to determine the path of least resistance and lowest risk between fire crew location and safety zone. To maintain a margin of safety (Beighley 1995), firefighters must have a keen awareness of both fire behaviour and their own ability to traverse a given landscape. There is an extensive body of literature and several well established tools for modeling fire behaviour (e.g. Andrews 2014; Finney 2006, 2004), and some data on fire crew physiological performance (Ruby *et al.* 2003). However, few studies have explored the interaction between landscape conditions and escape-route travel.

.

There are several landscape conditions that can affect travel rate in a wildland environment, including terrain slope (henceforth, ‘slope’), low-lying vegetation density (‘density’) and ground surface roughness (‘roughness’). Of these factors, slope has been the most extensively studied for its effects on travel rate. Butler *et al.* (2000) examined the effects of slope on travel rate using data from two fires with significant firefighter fatalities, South Canyon and Mann Gulch. Alexander *et al.* (2005) performed experiments with Alberta firefighters to determine the effects of not only slope, but also vegetation type, load carriage and trail improvement on travel rates. Tobler’s Hiking Function (THF) is an empirically derived model for estimating travel rates based on slope Tobler (1993) that has been widely used in a variety of contexts, including urban evacuation modeling (Wood and Schmidtlein 2012), outdoor recreation planning (Pettebone *et al.* 2009) and historical migration simulation (Kantner 2004), but has rarely been applied to the wildland firefighting environment, one exception being (Fryer *et al.* 2013). Another common slope-travel rate function is Naismith’s Rule, developed in 1892 by Scottish mountaineer William Naismith, which states that hiking 1 flat mile (~1600 m) should take 20 min with an additional 30 min for every 1000 feet (~300 m) of elevation gain, though it does not account for downhill travel (Norman 2004). More recently, Davey *et al.* (1994) derived a function based on a series of treadmill experiments that predicts sustainable uphill travel rates over long distances based on a baseline travel rate on flat slopes. Though mathematically similar to Naismith’s Rule and THF, the function of Davey *et al.* (1994) provides a flexible framework for adjusting to individual-level fitness. Studies that have quantified slope effects on travel rate universally demonstrate that travelling up and down steep slopes reduces travel rate. However, methodological

.

differences make it difficult to compare experimental data relevant to firefighter evacuation (e.g. Alexander *et al.* 2005) to models like THF, Naismith's Rule and Davey *et al.* (1994). Given the importance of slope as a predictor of travel rate, and the importance of travel rate on the effectiveness of escape routes, continued study is essential.

Few studies have examined the effects of vegetation and ground surface conditions on travel rates. Alexander *et al.* (2005) compared experimentally derived travel rates to a range of vegetation types, as categorised by Canadian Fire Behavior Prediction fuel type. Taller, denser spruce (*Picea* spp.) and lodgepole pine (*Pinus contorta*) fuel types resulted in slower travel rates than shorter, less dense grass and slash fuel types. Anguelova *et al.* (2010) modelled pedestrian evacuation due to a wildfire using a qualitative, heuristic approach to characterise the effects of common vegetation types in Southern California on relative travel rates. However, the use of categorical fuel and vegetation types in these studies limits applying these relationships on a broad scale. No studies to date have explored the effects of roughness on escape route travel explicitly, but research in the field of applied physiology has produced relevant results. The Pandolf equation is a function for estimating the metabolic cost of travelling across various types of terrain and land cover, using a variety of 'terrain factors' first introduced by Soule and Goldman (1972), which are categorical multiplicative factors used for estimating energy expenditure including blacktop road (1.0), dirt road (1.1), light brush (1.2), heavy brush (1.5), loose sand (2.1) and soft snow (2.5) (Pandolf *et al.* 1977). Schmidtlein and Wood (2015) used these terrain coefficients to model evacuation times in the event of a tsunami, but point out how their categorical nature does not easily

.

translate to more commonly used measures of land cover and highlight the importance of continued study to determine the degree to which such coefficients match reality.

Two fatality events, the 1994 South Canyon fire and the 2013 Yarnell Hill fire, highlight the critical effect that slope, density and roughness can have on travel rates. On the South Canyon fire, firefighters perished when trying to outrun flames up rocky slopes as steep as 55% (298) in an area dominated by dense Gambel oak and pinyon–juniper woodlands (Butler *et al.* 2000). On the Yarnell Hill fire, firefighters were entrapped as they travelled along an escape route through terrain characterised by boulders and covered with thick chaparral brush (Arizona State Forestry Division 2013).

To maximise the effectiveness of escape routes, we need to deepen our understanding of how slope, density and roughness affect travel rate in a precise, quantitative manner. These three landscape conditions can all be readily modelled using airborne light detection and ranging (LiDAR) data. LiDAR is a type of active remote sensing system in which pulses of laser light are emitted from an airborne platform towards the earth's surface and reflected back to the sensor, the timing of which enables the precise measurement of three-dimensional ground and aboveground structure (Lefsky *et al.* 2002). Airborne LiDAR has been used extensively for mapping terrain (e.g. Kraus and Pfeifer 2001; Reutebuch *et al.* 2003), vegetation structure (e.g. Bradbury *et al.* 2005; Hudak *et al.* 2008) and roughness (e.g. Glenn *et al.* 2006; Sankey *et al.* 2010). As such, the use of LiDAR has great potential for mapping escape routes. However, in the absence of a complete understanding of how these landscape conditions affect travel, the effectiveness of such an approach is limited. Accordingly, the objectives of this study are to: (1) perform an experiment to test the effects of slope, density and roughness on travel

.

rates, and (2) use the resulting data to develop a LiDAR-based geospatial model for optimising firefighter escape routes and estimating travel time to safety on a spatial scale most useful for wildland firefighting operations.

2.3 Methods

For this study, an airborne LiDAR dataset spanning Utah's Wasatch Front was obtained from the OpenTopography LiDAR data portal (opentopography.org). The data were acquired by Watershed Sciences, Inc. on behalf of the State of Utah between October 2013 and May 2014 and have an average point density of 11.93 points m^{-2}. The data are reported to have a respective average vertical accuracy of 2.43, 3.68 and 5.41 cm in hard surface, shrub and forested areas. A subset of the broader Wasatch Front dataset within Levan Wildland Management Area (39°35'15"N, 111°49'56"W) was chosen as the study area based on diversity of topography and vegetation, public land ownership, and road accessibility (Fig. 2.1). Elevations range between 1650 and 1775 m with dominant vegetation types of Utah juniper (*Juniperus osteosperma*) woodlands, big sagebrush (*Artemisia tridentata*) shrublands and mixed perennial grasslands.

To test the effects of slope, density and roughness on travel rates, an experiment was conducted in which volunteer study participants were timed as they walked a series of linear transects. Twenty-two 100-m transects were placed to capture a range of vegetation and topographic conditions (Fig. 2.1). They were selected from a randomly generated set of transects to minimise within- and maximise between-transect landscape condition variability. Transects were established in the field using a Trimble Geo 7X GPS (Trimble, Inc., Sunnyvale, CA, USA, www.trimble.com/Survey/Trimble-Geo-7x.aspx, accessed 13 September 2017) with ≥200 point averaging for transect start and end points

.

and a Laser Technology TruPulse 360 rangefinder (Laser Technology, Inc., Centennial, CO, USA, www.lasertech.com, accessed 13 September 2017) for azimuth and distance measurements. Sign posts were placed at each transect start and end, and coloured flagging was placed in between at intervals of 5–10 m, depending on visibility.

There were 31 study participants, none of whom had previously worked as firefighters (Table 2.1). Participants were partnered together and each individual walked the transects twice, once in each direction, and timed themselves as they walked, from which travel rates were computed. Participants walked the numbered transects in sequential order, but to avoid the potentially confounding effects of fatigue, partner groups were each assigned different starting transects. The experiment took place over 2 days, each lasting ~6 h, with a 30-min lunch break in the middle of the day. Participants were additionally allowed to rest while their partner was walking the transect. Given that individuals have different average walking rates (e.g. because of different fitness levels, heights, weights, gaits), participants were asked to maintain a consistent level of effort when walking each transect. Additionally, participants were asked to stay as close to the flagged transect centerline as possible except when it intersected impassable vegetation, in which case participants were permitted to walk around obstacles.

Travel rates were compared with LiDAR-derived estimates of slope, roughness and density. These metrics were generated for each transect using a combination of *LAStools* LiDAR processing software (radpidlasso GmbH, Gilching, Germany, www.rapidlasso.com), ESRI *ArcGIS* geospatial software (ESRI Inc., Redlands, CA, USA, www.esri.com, accessed 13 September 2017), and *R* statistical software (R Core Team, Vienna, Austria, www.r-project.org, accessed 13 September 2017). LiDAR data

.

were first classified into ‘ground’ and ‘non-ground’ points, using the *lasground* algorithm (Isenburg 2015). Several iterative classifications were performed, adjusting algorithm parameters as needed until the classification was deemed satisfactory according to a careful visual interpretation and comparison of the resulting classified LiDAR point cloud to high-resolution aerial imagery. Although no field validation was performed to obtain a quantitative, point-level accuracy assessment, it is likely that misclassifications between very low-lying non-ground points and ground points occurred. Slope was calculated by first creating a digital terrain model (DTM) at a spatial resolution of 1 m using the *las2dem* algorithm. For each transect (*t*), average slope (*s*) was then computed in degrees according to the difference in elevation in metres (*e*) at the start (*a*) and end (*b*) of each transect and the horizontal distance in metres (*h*) between *a* and *b*, such that:

$$s_t = \tan\left(\frac{e_b - e_a}{h}\right) \quad (2.1)$$

Roughness was calculated following an approach similar to that of Glenn *et al.* (2006) as the difference between a fine-scale DTM (0.25-m spatial resolution) and a ‘smoothed’ DTM (also 0.25 m) generated by calculating a focal mean of elevation values within a 2.5-m-radius circular kernel. The resulting raster dataset contained pixel values representing local deviations (e.g. bumps, pits) from the broader topography (Fig. 2.2). Linear transects were buffered by 5 m and the absolute values of the roughness raster data were averaged within each buffer to obtain a transect-level roughness in metres.

As vegetation density in different portions of the vertical canopy profile will have different effects on travel rates, it was first necessary to determine a suitable range of aboveground heights that would most directly affect travel. For example, very dense

.

vegetation in a very high or very low height stratum will likely have little effect on travel rates, as one could readily traverse under or over the vegetation unimpeded. LiDAR point clouds can be used to estimate vegetation density in distinct height strata by calculating normalised relative point density (NRD). NRD is a calculation of the relative proportion of point returns that fall within a given height range as compared with the total number of points that fall within and below that height range, such that:

$$NRD_{ij} = \frac{\sum_i^j n}{\sum_0^j n} \tag{2.2}$$

where *n* is the number of LiDAR point returns, *i* is the floor (low value) of the height range and *j* is the ceiling (high value) of the height range (USDA Forest Service 2014). To calculate NRD, aboveground height for each non-ground LiDAR point was first calculated using the *lasheight* algorithm, which uses the ground points to generate a triangulated irregular network (TIN) representing the ground surface, and then computes the height of each non-ground point above the TIN surface. Transects were buffered by 5 m, and the point cloud was extracted within the buffer area. Eqn 2.2 was then used to calculate a single NRD value for the entire transect. Fig. 2.3 depicts an example height range along a 100-m transect, where i = 0.15 m and j = 2.75 m. NRD values range from 0 to 1, with 1 being indicative of very dense vegetation in a given height range and 0 representing very little or no vegetation.

In order to determine the height range that had the most significant effect on travel rates, a series of linear mixed effects regression (LMER) analyses were performed. As stated earlier, some study participants consistently walk faster than others regardless of landscape conditions, and, although this is potentially useful information, of primary

.

interest are the relative effects (i.e. how much does vegetation density reduce travel rate independent of individual performance?). LMER modeling fits a series of models with variable (or, 'random') y-intercepts, providing an account of the fixed effects (the underlying trend) and the random effects (variability caused by individuals).

Two different LMER analyses were run using travel rate as the dependent variable. The first LMER analysis was designed to determine optimal NRD height range that best predicted travel rates. In order to minimise the confounding effects of slope, only data from transects with slopes of less than 58 (n = 16) were used in this analysis. For every possible contiguous height range between 0 and 5 m, at intervals of 5 cm, a LMER model was generated in *R* using the *lme4* package (Bates *et al.* 2014) to test the predictive power of NRD on travel rates and assessed for model fit. Models were assessed for fit using Nakagawa and Schielzeth (2013)'s measures for marginal and conditional R^2 (henceforth R^2_m and R^2_c), representing variance explained by the fixed effects and the variance explained by both the fixed and random effects respectively as implemented in *R* using the *MuMIn* package (Bartoń 2016). NRD for the height range that was able to best predict travel rates was selected for further use throughout the study as a representation of density. The second LMER analysis assessed the combined effects of slope, density, and roughness on travel rates, again accounting for variability individuals' travel rates. The best-fit fixed effects LMER model took the form:

$$travel\ rate = \alpha + \beta_1 density + \beta_2 roughness + \beta_3 slope + \beta_4 slope^2 \quad (2.3)$$

where α is the y-intercept, representing travel rate for zero density, roughness and slope, and β are multiplicative model coefficients, representing relative effects of the landscape variables on travel rates. In order to use these travel impedance model coefficients

.

derived from transect-level experimentation in a landscape-level geospatial model for escape route optimisation, each of the three landscape variables was computed on a per-pixel basis across the entire study area at a 5-m spatial resolution. Rasterised landscape variables were then multiplied by their model coefficients to derive travel impedance raster data throughout the study area. A route optimisation analysis was then performed in *R* using the *raster* and *gdistance* packages (Hijmans and van Etten 2014; van Etten 2012). The *gdistance* package uses transition matrices to calculate the relative resistance of moving between eight directionally adjacent cells in a raster dataset. For each of the landscape conditions of interest, a transition matrix was generated such that for each cell, a travel cost (s) was computed for travelling to each of its adjacent cells, according to the LMER model coefficients (β_1, β_2, β_3 and β_4 above). The transition matrices were combined to enable an analysis of travel time for travelling between any two locations throughout the study area. Lastly, a series of simulations were performed to create escape routes between simulated fire crew and safety zone locations. Each route was generated automatically to identify the fastest route to safety, according to the combined transition matrix, using Dijkstra's algorithm (Dijkstra 1959). Dijkstra's algorithm computes the relative travel impedance of all possible routes from origin to destination based on a defined set of nodes (raster cells) and paths between them (connections between adjacent cells) and identifies the single, most efficient path.

2.4 Results

Fig. 2.4 depicts the three landscape parameters of interest (slope, density, and roughness) throughout the study area with the 22 transects overlaid to highlight the range of conditions captured in the experiment. Slopes ranged from 0 to 39.48°, density (0.15–

.

2.75 m) ranged from 0 to 100%, and roughness ranged from 0 to 0.4 m. The majority of the juniper woodlands were found on steeper slopes at higher elevations, with sagebrush and grasslands dominating the lower-slope, lower-elevation terrain. In general, juniper woodlands tended to have the highest vegetation density, though a few of the sagebrush-dominant transects had higher vegetation densities (e.g. transects 15 and 16, Table 2.2). Roughness values were highest on steeper slopes and in dry streambeds, where erosional and depositional processes have created rocky ground surfaces.

In all, there were 1276 timed walks, with 10 subjects walking 22 transects, 19 subjects walking 20 transects, and two subjects walking 19 transects, all in both transect directions. All resultant travel rates were used in the subsequent analyses, with no outlier removal. The results of the first LMER analysis to determine the NRD height range that best predicted experimentally derived travel rates on slopes <5°, as approximated by R^2_m, can be seen in Fig. 2.5 and Table 2.3. Those height ranges with floors of 2 m or higher (e.g. 2–3 m, 3–4 m) had very little predictive power, higher (e.g. 2–3 m, 3–4 m) had very little predictive power, indicating that vegetation solely above the heads of study participants (average height 1.76 m) had little effect on travel rates. Conversely, those ranges with ceilings below 1 m (e.g. 0–0.5 m, 0–1 m) have low predictive power as well, suggesting that low-lying density alone does not account for much of the variability in travel rates. Consistently, the height ranges with floors between 0 and 0.5 m and ceilings between 2 and 4 m tend to be the best predictors of travel rates. Although several similar height ranges resulted in similarly high predictive power (Table 2.3), the single best height range of prediction was 0.15–2.75 m, with an R^2_m of 0.54 and R^2_c of 0.84 (Fig. 2.5). This range was used throughout the remaining analyses.

.

Fig. 2.6 highlights the fairly wide dispersal of travel rate values at each transect, as represented by the spread in the *y* direction at each *x* location. This spread represents the tendency for some individuals to travel faster than others regardless of landscape conditions, and was accounted for by using LMER.

The second LMER analysis to determine the combined effects of slope, density, and roughness on travel rates took the following form ($R^2_m = 0.59$; $R^2_c = 0.82$):

$$travel\ rate = 1.662 - 1.076 \times density - 9.011 \times roughness - (5.191 \times 10^{-3}) \times slope - (1.127 \times 10^{-3}) \times slope^2 \quad (2.4)$$

Each of the landscape parameters had a significant ($P < 0.001$) negative effect on travel rates, suggesting that as slope, density and roughness increase, travel rates decrease (Table 2.4). Fig. 2.7 provides a visualisation of the fixed and random effects of each landscape parameter. In order to display these relationships in two dimensions, for each landscape parameter (e.g. slope), the other two (e.g. density and roughness) were assumed to be the median value of those parameters among all of the transects. As can be seen from the magnitude of the standardised model coefficients ($\beta_{standardised}$, Table 2.4), and an analysis of variable-specific partial R^2_m, density had the greatest effect on travel rates, followed by slope and roughness.

Using the model coefficients from Table 2.4, Dijkstra's algorithm (Dijkstra 1959), as implemented in the *R gdistance* package (van Etten 2012) was performed to generate a series of simulated least-cost escape routes throughout the study area. Example resulting escape routes in Fig. 2.8 highlight the anisotropic effects of slope across this landscape, where the least-cost route from *a* to *b* differs from that of the reverse direction. Whereas the least-cost routes are actually longer than the straight-line distance between these two

.

points, the travel time along the optimised routes were lower than the straight-line routes (Table 2.5). Similarly, whereas the *b* to *a* route was longer than the *a* to *b* route, the travel time from *b* to *a* is shorter.

A series of 1000 escape-route simulations was performed between randomly generated location pairs to illustrate the effects of landscape parameters on route designation (Fig. 2.9). Slope has a major effect on route placement, given the greater amount of route overlap in areas where slopes are low and the sparseness in steep areas. Density is more locally variable on the landscape, allowing for least-cost paths to traverse small avenues of comparably low density within broader swaths of dense vegetation. Roughness is inconsistently distributed throughout the study area, with sparse pockets of high roughness typically found in drainage channels bearing little apparent effect on the placement of escape routes. The straight north–south line with a high degree of escape route overlap that appears in the western portion of the study area is a road, highlighting the model's implicit bias towards low-slope, low-density and smooth surfaces.

2.5 Discussion

This study examined the effects of slope, density and roughness on travel rates in order to develop a geospatial model for wildland firefighter escape route optimisation. It represents a valuable contribution to the existing body of research surrounding the effects of slope on travel rates, and a novel attempt at quantifying the effects of density and roughness. At present, escape routes are designated by firefighting personnel based on the recommendations of the National Wildfire Coordinating Group's Incident Response Pocket Guide, which suggest avoiding steep uphill escape routes, and scouting for loose soils, rocks, and vegetation (National Wildfire Coordinating Group 2014). Although

.

these are important recommendations, the language is inherently subjective (e.g. ‘steep’, ‘loose’), which can result in judgment error. This study introduces a standardised method for quantifying these variables and providing an experimentally derived account of their effects on travel. It also provides a framework for mapping travel rates across large areas, something that has not previously been possible. Provided that there are LiDAR data available within a given area, the resulting geospatial escape route optimisation model can be used as a decision support tool, providing fire crew members with objective insight to aid in the identification of efficient escape routes.

An important finding from this study was the determination of the aboveground density height range that most directly affected travel rates (0.15–2.75 m). The range floor (0.15 m) demonstrates that vegetation shorter than 15 cm in stature will most likely have little or no effect on one’s ability to traverse a given landscape. The range ceiling, however, is nearly a metre taller than the mean height of study participants (1.76 m). Although we did not collected GPS data to track individual movement, anecdotal evidence gleaned from experimental observation suggested obstacle avoidance, rather than passage through obstacles, was a primary cause of travel rate reduction. Given the subjectivity associated with obstacle avoidance and individual route selection, it is possible that study participants tended to avoid vegetation slightly overhead based on perception of travel efficiency, even if passage under said vegetation would not greatly impede travel. It is also possible that the specific vegetation types found within the study area are partly responsible for the modelled importance of overhead vegetation. Particularly in the case of Utah juniper, the densest portion of the canopy lies between ~2 and 4 m in height (Fig. 2.10). It is likely that density in these higher portions of the

.

canopy are highly correlated with density in the lower portions of the canopy as well. In other words, dense vegetation lying above the heads of study participants, although not directly affecting travel, likely indicates similarly dense vegetation at height ranges that do directly affect travel.

Although the 0.15–2.75-m height range was identified as the best range for predicting travel rates, as Table 2.3 highlights, there are several very similar ranges that possess similar predictive power. When combined with the inherent error in the ground point classification process and subtle LiDAR vertical inaccuracies, we can more broadly state that vegetation that generally occupies the same vertical space as a human (e.g. 0–3 m) most directly impedes travel.

This study has several assumptions and limitations that warrant further discussion. Perhaps the most important limitation is that the experiments were performed with non-firefighting personnel and without typical firefighting gear. That said, the test population was not entirely dissimilar to the firefighting community, demographically. According to the National Wildland Firefighter Workforce Assessment, almost 50% of aid- and tech-level USDA Forest Service firefighting personnel were between the ages of 26 and 35, as compared with the mean age of our study participants, which was 27 (USDA Forest Service 2010). Additionally, given the physical demands of the firefighting profession, firefighters tend to be of a high fitness level. By comparison, the study population was of generally above-average fitness, exercising a self-reported average of 7 h per week. One key difference is that this study population had a relatively large female population as compared with that of the firefighting community (39 v. 16% in the USDA Forest Service; USDA Forest Service 2010).

.

Regardless of the specific sample population used to derive the relative effects of landscape conditions, estimating travel rates should be done with great caution, particularly when simulating escape routes travel in a potentially dangerous wildfire environment. The most valuable contribution of this study is the analysis of relative effects of landscape conditions on travel rates, which are more robust to slight differences in individuals' heights, weights and fitness levels. Our data confirm this robustness, with an R^2_c value of 0.82, which suggests that when accounting for the small differences in individual travel rate biases, 82% of the variance in overall travel rate is explained by slope, density, and roughness. The resulting model enables the automated generation of the fastest route to safety, irrespective of specific resulting travel rates and times.

It is worth noting that study participants walked, rather than ran, the transects. If subjects were asked to run the transects, the resulting between-subject variability would make a robust analysis much more difficult. Additionally, the effects of fatigue between running the first and last of 22 transects would be more pronounced than those of walking, making the within-subject variability problematic for modeling purposes. Although one might typically associate escape routes being a measure of last resort, the ideal escape route evacuation scenario is one in which a fire crew proceeds along an escape route in line at a controlled, walking pace. Although subjects were asked to maintain a consistent level of effort while walking transects, there remained a level of uncertainty in the computation of relative travel impedance due to a lack of quantitative control for energy expenditure levels. To further refine the relationship between landscape conditions and travel rates would require the collection of more robust measures of physical exertion, such as oxygen consumption rates, which was beyond the

.

scope of our analysis. In addition, having subjects walk the same transects several times could have provided an estimate of uncertainty; however, given experimental time constraints, this would have limited the total number of transects and, by proxy, the range of landscape conditions tested. Fig. 2.11 in the Supplementary material provides a graphical depiction of the relative consistency of travel rates, according to how each study participant's travel rates ranked among all participants for each transect.

Another limitation of this study is the limited range of landscape conditions sampled throughout the 22 transects. Although a wide range of conditions was captured, obtaining an exhaustive sample was impossible given the practical constraints of testing human subjects. This is particularly true of slope, where our maximum sampled slope was ~15°. As a result, we must extrapolate the effects on travel rates of slopes steeper than 15°, which may in reality take a different form than our proposed model. For example, THF, Naismith's Rule and Davey *et al.* (1994)'s function all flatten out towards the 'tails' on very steep slopes, but never quite reach a travel rate of zero, whereas our model calculates a travel rate of zero above slopes of ~36° and below slopes of ~-40° (Fig. 2.12). The model fit presented in Fig. 2.12 represents the effects of slope assuming zero density and roughness. As Fig. 2.12 depicts, the effects of slope as determined in our model are less pronounced than the other three models, likely due to differences in methodology. Whereas our study provides an account of the effects of slope over relatively short distances in wildland environments (100 m), the other three are based on long distance hiking on improved trails or treadmills.

The strength of the approach taken in this study lies in the broad applicability of LiDAR metrics tested. Regardless of geography, the quantitative measures that were

.

computed from LiDAR data can be calculated in any environment. However, airborne LiDAR pulse density and overstorey vegetation conditions can have significant effects on the precision with which these measures are computed. The calculation of slope is fairly robust to these limitations, given the coarse scale of analysis. However, accurate estimation of understorey vegetation density and roughness relies on a sufficient amount of LiDAR pulse energy reaching the understorey and ground surface, requiring a balance between LiDAR pulse density and overstorey vegetation density. Though no sensitivity tests were performed to determine the effect of pulse density or overstorey conditions on characterising landscape conditions, it is likely that lower pulse densities or denser upper vegetation canopies than those in our study would reduce the effectiveness of our approach. The very nature of the roughness calculation we performed relies on assessing the difference between microtopography and macrotopography. As ground point densities decrease, those two measures begin to converge, reducing the ability to characterise small perturbations in the ground surface. Similarly, the understorey vegetation density calculation assumes that LiDAR pulse spacing will be sufficiently dense, so as to enable interaction with multiple features within the vertical canopy profile. With a much lower pulse density, deciphering between those points that reflect off of the top of the canopy and the middle of the canopy becomes much more difficult. Vegetation density, in particular, would also be difficult to characterise in vegetation types with very dense upper canopies, where relatively little airborne LiDAR pulse energy can reach the understorey. However, particularly in the fire-prone coniferous forests throughout the western United States, with comparably permeable upper canopies, this method should translate well.

.

A key assumption made in the development of this methodology is that the fastest route to safety is always the best route to safety, when in reality, this may not be the case. There are two key variables not assessed in our model: (1) road or trail access and (2) the location of the wildland fire. As Alexander *et al.* (2005) revealed, travelling along improved trails (flagged, cleared of brush) significantly reduced travel time along an escape route. Although this is implicitly accounted for in our model (presumably roads or trails have lower slope, density and roughness than off-trail areas), it is not explicitly built into the model. In a wildland firefighting environment, where high winds and smoke can greatly reduce visibility, travelling along a clearly defined road or trail could prove to be highly advantageous, even if slower than the 'optimal' route. That being said, by using a GPS and flagging the route identified by our algorithm, firefighters could reduce travel time by a potentially critical amount. Second, this model makes no attempt to characterise fire behaviour or identify current fire location. As such, it is conceivable that the fire would spread in a direction that would render the escape routes unsuitable or even fatal, as in the case of the Yarnell Hill fire in 2013. To address these points, future work could include model refinement to include an optional bias towards roads or trails and incorporation of fire location or a fire behaviour model, such as was done by Fryer *et al.* (2013) and Anguelova *et al.* (2010), to bias the model away from potentially dangerous routes.

2.6 Conclusions

The infusion of high resolution-high precision geospatial data, such as airborne LiDAR, into fire safety planning has the potential to greatly improve the consistency, reliability and efficiency of designating escape routes. However, escape routes are merely

.

one component of the LCES system and must be connected to a safety zone or other low-risk area. As such, this research compliments recent work by Dennison *et al.* (2014) and Campbell *et al.* (2017), who have demonstrated methods for taking advantage of the advanced capabilities of LiDAR for safety zone identification and evaluation. Taken together, these methodologies can eliminate much of the potential for costly errors in the decision-making process when implementing LCES.

This study provides several important fire safety management implications:

- When designating escape routes, every attempt should be made to avoid steep slopes, dense vegetation, and rough ground surfaces.
- The use of airborne LiDAR to precisely quantify these landscape conditions can help select the most efficient escape routes.
- Mean walking travel rate on flat slopes, with minimal vegetation and ground surface roughness was 1.66 ms^{-1}.
- Travelling up slopes of 5, 10 and 15° reduced the travel rate by 3, 10 and 20% respectively.
- Travelling down slopes of 5, 10 and 15° reduced the travel rate by 0, 4 and 11% respectively.
- Travelling through dense juniper (NRD = 0.33) and dense sagebrush (NRD = 0.35) reduced the travel rate by 22 and 23% respectively.
- Travelling along rough ground surfaces (roughness = 3.57 x 10^{-2} m) reduced the travel rate by 19%.

Particularly in light of the push to collect nationwide LiDAR data throughout the United States within a decade as part of the USGS 3D Elevation Program (Snyder 2012),

.

methods such as those presented in this study have the potential to enhance wildland firefighting safety. More work is certainly needed to validate and refine the results obtained in our experiments, and to test the additional effects of carrying packs, increased travel distance, and other external conditions such as temperature and humidity on firefighter travel rates, but this study represents a novel contribution in a direction that, as yet, has remained largely unexplored in the scientific and applied literature.

2.7 Acknowledgements

Funding for this research was provided by the USDA Forest Service National Fire Plan through the Office of Research, the National Wildfire Coordinating Group Fire Behavior Subcommittee, and the Wildland Fire Management Research Development and Application Program, Cooperative Agreements 14JV11221637123 and 15CR11221637105. We owe a great debt of gratitude to the volunteer study participants whose efforts enabled the success of the field experiment and to Dr. Andrea Brunelle for her assistance in recruiting.

.

Table 2.1. Study participant summary.

	n	Mean age (years)	Mean height (m)	Mean weight (kg)	Mean exercise (h week^{-1})
All subjects	31	26.97	1.76	73.22	7.00
Male	19	26.11	1.81	81.65	7.78
Female	12	28.33	1.67	59.87	5.83

.

Table 2.2. Transect landscape parameter mean values.

Transect	Length (m)	Slope (°)	Density (%)	Roughness (m)
1	99.77	3.04	33.24	2.02×10^{-2}
2	99.96	3.55	25.17	1.91×10^{-2}
3	99.77	3.52	31.50	1.81×10^{-2}
4	99.80	3.71	16.83	1.78×10^{-2}
5	100.04	1.74	9.76	2.06×10^{-2}
6	100.07	3.29	3.57	2.18×10^{-2}
7	100.01	0.09	1.86	2.47×10^{-2}
8	100.20	15.23	4.75	2.61×10^{-2}
9	102.49	13.22	9.35	3.57×10^{-2}
10	99.70	14.61	17.87	2.16×10^{-2}
11	100.77	14.02	16.72	2.46×10^{-2}
12	99.97	2.60	4.08	1.64×10^{-2}
13	99.69	3.15	13.27	1.76×10^{-2}
14	99.99	2.07	19.94	1.97×10^{-2}
15	100.31	2.96	34.17	2.25×10^{-2}
16	100.48	2.16	34.65	1.89×10^{-2}
17	100.52	1.98	27.44	2.41×10^{-2}
18	100.51	0.44	13.79	2.18×10^{-2}
19	100.17	2.21	5.61	1.71×10^{-2}
20	99.95	1.61	2.98	1.80×10^{-2}
21	99.96	15.90	40.20	2.04×10^{-2}
22	100.06	15.57	30.47	1.83×10^{-2}

.

Table 2.3. Results from regression analyses to determine optimal light detection and ranging (LiDAR) normalised relative point density (NRD) height range for predicting travel rate along slopes of less than 5°.

Rank	NRD height range	R^2_m	R^2_c
1	0.15–2.75 m	0.540	0.839
2	0.15–2.70 m	0.540	0.838
3	0.15–2.65 m	0.539	0.838
4	0.15–2.60 m	0.539	0.837
5	0.15–2.80 m	0.539	0.837
…	…	…	…
5053	4.85–4.90 m	0.008	0.272

.

Table 2.4. Fixed effects for model predicting travel rates. Probabilities are significant at: ***, $\alpha = 0.001$. Residual degrees of freedom = 1269.

Parameter	β	s.e.	$\beta_{standardised}$	t	p
intercept (α)	1.662	0.025			
density	–1.076	0.024	–0.551	–45.67	<0.001***
roughness	–9.011	0.743	–0.171	–12.13	<0.001***
slope	-5.191×10^{-3}	3.675×10^{-4}	–0.168	–14.12	<0.001***
slope^2	-1.127×10^{-3}	3.649×10^{-5}	–0.263	–30.89	<0.001***

.

Table 2.5. Resulting travel distances, times and rates for simulated escape routes.

Route	Straight-line distance (m)	Route distance (m)	Travel time (s)	Straight line mean travel rate (m s^{-1})	Route mean travel rate (m s^{-1})
a → b	941.5	1038.9	969.6	0.97	1.07
b → a	941.5	1157.8	950.0	0.99	1.22

.

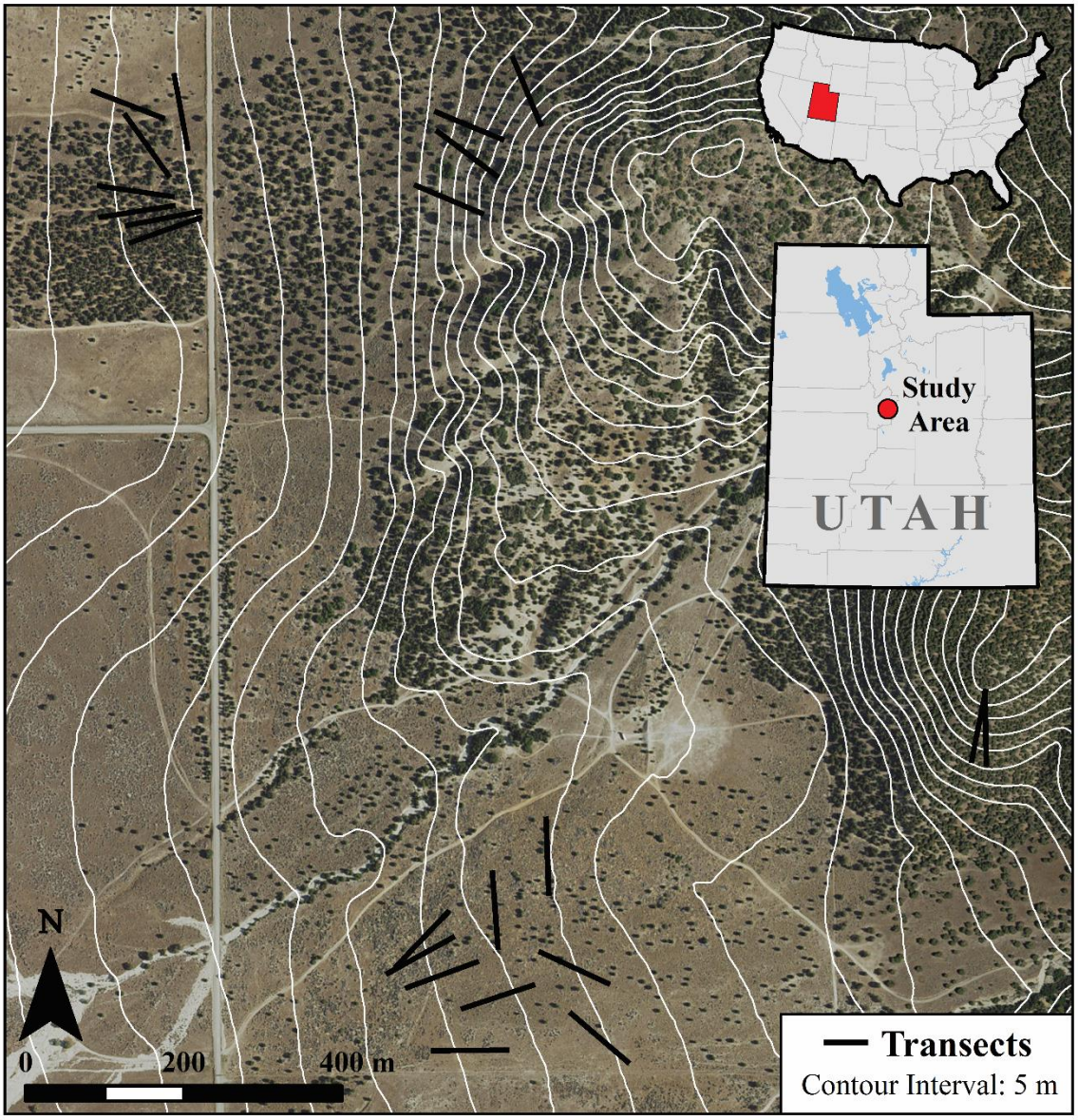

Fig. 2.1. Study area map, with background imagery care of ESRI (ESRI Inc., Redlands, CA, USA, www.esri.com).

.

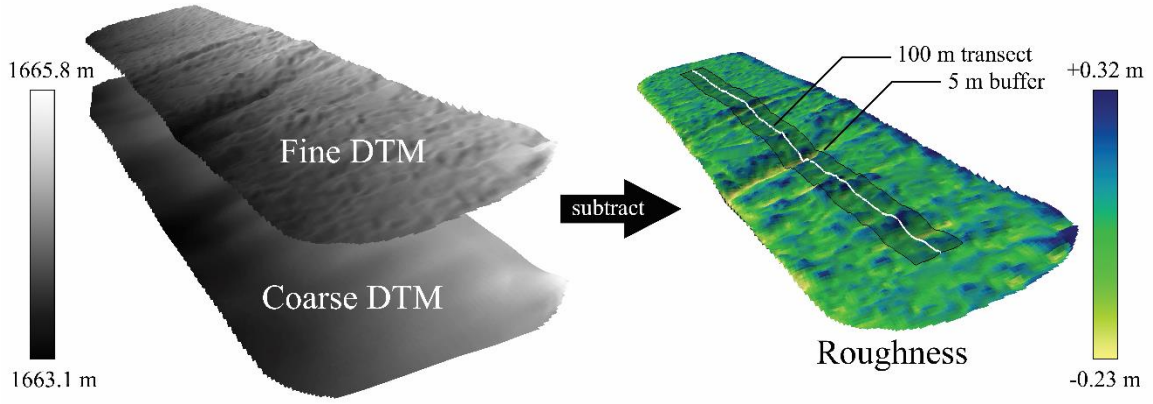

Fig. 2.2. Roughness calculation; digital terrain model (DTM) elevation values exaggerated 3x to highlight texture.

.

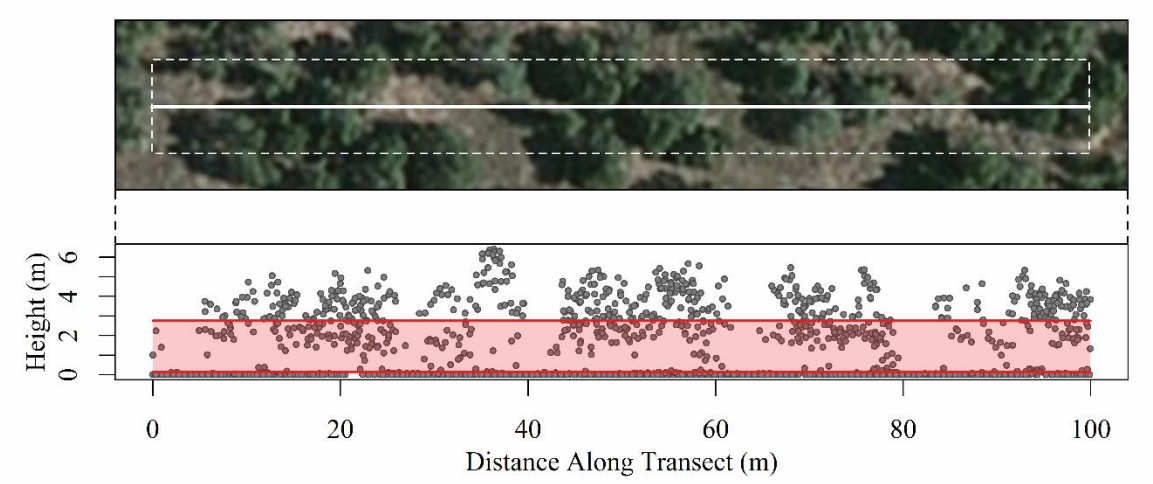

Fig. 2.3. Example transect with associated light detection and ranging (LiDAR) point cloud cross-section and example height range (0.15–2.75 m); heights scaled for clarity, with background imagery care of ESRI (ESRI Inc., Redlands, CA, USA, www.esri.com).

.

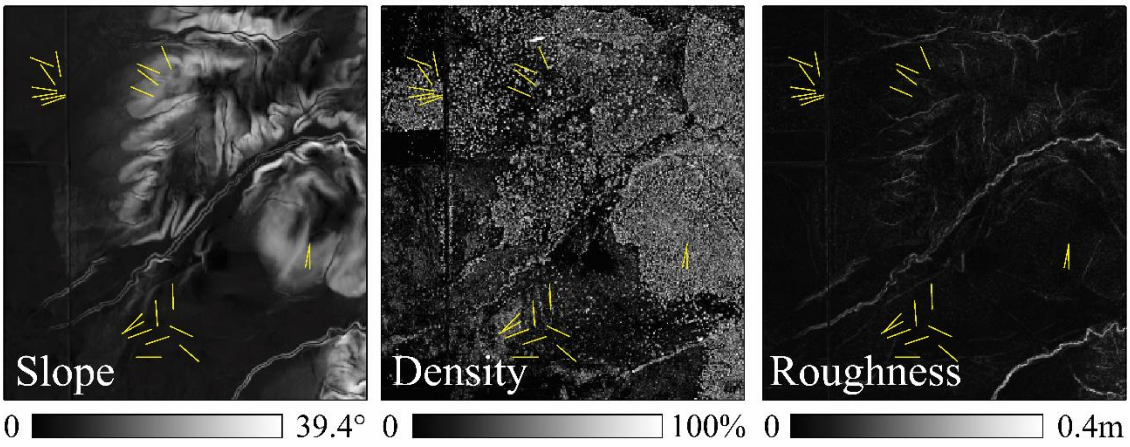

Fig. 2.4. Landscape parameters with transects.

.

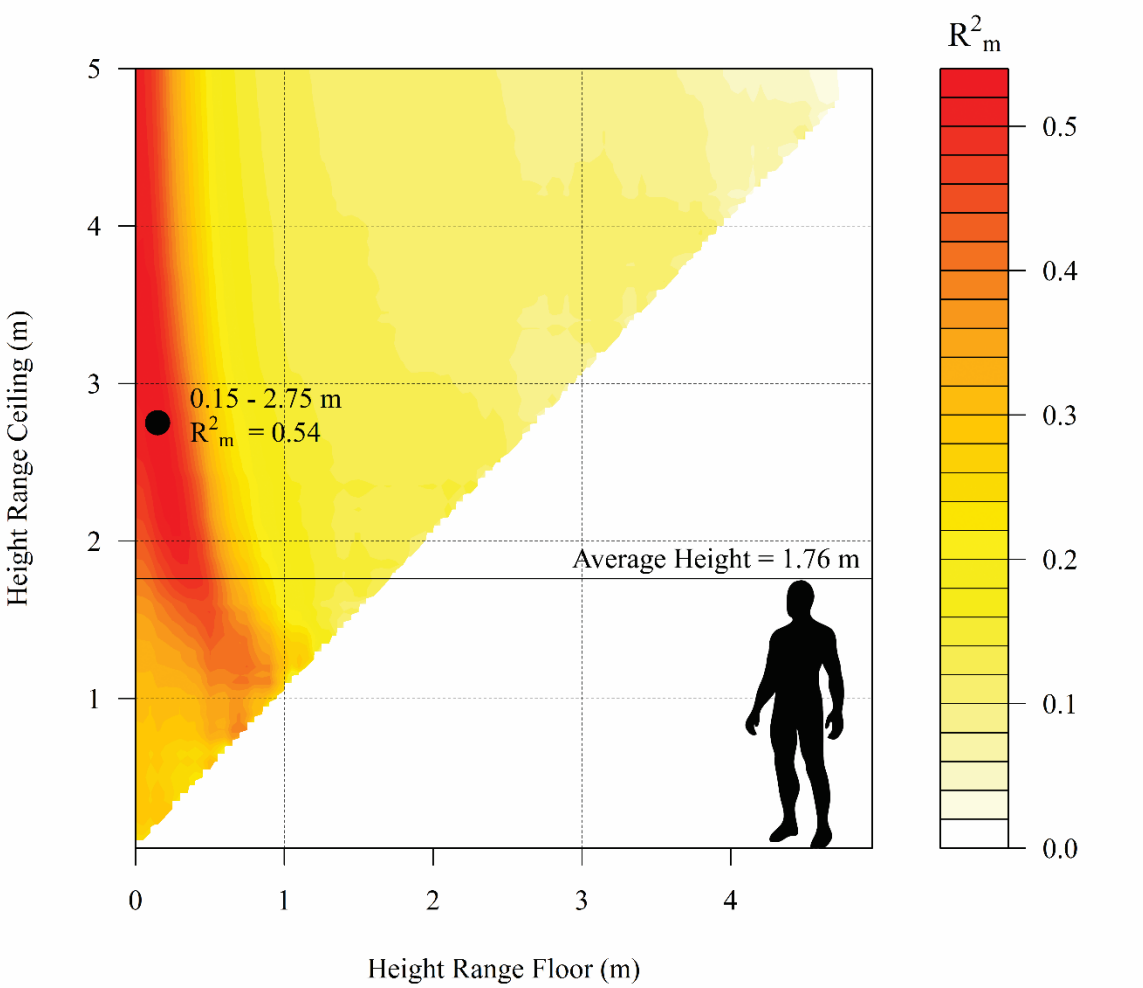

Fig. 2.5. Power of light detection and ranging (LiDAR) normalised relative point density (NRD) height ranges from 0 to 5 m for predicting travel rates along slopes of <5° as approximated by Nakagawa and Schielzeth (2013)'s measure for marginal R^2 (R^2_m) compared with average study subject height. Best interval (0.15–2.75 m) shown.

.

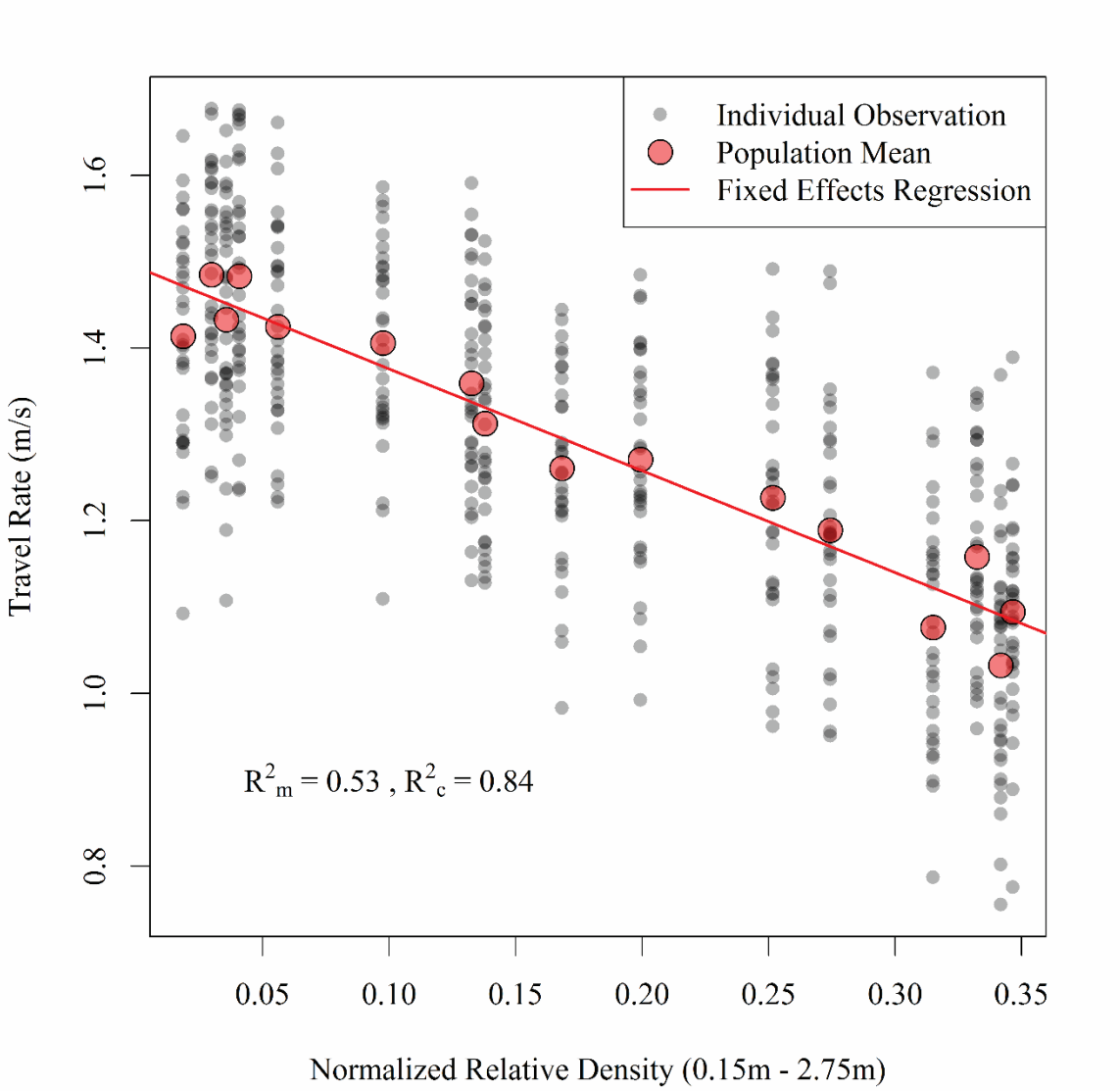

Fig. 2.6. Effect of density, as approximated by the optimal light detection and ranging (LiDAR) normalised relative point density (NRD) height range (0.15–2.75 m), on travel rates along slopes less than 5°.

.

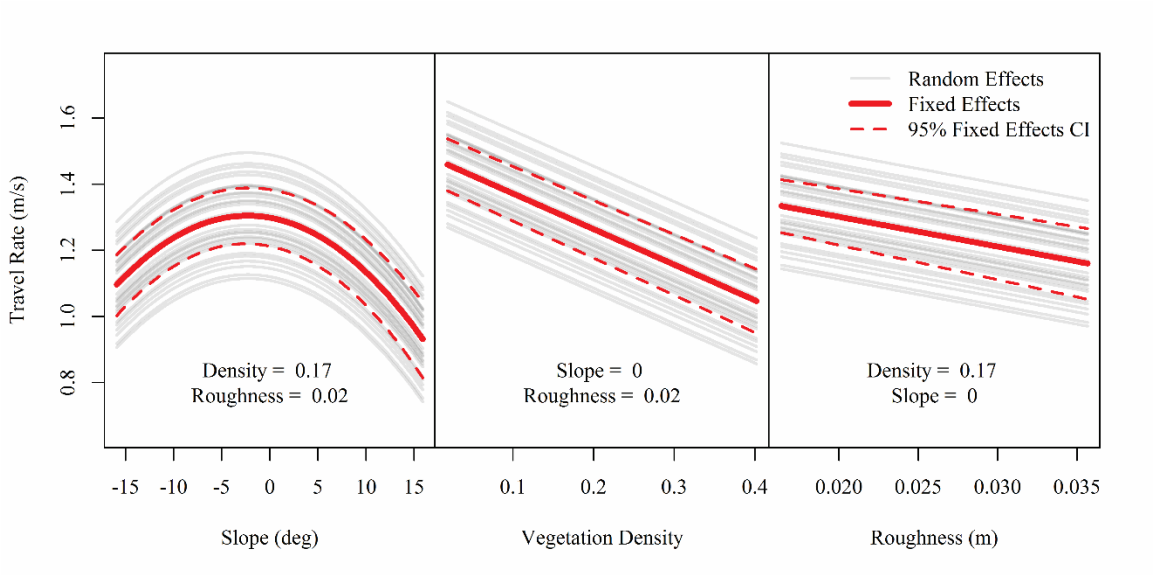

Fig. 2.7. Predicted results of linear mixed effects regression (LMER) for each landscape condition within the range of values found on transects throughout the study area, assuming a median value of the other two conditions.

.

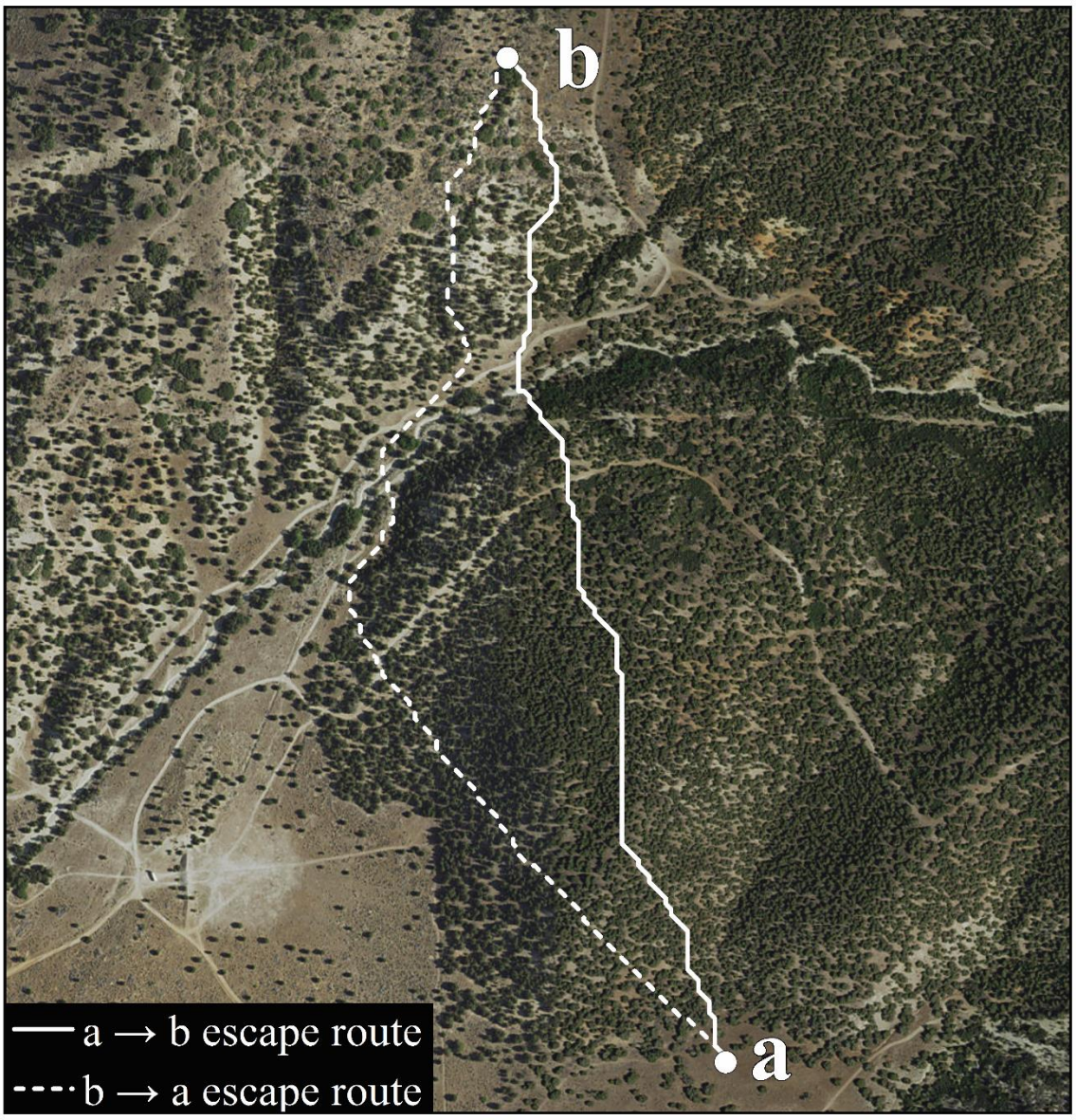

Fig. 2.8. Two simulated escape routes representing the least-cost paths between points *a* and *b* in both directions; background imagery: ESRI (ESRI Inc., Redlands, CA, USA, www.esri.com).

.

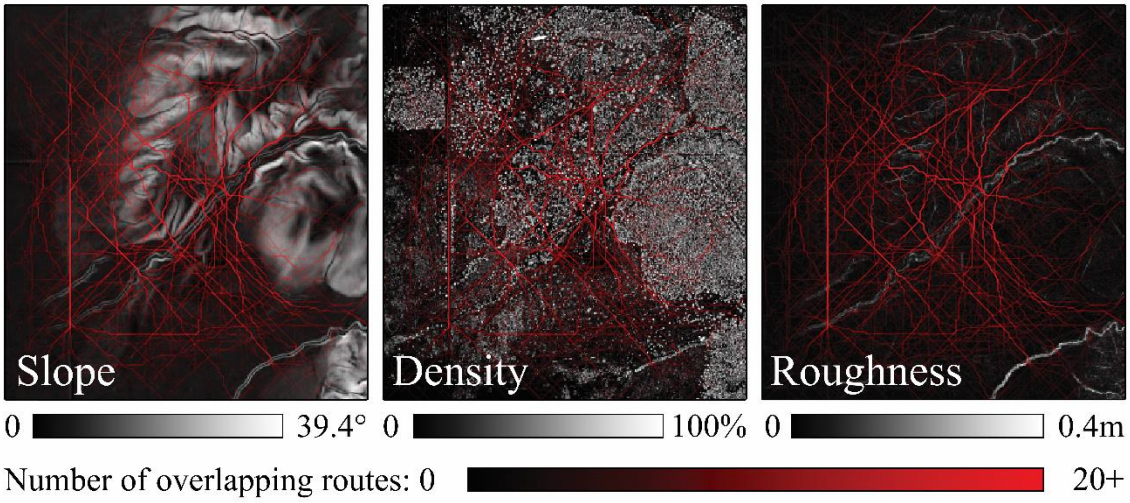

Fig. 2.9. Results of least-cost routes between 1000 randomly generated point location pairs throughout the study area with route overlap displayed against landscape parameters.

.

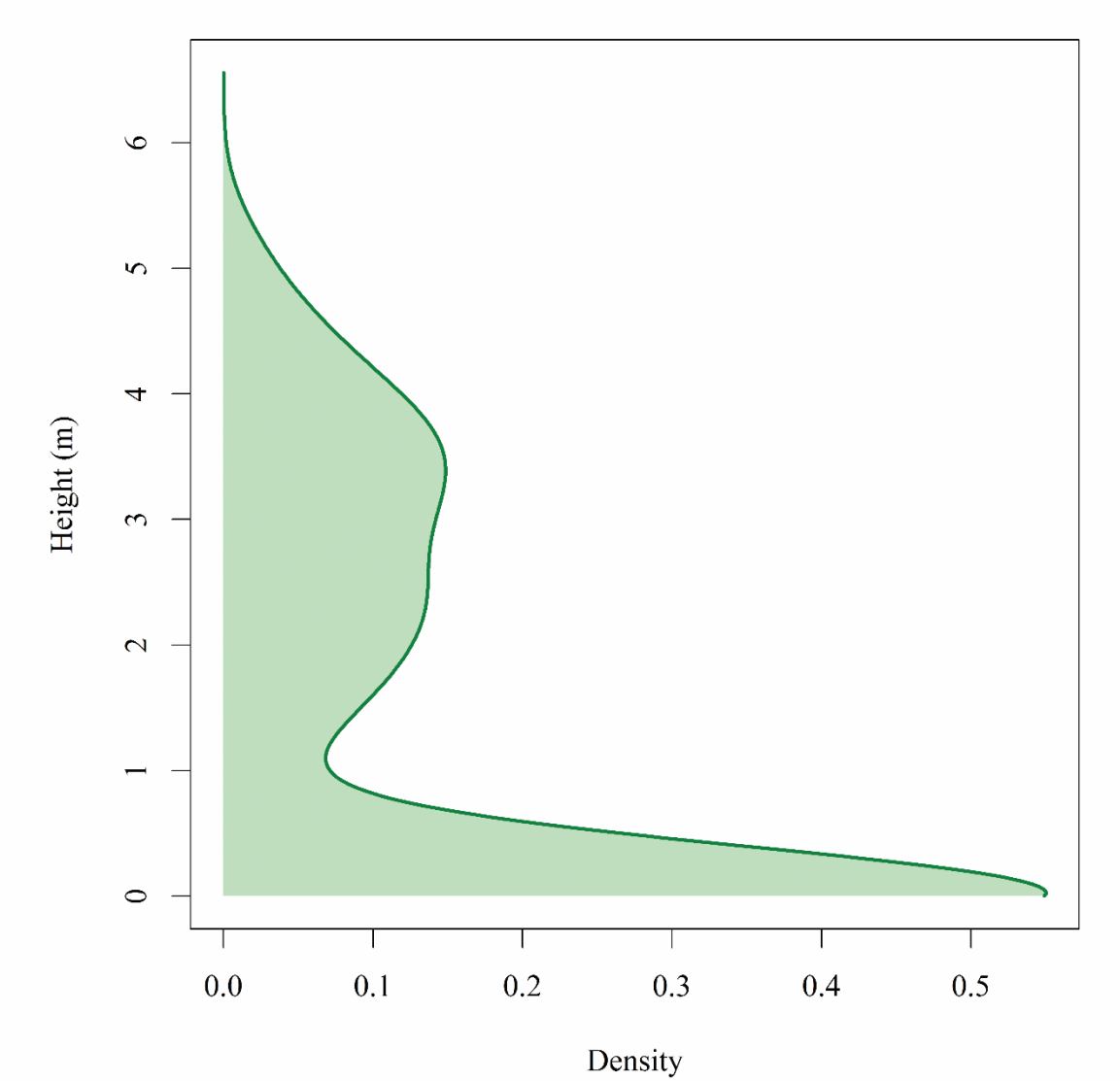

Fig. 2.10. Density plot of light detection and ranging (LiDAR) point return heights, measured as a proportion of all returns, for a transect with dense juniper.

.

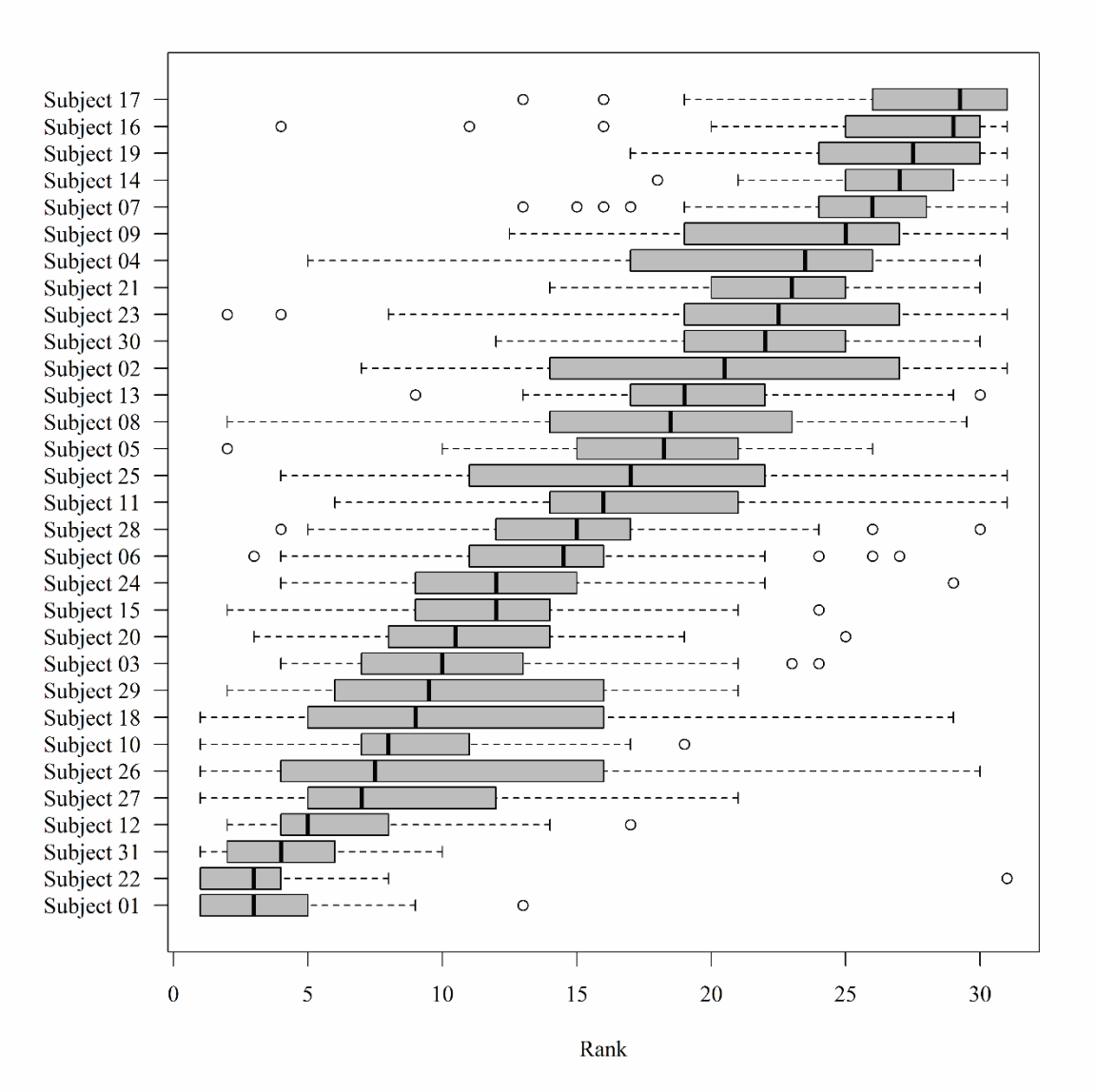

Fig. 2.11. How each study participant's travel rates ranked among all participants for each transect

.

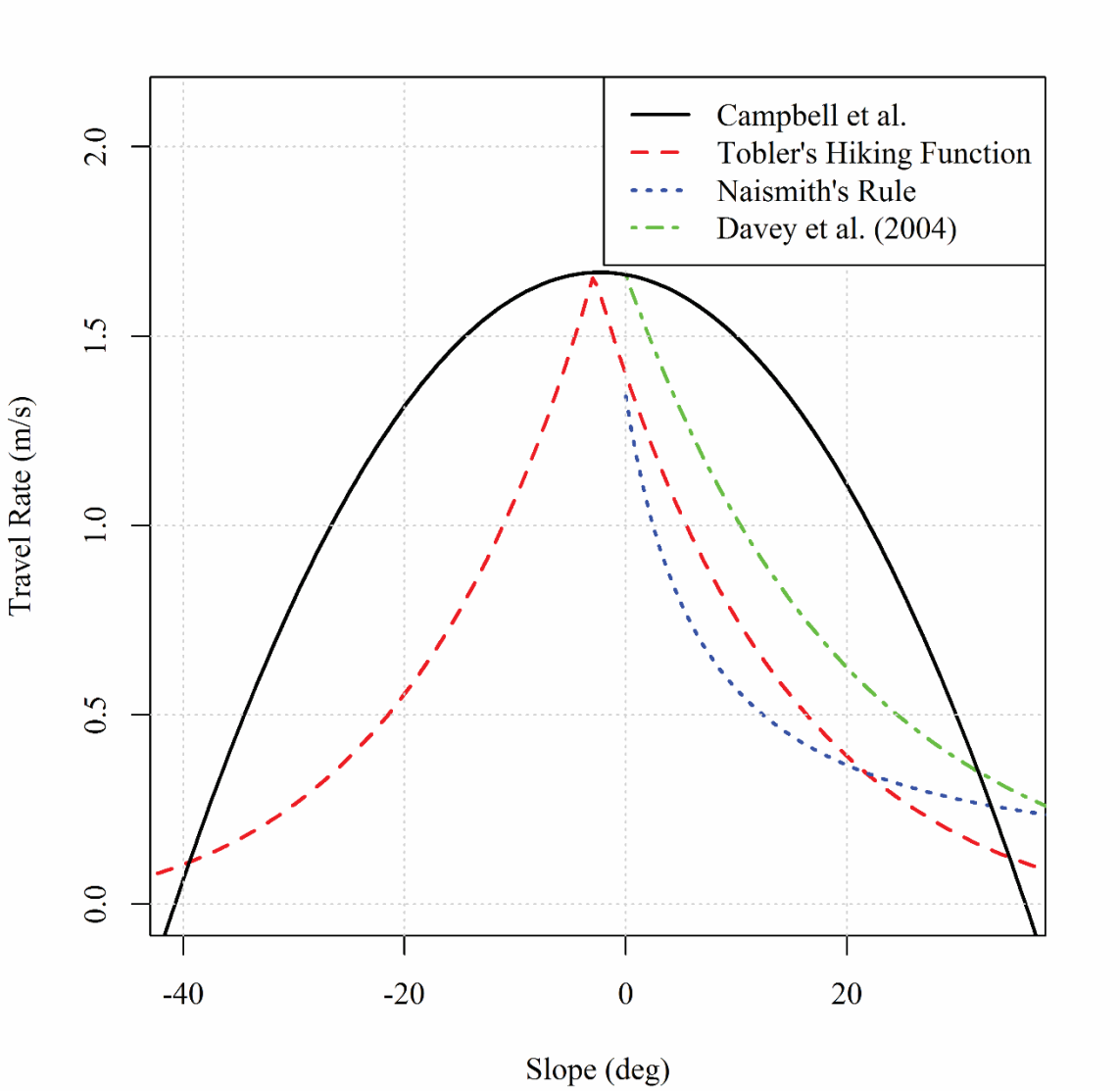

Fig. 2.12. Comparison of model results (calculated assuming zero vegetation density and zero ground surface roughness) to three well-established models used to estimate the effects of slope on travel rate. Davey *et al.* (1994)'s model was calibrated to match our model's 0° slope travel rate.

.

2.6 References

Alexander ME, Baxter GJ, Dakin GR (2005) Travel rates of Alberta wildland firefighters using escape routes. In 'Eighth International Wildland Fire Safety Summit', 26–28 April 2005, Missoula, MT, USA. (Eds BW Butler, ME Alexander) pp. 1–11. (International Association of Wildland Fire: Missoula, MT, USA)

Andrews PL (2014) Current status and future needs of the BehavePlus Fire Modeling System. *International Journal of Wildland Fire* **23**, 21–33. doi:10.1071/WF12167

Anguelova Z, Stow DA, Kaiser J, Dennison PE, Cova T (2010) Integrating fire behavior and pedestrian mobility models to assess potential risk to humans from wildfires within the US–Mexico border zone. *The Professional Geographer* **62**, 230–247. doi:10.1080/00330120903543756

Arizona State Forestry Division (2013) Yarnell Hill fire: serious accident investigation report. 23 September 2013. Available at http://wildfiretoday.com/documents/Yarnell_Hill_Fire_report.pdf [Verified 9 February 2017]

Bartón K (2016) MuMIn: multi-model inference. R package version 1.15.6. Available at http://CRAN.R-project.org/package=MuMIn [Verified 20 December 2016]

Bates D, Maechler M, Bolker B, Walker S (2015) Fitting linear mixed effects models using lme4. *Journal of Statistical Software* **67**, 1–48. doi:10.18637/JSS.V067.I01

Beighley M (1995)Beyond the safety zone: creating a margin of safety. *Fire Management Notes* **55**, 22–24.

Bradbury RB, Hill RA, Mason DC, Hinsley SA, Wilson JD, Balzter H, Anderson GQ, Whittingham MJ, Davenport IJ, Bellamy PE (2005) Modelling relationships between birds and vegetation structure using airborne LiDAR data: a review with case studies from agricultural and woodland environments. *The Ibis* **147**, 443–452. doi:10.1111/J.1474919X.2005.00438.X

Butler BW, Cohen JD, Putnam T, Bartlette RA, Bradshaw LS (2000) A method for evaluating the effectiveness of firefighter escape routes. In '4th International Wildland Fire Safety Summit', 10–12 October 2000, Edmonton, AB, Canada. (Eds BW Butler, KS Shannon) pp. 42–53. (International Association of Wildland Fire: Missoula, MT, USA)

Campbell MJ, Dennison PE, Butler BW (2017) Safe separation distance score: a new metric for evaluating wildland firefighter safety zones using LiDAR. *International Journal of Geographical Information Science* **31**, 1448–1466. doi:10.1080/13658816.2016.1270453

.

Davey RC, Hayes M, Norman JM (1994) Running uphill: an experimental result and its applications. *The Journal of the Operational Research Society* **45**, 25–29. doi:10.1057/JORS.1994.3

Dennison PE, Fryer GK, Cova TJ (2014) Identification of firefighter safety zones using LiDAR. *Environmental Modelling & Software* **59**, 91–97. doi:10.1016/J.ENVSOFT.2014.05.017

Dijkstra EW (1959) A note on two problems in connexion with graphs. *Numerische Mathematik* **1**, 269–271. doi:10.1007/BF01386390

Finney MA (2004) FARSITE: fire area simulator-model development and evaluation. USDA Forest Service, Rocky Mountain Research Station, Research Paper RMRS-RP-4. (Ogden, UT, USA)

Finney MA (2006) An overview of FlamMap fire modeling capabilities. In 'Fuels management—how to Measure Success: Conference Proceedings', 28–30 March 2006, Portland, OR, USA. (Eds PL Andrews, BW Butler) pp. 213–220. (USDA Forest Service, Rocky Mountain Research Station: Fort Collins, CO, USA)

Fryer GK, Dennison PE, Cova TJ (2013) Wildland firefighter entrapment avoidance: modelling evacuation triggers. *International Journal of Wildland Fire* **22**, 883–893. doi:10.1071/WF12160

Gleason P (1991) LCES – a key to safety in the wildland fire environment. *Fire Management Notes* **52**, 9.

Glenn NF, Streutker DR, Chadwick DJ, Thackray GD, Dorsch SJ (2006) Analysis of LiDAR-derived topographic information for characterizing and differentiating landslide morphology and activity. *Geomorphology* **73**, 131–148. doi:10.1016/J.GEOMORPH.2005.07.006

Hijmans RJ (2015). raster: geographic data analysis and modeling. R package version 2.5–2. Available at http://CRAN.R-project.org/ package=raster [Verified 20 December 2016]

Hudak AT, Crookston NL, Evans JS, Hall DE, Falkowski MJ (2008) Nearest neighbor imputation of species-level, plot-scale forest structure attributes from LiDAR data. *Remote Sensing of Environment* **112**, 2232– 2245. doi:10.1016/J.RSE.2007.10.009

Kantner J (2004) Geographical approaches for reconstructing past human behavior from prehistoric roadways. In 'Spatially Integrated Social Science: Examples in Best Practice'. pp. 323–344. (Oxford University Press: Oxford, UK)

.

Kraus K, Pfeifer N (2001) Advanced DTM generation from LIDAR data. *The International Archives of the Photogrammetry, Remote Sensing and Spatial Information Sciences* **34**, 23–30.

Lefsky MA, Cohen WB, Parker GG, Harding DJ (2002) LiDAR Remote Sensing for Ecosystem Studies LiDAR, an emerging remote sensing technology that directly measures the three-dimensional distribution of plant canopies, can accurately estimate vegetation structural attributes and should be of particular interest to forest, landscape, and global ecologists. *Bioscience* **52**, 19–30. doi:10.1641/0006-3568(2002)052[0019:LRSFES]2.0.CO;2

Nakagawa S, Schielzeth H (2013) A general and simple method for obtaining R2 from generalized linear mixed-effects models. *Methods in Ecology and Evolution* **4**, 133–142. doi:10.1111/J.2041-210X.2012.00261.X

National Fire Protection Agency (2011) Firewise communities: firefighter safety in the WUI. Available at http://learningcenter.firewise.org/Firefighter-Safety/3-4.ph [Verified 20 December 2016]

National Wildfire Coordinating Group (2014) Incident response pocket guide. Available at http://www.nwcg.gov/sites/default/files/products/ pms461.pdf [Verified 20 December 2016]

National Wildfire Coordinating Group (2016) Glossary A–Z. Available at http://www.nwcg.gov/glossary/a-z [Verified 20 December 2016]

Norman JM (2004) Running uphill: energy needs and Naismith's Rule. *The Journal of the Operational Research Society* **55**, 308–311. doi:10.1057/ PALGRAVE.JORS.2601671

Pandolf KB, Givoni B, Goldman RF (1976) Predicting energy expenditure with loads while standing or walking very slowly. US Army Research Institute of Environmental Medicine Paper USARIEM-M-3/77.(Natick, MA, USA)

Pettebone D, Newman P, Theobald D (2009) A comparison of sampling designs for monitoring recreational trail impacts in Rocky Mountain National Park. *Environmental Management* **43**, 523–532. doi:10.1007/ S00267-008-9261-9

Reutebuch SE, McGaughney RJ, Andersen HE, Carson WW (2003) Accuracy of a high-resolution LiDAR terrain model under a conifer forest canopy. *Canadian Journal of Remote Sensing* **29**, 527–535. doi:10.5589/M03-022

Ruby BC, Leadbetter GW III, Armstrong DW, Gaskill SE (2003) Wildland firefighter load carriage: effects on transit time and physiological responses during simulated

.

escape to safety zone. *International Journal of Wildland Fire* **12**, 111–116. doi:10.1071/WF02025

Sankey JB, Glenn NF, Germino MJ, Gironella AIN, Thackray GD (2010) Relationships of aeolian erosion and deposition with LiDAR-derived landscape surface roughness following wildfire. *Geomorphology* **119**, 135–145. doi:10.1016/J.GEOMORPH.2010.03.013

Schmidtlein MC, Wood NJ (2015) Sensitivity of tsunami evacuation modeling to direction and land cover assumptions. *Applied Geography* **56**, 154–163. doi:10.1016/J.APGEOG.2014.11.014

Snyder GI (2012)The 3D elevation program: summary of program direction. US Department of Interior Geological Survey Fact Sheet 2012–3089. (Reston, VA, USA)

Soule RG, Goldman RF (1972) Terrain coefficients for energy cost prediction. Journal of *Applied Physiology* **32**, 706–708.

Tobler W (1993) Three presentations on geographical analysis and modeling. University of California at Santa Barbara, National Center for Geographic Information and Analysis Technical Report 93–1. (Santa Barbara, CA)

USDA Forest Service (2010) National wildland firefighter (NWFF) workforce assessment. (USDA Forest Service) Available at https://www.fs. fed.us/fire/management/assessments/phase1/NWFF_ReportPhaseI.pdf [Verified 20 December 2016]

USDA Forest Service (2014) First order LiDAR metrics: a supporting document for LiDAR deliverables. (USDA Forest Service, Remote Sensing Applications Center) Available at https://www.fs.fed.us/eng/rsac/LiDAR_training/pdf/LiDARMetricsDescriptionOfDeliverables_Generic_12_15_14.pdf [Verified 20 December 2016]

van Etten J (2015) gdistance: distances and routes on geographical grids. R package version 1.1–9. Available at http://CRAN.R-project.org/ package=gdistance [Verified 20 December 2016]

Wood NJ, Schmidtlein MC (2012) Anisotropic path modeling to assess pedestrian-evacuation potential from Cascadia-related tsunamis in the US Pacific Northwest. *Natural Hazards* **62**, 275–300. doi:10.1007/ S11069-011-9994-2

Ziegler JA (2007) The story behind an organizational list: a genealogy of wildland firefighters' 10 standard fire orders. *Communication Monographs* **74**, 415–442. doi:10.1080/03637750701716594

.

CHAPTER 3

QUANTIFYING UNDERSTORY VEGETATION DENSITY USING SMALL FOOTPRINT AIRBORNE LIDAR

3.1 Abstract

The ability to quantify understory vegetation structure in forested environments on a broad scale has the potential to greatly improve our understanding of wildlife habitats, nutrient cycling, wildland fire behavior, and wildland firefighter safety. Lidar data can be used to model understory vegetation density, but the accuracy of these models is impacted by factors such as the specific lidar metrics used as independent variables, overstory conditions such as density and height, and lidar pulse density. Few previous studies have examined how these factors impact estimation of understory density. In this study, we compare two widely-used lidar-derived metrics, overall point relative density (ORD) and normalized point relative density (NRD) in an understory vertical stratum, for their abilities to accurately model understory vegetation density. We also use a bootstrapping analysis to examine how lidar pulse density, overstory vegetation density, and canopy height can affect the ability to characterize understory conditions. In doing so, we present a novel application of an automated field photo-based understory cover estimation technique as reference data for comparison to lidar. Our results highlight that NRD is a far superior metric for characterizing understory density than ORD (R^2_{NRD} = 0.44 vs. R^2_{ORD} = 0.14). In addition, we found that pulse density had

the strongest positive effect on predictive power, suggesting that as pulse density increases, the ability to accurately characterize understory density using lidar increases. Overstory density and canopy height had nearly identical negative effects on predictive power, suggesting that shorter, sparser canopies improve lidar's ability to analyze the understory. Our study highlights important considerations and limitations for future studies attempting to use lidar to quantify understory vegetation structure.

3.2 Introduction

Understory vegetation plays a large number of critical roles in forest ecosystems. It is often the most species-rich and diverse portion of a forest (Eskelson et al., 2011). Low-lying vegetation cover provides prey species with visual cover to aid in avoiding predation (Lone et al., 2014). For forest-dwelling mammals, much of the nutritious and palatable forage is found in the understory (Nijland et al., 2014). The quantity and size of tree regeneration has important implications not only for forest health, but also economic importance for timber production (Korpela et al., 2012). Understory biomass contributes to carbon sequestration and soil nutrient cycling (Estornell et al., 2011; Suchar and Crookston, 2010). Understory plants also play an important role in maintaining soil structure and reducing erosion (Suchar and Crookston, 2010). Surface fuel loading and bulk density are some of the most important predictors of wildland fire intensity and rate of spread (Keane, 2014). The presence of ladder fuels in the understory of a forested environment can facilitate the transition from a surface fire to a crown fire, which can have dramatic impacts on post-fire ecosystems (Kramer et al., 2016; Stephens, 1998). Understory vegetation density has also been linked to firefighter safety, given that more dense understories can reduce the ability to efficiently traverse wildland environments

.

(Campbell et al., 2017a) and impact safety zone suitability (Campbell et al., 2017b). For these reasons and many others, it is essential to be able to quantify the abundance and spatial distribution of understory vegetation in forested environments.

There are many ways to characterize understory vegetation in the field (Higgins et al., 2005). One of the most common methods for doing so is through the use of cover boards, which rely on visually estimating of the relative proportion of a board of known dimensions that is being obscured by vegetation from a given vantage point (Jones, 1968; Nudds, 1977). Although field-based methods tend to be both highly precise and accurate, implementation is costly, time-consuming, and even the most extensive field campaigns result in a mere sample of the broader landscape. When field data collections designed to sample the landscape in an unbiased and representative manner are used in conjunction with remote sensing, however, field estimates of understory structure can be used as training data for predictive models, thus enabling the broad-scale imputation of vegetation biometrics. Although cover boards have been rarely used as such, they have much potential for use in conjunction with remote sensing technologies such as airborne light detection and ranging (lidar) (Kramer et al., 2016). A widely-acknowledged limitation of cover board analysis, however, is that the subjectivity inherent to the visual estimation of cover board cover is prone to error (Collins and Becker, 2001; Limb et al., 2007; Morrison, 2016). This has motivated the more recent implementation of digital image processing into the semi-automated analysis of cover board photos (Jorgensen et al., 2013).

In recent decades, lidar has emerged as a leading technology in the mapping of three-dimensional vegetation structure. Lidar is particularly useful in characterizing

.

understory structure, as narrow beams of laser light emitted in rapid succession from an airborne sensor can exploit small gaps in a forested canopy. The pulses interact with features in the understory (tree leaves, branches, and boles, shrubs, grasses, and forbs) and reflect back to the sensor; the timed pulse returns can provide detailed information on understory structure. Particularly in the past 15 years, as lidar technology and associated data processing capacities have improved, the number of studies involving the use of lidar to characterize understory conditions has grown rapidly (Alexander et al., 2013; Campbell et al., 2017a; Chasmer et al., 2006; Clark et al., 2004; Estornell et al., 2011; Korpela et al., 2012; Kramer et al., 2016; Maltamo et al., 2005; Martinuzzi et al., 2009; Morsdorf et al., 2010; Mutlu et al., 2008; Nijland et al., 2014; Riaño et al., 2003; Singh et al., 2015; Su and Bork, 2007). To accurately model these conditions, however, first requires a careful selection of appropriate ground reference information capable of linking ground conditions to remotely sensed data, such as cover board analysis. In addition, the selection of relevant lidar-derived metrics for statistical comparison is of critical importance. Many such metrics have been used throughout the literature, but two height stratum-based metrics have dominated in characterizing the understory: overall relative point density (ORD) and normalized relative point density (NRD). A roughly equal number of studies have employed the use of ORD (Hudak et al., 2008; Maltamo et al., 2005; Martinuzzi et al., 2009; Mutlu et al., 2008; Riaño et al., 2003; Singh et al., 2015) and NRD (Campbell et al., 2017a; Goodwin et al., 2007; Kramer et al., 2016; Lone et al., 2014; Seielstad and Queen, 2003; Skowronski et al., 2007; Su and Bork, 2007), but none has compared the two for their respective predictive capabilities. Lastly, there are many factors that can affect the accuracy of the resulting structural models that must be

.

carefully considered when attempting to characterize the understory, including lidar pulse density, overstory vegetation density, and canopy height.

The objectives of this study are to (1) develop a method for automated cover board photo analysis for use as reference data for lidar understory density estimation; (2) compare two widely-used lidar vertical stratum metrics (overall relative point density and normalized relative point density) with respect to their ability to accurately characterize understory vegetation density; and (3) determine the relative effects of lidar pulse density, overstory vegetation density, and canopy height on the ability to accurately characterize understory vegetation density.

3.3 Background

3.3.1 Characterizing understory structure using cover boards

There are a number of ways to characterize forest understory structure in the field. (Higgins et al., 2005) present a comprehensive review of these methods. Some of the most oft-employed field methods for estimating understory cover are visual obstruction methods. Though the specific methods vary slightly, the assessment is generally based on the determination of the degree to which a distant reference object of known dimensions is being covered by vegetation from a given vantage point. The underlying assumption is that denser vegetation will result in a greater proportion of the object being covered. The two most common reference objects are cover poles (Robel et al., 1970) and cover boards (Jones, 1968; Nudds, 1977), the former enabling obstruction estimation in one dimension, the latter in two. Cover poles are simpler to analyze, given the ease with which one can quantify the proportion of vegetation cover in a single dimension, but cover boards, with their larger sample area, provide more detailed information to the analysis. Cover boards

.

have been used extensively, particularly in wildlife habitat studies (Duebbert and Lokemoen, 1976; Griffith and Youtie, 1988; Jones, 1968; Musil et al., 1994; Sage et al., 2004; Winnard et al., 2013).

The main problem with cover board analyses is the subjectivity of field- or photo-based cover interpretation. Studies have repeatedly demonstrated significant variability in individual analysts' cover estimates (Collins and Becker, 2001; Limb et al., 2007; Morrison, 2016). A number of authors have attempted to overcome the issue of interpreter subjectivity by capturing a digital photo of the cover board and subsequently classifying between board and non-board pixels in some semi-automated fashion (Boyd and Svejcar, 2005; Carlyle et al., 2010; Jorgensen et al., 2013; Limb et al., 2007; Marsden et al., 2002; Winnard et al., 2013). Limb et al. (2007) compared this procedure to visual interpretation of a cover board and cover pole, finding that the classification approach greatly reduced the variability in cover estimates and attained the highest degree of correlation with field-sampled biomass. However, many of these studies rely on manually thresholding the pixel value brightness to distinguish between board and vegetation, which can be even more error-prone than visual interpretation (Booth et al., 2005; Jorgensen et al., 2013). Accordingly, a small number of studies have begun using more advanced image analysis, including supervised classification (Jorgensen et al., 2013).

Another key limitation of cover board-based studies – and, by extension all solely field-based studies – is that they represent a mere sampling of the broader landscape. Remote sensing is one potential solution to this problem, provided that a robust, statistical relationship can be determined between a field-based measure such as cover board cover and some remote sensing dataset capable of characterizing understory

.

vegetation structure, such as lidar. To our knowledge, there has only been one published study to date that has attempted to bridge this divide (Kramer et al., 2016). Kramer et al. (2016) used cover board cover as training data in a lidar-based model aimed at quantifying ladder fuels for fire behavior prediction, demonstrating a high degree of predictive power. In a plot-level study of deer predation, Lone et al. (2014) used both cover board and lidar-derived estimates of understory cover as predictors in a logistic regression model, finding that both variables were strong predictors of predation; however, there was no analysis of the degree to which the two measures were correlated. Given that Kramer et al. (2016) and Lone et al. (2014) employed manual visual interpretation of cover board photos to assess understory cover, no studies, to date, have linked digitally-classified cover board photos to lidar-derived understory metrics.

3.3.2 Characterizing understory structure using lidar

Airborne discrete-return lidar has been widely used for modeling overstory forest conditions, such as height (Ben-Arie et al., 2009; Hopkinson et al., 2006; Khosravipour et al., 2015; Popescu et al., 2002), basal area (Bright et al., 2013; Chen et al., 2007; Hudak et al., 2006; Lefsky et al., 1999), canopy cover/closure (Ahmed et al., 2015; Holmgren et al., 2003; Korhonen et al., 2011; Smith et al., 2009), species composition (Brandtberg, 2007; Korpela et al., 2010; Vaglio Laurin et al., 2016), and leaf area index (Korhonen et al., 2011; Riaño et al., 2004; Richardson et al., 2009; Tang et al., 2014). However, comparably few studies have examined the ability of lidar to characterize understory conditions. Among these studies, the most common approach to doing so is the area-based approach of Næsset (2002). This method relies on statistically relating one or more

.

lidar-derived metrics within an area of a given size and dimensions to some ground-based vegetation biometric data collected within that same area (Næsset, 2002). The development of an associated predictive model based on that relationship enables broad-scale biometric mapping across un-sampled areas (Wulder et al., 2013). A variety of different statistical modeling techniques have been employed to develop these predictive relationships, including more traditional, parametric modeling techniques such as ordinary least squares regression (Clark et al., 2011), multiple regression (Hudak et al., 2006), and stepwise regression (Drake et al., 2002), and more advanced, non-parametric modeling techniques such as *k*-nearest neighbor (Falkowski et al., 2010), support vector machines (Dalponte et al., 2011), and random forests (Martinuzzi et al., 2009). Parametric models have the advantage of conceptual simplicity, being based on linear relationships between a set of predictor (or independent) variables and a single response (or dependent) variable, the results of which can be easily interpreted and evaluated for logical consistency (Penner et al., 2013). However, non-parametric models – particularly advanced machine learning algorithms such as random forests – can often result in higher imputation accuracies, albeit at the expense of model transparency and potential for overfitting (Hudak et al., 2008; Latifi et al., 2010).

One of the most important steps in the area-based analytical process is the selection of lidar metrics. Evans et al. (2009) provide an extensive list of metrics that have been used throughout the lidar literature. These metrics, ranging from basic descriptive statistics such as mean, standard deviation, and range, to more advanced parameters such as skewness and kurtosis, can be computed on an entire lidar point cloud extracted within a given *x* by *y* area (e.g. mean lidar point return height within a 30 x 30

.

m area) (Evans et al., 2009). However, one of the great strengths of lidar is the ability to analyze point clouds in discrete vertical strata. Thus, instead of computing these metrics on the entire vertical extent of a given area, you can first subdivide the point cloud into a series of voxels, based on one or more aboveground height thresholds. This approach is particularly useful when attempting to characterize understory structure in forested environments (Goodwin et al., 2007; Mutlu et al., 2008; Riaño et al., 2003; Seielstad and Queen, 2003; Skowronski et al., 2007).

Two important vertical stratum metrics that are often used in analyzing understory structure are overall relative point density (ORD) and normalized relative point density (NRD) (USDA Forest Service, 2014). A key assumption of both ORD and NRD is that as vegetation density increases, the likelihood of a given lidar pulse interacting with vegetation increaseS, thus increasing the proportion of aboveground vegetation point returns. ORD for a given height range between *i* and *j* is defined as the number of points (*n*) that fall between *i* and *j* divided by the total number of points in a given area, from the ground level (height = 0) to the height of the highest point (*k*) such that:

$$ORD_{(i,j)} = \frac{\sum_i^j n}{\sum_0^k n} \tag{3.1}$$

NRD is very similar, but it characterizes point density as compared only to the number of points within a given height range and below, such that:

$$NRD_{(i,j)} = \frac{\sum_i^j n}{\sum_0^j n} \tag{3.2}$$

.

This is an important distinction, as NRD is theoretically more robust to differences in overstory conditions (USDA Forest Service, 2014). In the presence of a dense overlying canopy, much of the lidar pulse energy is likely to be absorbed in the upper canopy, thus reducing the amount of energy, and in turn the proportion of point returns, in the understory, regardless of actual understory density. Figure 3.1 contains a figurative example of lidar point cloud in a conifer forest with both a dense overstory and a dense understory of regeneration. As can be seen, the majority of the point returns are found within the overstory as a result of lidar pulse occlusion. If one were to calculate understory ORD in this example, the result would be relatively low (e.g. 0.1), suggesting that understory density is low, when it is, in fact, relatively high. Conversely, NRD, ignoring the overstory returns, would be much higher (e.g. 0.6), more accurately representing true understory density. Despite the apparent conceptual advantage of NRD over ORD, particularly for characterizing understory structure, there is no clear evidence in the literature as to which metric results in improved model accuracy. Nor is there any sort of agreement on which metric to use, with a large number of studies using ORD (Hudak et al., 2008; Maltamo et al., 2005; Martinuzzi et al., 2009; Mutlu et al., 2008; Riaño et al., 2003; Singh et al., 2015), and a similar number using NRD (Campbell et al., 2017a; Goodwin et al., 2007; Kramer et al., 2016; Lone et al., 2014; Seielstad and Queen, 2003; Skowronski et al., 2007; Su and Bork, 2007). No studies to date have directly compared the respective efficacy of ORD and NRD at characterizing understory conditions.

.

3.3.2.1 Characterizing understory structure with ORD

Riaño et al. (2003) characterized understory conditions using lidar by first performing a cluster analysis to distinguish between overstory and understory returns, and then computing both understory cover using ORD, and understory height by calculating the 99th percentile of understory returns. Maltamo et al. (2005) modeled understory tree number and heights using lidar, finding that ORD bore no significant predictive power for estimating either parameter, instead finding that maximum lidar return height, proportion of all vegetation returns, and height percentiles were more effective predictors. Mutlu et al. (2008) fused lidar ORD data calculated in a series of height bins ranging from 0 to 2 m in height with QuickBird imagery to generate a high-resolution surface fire behavior fuel type map. Martinuzzi et al. (2009) modeled understory shrub cover and standing dead snags using random forest modeling of a range of predictor variables, determining that three predictors were most valuable for characterizing understory structure: (1) ORD of ground points; (2) ORD between 1 and 2.5 m; and a slope-aspect transformation terrain variable. Singh et al. (2015) included several understory ORD metrics in a random forest model for the detection of an invasive understory plant in North Carolina, but found that they bore little importance in the resultant best-fit prediction model.

3.3.2.2 Characterizing understory structure with NRD

Seielstad and Queen (2003) provided one of the earliest examples of lidar-based understory vegetation structural characterization, demonstrating how NRD (referred to as "obstacle density") between 0 and 6 feet in aboveground height can be used to distinguish between several of Anderson's (1982) 13 fire behavior surface fuel models. Goodwin et

.

al. (2007) compared NRD between 0.5 and 4 m in height to field-based ocular estimates of understory cover, finding that NRD alone was a strong predictor of cover. Skowronski et al. (2007) analyzed ladder fuels in the understory through the analysis of a series of vertical strata, finding that NRD between 1 and 2 m in height and NRD between 2 and 3 m in height were strongly correlated to the presence of ladder fuels. Su and Bork (2007) used a clustering technique to separate understory from overstory returns, and further between shrub and herbaceous layers. They attempted to model shrub and herbaceous cover using NRD as the sole predictor; however, no significant relationships were found. Wing et al. (2012) used a modified form of NRD, which involved an intensity-based filter aimed at minimizing the inclusion of ground points. However, they also used ORD to characterize overstory conditions.

3.3.2.3 Effects of pulse density

Airborne lidar is, in essence, a sampling instrument. Laser pulses are emitted in rapid succession from a sensor aboard an aircraft towards the ground surface. They interact with one or more surfaces on or above the ground and reflect back to the sensor, the timing of which enables the precise measurement of sensor-surface distance. When combined with onboard GPS and inertial measurement unit, the resulting point returns form a cloud containing millions of individual points, each of which has an *x*, *y*, and *z* coordinate, as well as a reflection intensity. The pulse frequency and emission angles depend on the specifications of the lidar instrument used. The pulse spacing is a function of frequency, angle, flying height, and speed. Higher altitudes and faster speeds result in higher pulse spacing (lower pulse density). Thus, with higher pulse density, you are getting a more detailed sampling of the earth's surface. There are more pulses per unit

.

area to potentially interact with more surfaces on the ground. Accordingly, it can be assumed, and indeed has been widely cited, that higher pulse density lidar data collections enable the generation of more precise, high-resolution estimates of three-dimensional structure (Estornell et al., 2011; Pesonen et al., 2008; Wing et al., 2012). While this general relationship is widely accepted, the specific effects of pulse density on the ability of lidar to accurately characterize understory structure have not been explored in the scientific literature.

3.3.2.4 Effects of overstory density

One of the great advantages of using airborne lidar in forested environments is the ability of individual laser pulses to exploit gaps in the overstory to reach understory vegetation and thus facilitate the structural characterization thereof. However, as the density of overstory vegetation increases, the size and number of those gaps decreases. Accordingly, it has been acknowledged by a number of authors that denser canopies reduce the ability to accurately characterize sub-canopy vegetation (Chasmer et al., 2006; Falkowski et al., 2008; Goodwin et al., 2007; Hill and Broughton, 2009; Maltamo et al., 2004; Martinuzzi et al., 2009; Mutlu et al., 2008; Richardson and Moskal, 2011; Su and Bork, 2007; Wing et al., 2012).

Chasmer et al. (2006) demonstrated how lidar pulse occlusion in dense forest canopies negatively impacts live crown base height estimation. Maltamo et al. (2004) highlighted the degree to which the presence of overstory trees negatively impacts both sub-canopy tree identification and height estimation. Falkowski et al. (2008) similarly found that subdominant trees were more difficult to delineate using automated tree identification algorithms as canopy cover increased. Su and Bork (2007) compared lidar-

.

understory cover model predictive power between open- and closed-canopy aspen forests; however, they were unable to obtain any statistically-significant predictive relationships in either environment, thus nullifying the comparative ability. Korpela et al. (2012) provide a detailed analysis of lidar pulse transmission in a forested environment, highlighting the effects of species-specific canopy cover on the likelihood of given pulses interacting with features in the understory. They also suggest a potentially significant effect of scan angle, indicating that including a variety of scan angles may provide more opportunity for canopy penetration. Wing et al. (2012) found no effect of canopy cover on understory cover prediction accuracy; however, they suggest that this may be a unique effect of the distinct vertical stratum differences between understory and overstory vegetation in the ponderosa pine (*Pinus ponderosa*) forests they were studying.

Several studies have quantified the effect of overstory vegetation cover and/or density on the resultant accuracy of lidar-derived digital terrain models (DTMs) (Clark et al., 2004; Hopkinson et al., 2006; Reutebuch et al., 2003; Su and Bork, 2006; Takahashi et al., 2006). These studies consistently demonstrate decreasing DTM accuracy with increasing overstory cover. However, very few studies have explicitly tested the effect of overstory conditions on the ability to characterize the understory, with the exception of Su and Bork (2007) who found no effect and Wing et al. (2012) who suggest that the specific vegetation type they studied may be anomalous with respect to its overstory-understory relationship. One of the key challenges of examining the effect of overstory density on the ability of lidar to characterize understory density is that there tends to be a negative correlation between overstory density and understory density, because as canopy cover increases, less light is able to reach the forest floor, limiting the ability of light-

.

dependent understory plants to regenerate (Alexander et al., 2013; Bartemucci et al., 2006; Kerns and Ohmann, 2004; Martinuzzi et al., 2009; Wing et al., 2012). Accordingly, when analyzing the effects of overstory lidar occlusion, one must be aware of this potentially confounding ecological relationship.

3.3.2.5 Effects of canopy height

While much of the canopy occlusion effect can be explained by overstory density, we hypothesize that there is an additional, independent effect of canopy height. This effect is likely to manifest primarily on off-nadir (higher emission angle) pulses. In the presence of very tall trees, even if those trees are widely spaced (low density), an angular lidar pulse is more likely to interact with multiple overstory surfaces prior to reaching the understory (Figure 3.2). For example, in a forest of 150 foot tall trees, a 20° pulse can interact with two trees almost 55 m apart. This may be a partial explanation for the lack of an effect of overstory cover on the ability to accurately characterize understory conditions found by Wing et al. (2012). They were working in forests typically characterized by tall and widely-spaced ponderosa pine trees. Although many have implicated the effects of overstory vegetation on lidar-based understory characterization, none have explicitly related the effect to a continuous measure of canopy height.

3.4 Methods

3.4.1 Study area

This study was conducted in the Monroe Mountain area of Fishlake National Forest in central Utah (Figure 3.3). This area was selected primarily due to the availability of recent, high-quality lidar data collected during leaf-on conditions. The

.

lidar data were acquired by Digital Mapping, Inc. on behalf of the USDA Forest Service and Utah Automated Geographic Reference Center between August and September of 2016 with an average point density of 16.43 pts/m^2. The 711 km^2 area ranges in elevation from 1711 m to 3418 m. The dominant vegetation types within the study area include black sagebrush (*Artemisia nova*) and big sagebrush (*Artemisia tridentata*) shrublands, pinyon-juniper (*Pinus edulis* and *Juniperus osteosperma*), Gambel oak (*Quercus gambelii*), and curlleaf mountain mahogany (*Cercocarpus ledifolius*) woodlands, and quaking aspen (*Populus tremuloides*), Engelmann spruce (*Picea engelmannii*), white fir (*Abies concolor*), and subalpine fir (*Abies lasiocarpa*) forests. The area has seen significant changes in vegetation conditions over the past few decades, including widespread beetle-induced Engelmann spruce mortality, and aspen decline due to decreased fire frequency and increased grazing (USDA Forest Service, 2017). In recent years, along with a number of partner organizations, the Forest Service has enacted extensive forest management in the Monroe Mountain area, including mechanical treatment and prescribed burning, to promote aspen regeneration. These changes have combined to produce a landscape mosaic of diverse forest types and conditions in both the understory and overstory.

3.4.2 Field data

3.4.2.1 Field site selection

In order to facilitate direct comparison to the lidar data, field data were collected exactly one year after the lidar data were acquired (between August and September of 2017). Field sites had to meet the following criteria to facilitate accessibility, promote data collection efficiency, and reduce potential edge effects. Sites had to be: (1) within

.

100 m of major roads; (2) at least 25 m from all roads and water features; (3) on slopes of less than 10 degrees; and (4) on public lands. In addition, with the primary goal being to analyze understory vegetation in forested environments, sites had to be located within areas where vegetation equal to or greater than 2 m in height occupied at least 20% of a given 30 x 30 m area. This required the creation of a canopy height model (CHM) from lidar. A study area-wide CHM was generated at a 1 m spatial resolution as the difference between a digital terrain model, interpolated from lidar points classified as "ground" points, and a digital surface model, interpolated from all first-return lidar points. A binary tree vs. non-tree classification was performed using a 2 m CHM height threshold. The classification was then aggregated to 30 m to determine relative tree cover.

The combination of these site placement criteria resulted in a relatively small area of eligibility. Within this area of eligibility, we employed a conditioned Latin hypercube sampling (CLHS) strategy in order to capture a broad range of vegetation conditions. CLHS is a stratified random sampling procedure that enables the selection of samples that simultaneously maximize the variability captured in each of a defined set of variables (Minasny and McBratney, 2006). The variables we chose to include were: (1) lidar-derived elevation; (2) lidar-derived understory (0.15 – 1.85 m) NRD (NRD_{under}); (3) lidar-derived overstory (> 1.85 m) NRD (NRD_{over}); (4) lidar-derived vegetation height; and (5) Landsat 8 OLI-derived normalized difference vegetation index. All lidar data processing was performed using *LAStools* (Isenburg, 2015).

Fifty sample points were placed within the area of eligibility using the CLHS algorithm, as implemented in the *clhs* package in R statistical software (R Core Team, 2016; Roudier, 2017) (Figure 3.3). Each point was then converted to a 10 m transect line,

.

by extending a line 5 m in each direction perpendicular to the terrain slope (along the contour), to ensure relatively flat transects.

3.4.2.2 Cover board photos

Cover boards are most often designed to facilitate visual photo interpretation, typically comprising a grid of alternately-colored boxes, like a checkerboard. Thus, when analyzing a cover board photo, one can readily judge how many boxes, or what portions of each box, are covered by vegetation, the averaging of which can provide an estimate of overall cover for the entire board. However, in order to reduce the potential for interpretation error and/or observer bias in cover estimation, we opted to create a cover board that could be analyzed in an objective, automated fashion. To do so, the board needed to be both easily distinguished from natural vegetation, and a single, uniform color. Through preliminary experimentation it was determined that a magenta-colored cover board would be highly spectrally separable from vegetation. Accordingly, we created a 1.5 x 1.5 m magenta cover board using heavy-duty canvas and PVC pipes (Figure 3.4). In addition, our preliminary work highlighted the fact that small differences in viewing angle could result in significant differences in the resultant cover estimate. Accordingly, we created a 1.5 x 1.5 m photo viewing grid, also using canvas and PVC, with 25 equally-spaced viewing holes through which cover board photos would be taken (Figure 3.4).

We navigated to each transect start point, staked the photo viewing grid into the ground, and collected a GPS point using a Trimble Geo7x with 200+ point averaging. We then used a tape to measure 10 m from the start point to the end point using a compass to navigate in the direction of the azimuth defined during the transect generation process.

.

We then staked the cover board into the ground and collected another GPS point. Lastly, we took photos through each of the viewing grid holes towards the cover board, totaling 25 photos per site using a SONY HX-50V digital camera, with a fixed, 8X optical zoom.

3.4.2.3 Photo classification

As a result of the field data collection effort, there were 1250 cover board photos (50 sites x 25 photos). Rather than attempt to visually estimate the cover in each of these photos, an automated "board" vs. "non-board" classification was performed as follows. A program was written in R using the *raster* package (Hijmans et al., 2016) to load each photo sequentially, and generate 4 random points within a square area generally occupied by the cover board (square length and height equal to 2/3 of the photo height). Each point was then visually interpreted as either "board" or "non-board". "Non-board" is an inclusive class that represents pixels containing anything besides the cover board, primarily live and dead vegetation. There were 5000 photo interpreted points in total, 4800 of which were randomly designated as training data, and 200 of which were designated as accuracy assessment data (100 "board" points, 100 "non-board" points).

For each of the 4800 training points, red, green, and blue (RGB) pixel value means were extracted within a 5x5 pixel square immediately surrounding it. A number of derivative variables were also calculated to improve classification accuracy (Table 3.1). We performed a stepwise logistic regression, beginning with a full model that contained all of the independent variables in Table 3.1 and iteratively removing them until an optimal balance between model complexity and variance explained, as approximated by the Akaike Information Criterion (AIC). The resulting model was used to classify "board" and "non-board" in all 1250 photos. We assessed overall and class-specific

.

user's and producer's accuracies of the photo classification using the accuracy assessment data.

Given that every photo was taken from a fixed distance (10 m), with a consistent zoom (8x), towards a board of the same size (1.5 x 1.5 m), relative cover could be easily calculated, provided that a relative scale could be determined between photo pixel size and cover board size. To calculate this scale, we first needed to identify a single photo from each transect that had at least one entire cover board dimension (either a full width or height) visible. There were only 4 transects where no such dimensions were clearly visible. For the remaining 46, a measurement was taken in Adobe Photoshop of equivalent number of pixels for each cover board height or width, depending on which was more clearly visible. From this, an effective per-pixel area could be calculated. This effective pixel area was then multiplied by the number of pixels classified as "board" for each photo, which was then compared to the entire board area (2.25 m^2) to determine relative cover. Overall understory cover was then calculated for each transect by taking the mean value for all 25 photos.

3.4.3 GIS and lidar data processing

The GPS points representing transect start and end points were differentially corrected using base station data from nearby Scipio, UT and converted to shapefile format for use in GIS. A line was drawn between points representing the transect, and a buffer created around each transect within which the lidar data would be analyzed. A 0.75 m rectangular buffer was generated around the transect line to represent the precise area between cover board and photo grid (10 m long x 1.5 m wide). However, given the small

.

uncertainty in the GPS data, we performed an additional buffer around the rectangle of 0.25 m (Figure 3.5).

Lidar point cloud data were extracted within each transect plus GPS uncertainty buffer. The following metrics were derived for each transect point cloud: (1) understory NRD from 0.15 – 1.85 m (NRD_{under}); (2) understory ORD from 0.15 – 1.85 m (ORD_{under}); (3) overstory ORD from > 1.85 m (ORD_{over}); (4) 95^{th} height percentile; and (5) pulse density. Even though the cover board ranged in height from 0.25 – 1.75 m, we opted to add 10 cm to both ends to account for small uncertainty in the vertical accuracy of lidar returns and to create a more inclusive voxel to increase the number of point returns analyzed. We did not calculate overstory NRD because overstory ORD and NRD are the same metric, since it was inclusive of all points higher than 1.85 m.

3.4.4 Analysis

In order to assess their respective abilities to predict understory vegetation density, individual ordinary least squares regression models were generated for ORD_{under} and NRD_{under}. Both ORD and NRD displayed non-normal, right-skewed distributions. Accordingly, log regression was performed in both cases. The models were compared according to the degree to which the lidar-based independent variables were able to explain variance in the cover board-based dependent variable, as approximated by R^2, and AIC.

In order to determine the relative effects of lidar pulse density, overstory vegetation density, and canopy height, we performed a bootstrapping analysis. Ten-thousand random samples of 20 were taken from the 50 original transect-level data points, without replacement. For each sample data subset, the mean pulse density, the

.

mean overstory ORD, and the mean 95th height percentile were calculated. In addition, a regression model was generated comparing understory NRD (independent variable) to cover board cover (dependent variable) for each subset as well, from which R^2 values were computed. We then compared the subset data pulse density, overstory ORD, and 95th height percentile to the resultant model R^2 in a series of individual ordinary least squares regression analyses to determine the relative effects of these variables on the degree to which understory NRD can predict understory vegetation density in a series of regression analyses. Lastly, in order to account for the potentially confounding effects arising from correlation between overstory ORD and 95th height percentile, we performed a multiple regression containing all three predictor variables (pulse density, overstory ORD, and 95th height percentile).

3.5 Results

In total, 1250 photos were classified according to a binary "board" vs. "non-board" classification (Figure 3.6). Of the 18 spectral variables generated for each photo, a stepwise regression algorithm determined that a combination of 8 variables was best for distinguishing between those image pixels that contained primarily board and those that contained primarily non-board (predominantly vegetation) (Table 3.2). Each predictor variable was significant at a level of $\alpha = 0.1$. The model coefficients were used to develop a prediction equation, such that:

$$y = 0.039R - 0.077G + 0.052B + 423.9R_{norm} + 8.678NDGB + 57.57NDBR - 237.0NDMC - 62.63NDYM - 0.015 \quad (3.3)$$

.

where variable names are listed in Table 3.2. Resulting pixel values greater than or equal to 0.5 were classified as board (1); those pixels with values less than 0.5 were classified as non-board (0). Randomly-selected accuracy assessment points were compared to the resultant classification (Table 3.3). Overall accuracy was high, at 97.5%. Inaccuracies arose solely in the commission of pixels classified as non-board, suggesting that the resulting classified images tended to slightly overestimate cover by a small margin.

For each transect, a single density estimate was obtained by taking the mean percent cover for each of the 25 gridded photos. Transect-level cover board density was then compared to lidar-derived ORD_{under} and NRD_{under} (Figure 3.7). NRD_{under} far outweighed ORD_{under} in terms of predictive power (R^2: 0.442 vs. 0.137) and model quality (AIC: -15.802 vs. 5.966). ORD_{under} bore almost no recognizable relationship to cover board density (Figure 3.7a).

The results of the bootstrapping analysis to determine the relative effects of pulse density, overstory vegetation density, and canopy height on the ability to accurately model understory density can be seen in Figure 3.8 and Table 3.4. Although there is much spread in the resulting scatterplots, each variable was found to have a statistically significant relationship to the NRD-cover board density model R^2 values in a multiple regression environment ($\alpha = 0.001$). As the standardized coefficients suggest, pulse density had the effect of greatest magnitude on R^2, followed by overstory density and canopy height, which had very similar effects. Accordingly, as pulse density increases, the ability to model understory density using lidar NRD_{under} increases. Conversely, as overstory vegetation density (as approximated by lidar ORD_{over}) increases, the ability to model understory density using lidar NRD_{under} decreases. And lastly, as canopy height (as

.

approximated by lidar 95th height percentile) increases, the ability to model understory density using lidar NRD_{under} decreases.

3.6 Discussion

Lidar is unique in its ability to characterize understory structure at a high spatial resolution across broad tracts of forest land. While this ability has widespread application in fields ranging from wildlife biology to wildland firefighter safety, there are some key considerations that require addressing before engaging in such an analysis. We have presented and quantified the effects of a number of these considerations in this study. The first consideration is the selection of appropriate understory lidar metrics for use in modeling understory vegetation density. Throughout the literature, there have been a wide array of metrics used for characterizing understory vegetation (Evans et al., 2009). In nearly every study we found, researchers used some form of a vertically-stratified lidar point density measure as either the single, or one of many predictor variables. The underlying assumption of such a measure is that denser vegetation in a given height stratum will have a greater likelihood that a given lidar pulse will interact with vegetative surfaces. Thus, an assessment of the relative proportion of lidar point returns that fall in that same height stratum should provide some information about the density of vegetation. Relative proportion, however, can be calculated in two primary ways: (1) number of points in a height stratum relative to the total number of points in a given area (overall relative point density, or ORD), and (2) number of points in a height stratum relative to the number of points in that stratrum and below (normalized relative point density, or NRD).

.

There is no agreement in the lidar literature about which metric should be used, as researchers have seemingly used ORD and NRD with relatively equal frequency and no one has yet compared the predictive power of the two. We compared ORD to NRD for their respective abilities in predicting understory density as measured in the field, finding that NRD was far superior in this regard. NRD was able to explain nearly half of the variance in field-measured understory density, whereas ORD explained next to none. This significant difference is likely a result of overstory conditions. The very nature of understory vegetation suggests that there is overlying vegetation. Many authors have pointed to the fact that overstory vegetation can result in lidar pulse energy occlusion, thus limiting the ability to characterize understory conditions. NRD accounts for differences in overstory vegetation, as it only takes into consideration those portions of a given lidar pulse that have already penetrated the canopy in computing relative proportion. ORD does not. Accordingly, if one's goal is to characterize understory conditions in a forested environment – particularly one with a dense overstory – the results of our study suggest using NRD. In the absence of an overstory, however, NRD and ORD are, in fact, the exact same measure.

The results of our study also suggest that NRD, though preferable to ORD, does not account for all overstory effects. The very fact that NRD only accounted for roughly half of the variance in field-measured density highlights this fact. Accordingly, we examined the effects of two overstory conditions on understory model fit. Using a bootstrapping analysis, we found that as overstory density and canopy height increase, the ability to effectively model understory conditions decreases. In addition, as pulse density increases, so too does the ability to model understory conditions. Thus, it comes

.

as no surprise that the superior ability of NRD to accurately quantify understory density is maximized with a high pulse density lidar dataset in areas with shorter, sparser canopies. For example, if we take the uppermost 97.5 percentile of pulse density (17.90 pulses/m^2) and the lowermost 2.5 percentile of overstory density (0.38) and canopy height (9.04 m) in our bootstrapped data – representing "ideal" conditions while avoiding extrapolation – the resultant R^2 for using NRD to predict understory would be 0.59, according to our multiple regression results. Presumably, with an even higher pulse density, and even lower overstory density and canopy height, this relationship could improve even more.

However, even in these optimal conditions, a noteworthy amount of variance is still left unexplained. There are several reasons why this may be the case. First, as in all lidar-based studies but particularly in those that examine near-ground vegetation conditions, the accuracy of the classification between ground and non-ground points is critical (Meng et al., 2010). The ground point classification is the basis upon which lidar point aboveground heights are calculated prior to calculation of metrics for predictive modeling. Particularly when working in as narrow of a height range with a low-end threshold as low as we did in this study (0.15 – 1.85 m), a few misclassified ground points can have a dramatic effect on resultant NRD calculations. The dataset we used in this study has a self-reported vertical root mean square error of 6.1 cm for ground points, and a 95% confidence interval of ± 11.9 cm. Thus, it is highly likely that some of the points we considered aboveground vegetation were in fact ground points, and vice versa. In this study area in particular, there was an abundance of downed coarse woody debris,

.

which a ground filtering algorithm may have difficulty distinguishing from the ground (Pesonen et al., 2008).

A second factor than may have negatively impacted the lidar-understory density relationship found in our study stems from the nature of our field data. As discussed earlier, cover boards are an invaluable tool for characterizing understory conditions, widely used for their efficiency of implementation, conceptual simplicity, and applicability in a range of disciplines. Our study represents one of the first attempts at using cover boards as ground reference data for direct comparison to lidar, with Kramer et al. (2016) being the only other published example to date. While it shows great promise as a source of training and validation data, there are limitations that emerge, primarily from the effects of viewing geometry. To avoid biasing our dataset towards open understories, we made every attempt to place our viewing grid on the precise, computer-generated GPS location to the extent that it was physically possible. Likewise, we attempted to place the cover board exactly 10 m from the viewing grid along a pre-defied azimuth. While this facilitated an unbiased sample, occasionally it resulted in, for example, the viewing grid falling right behind the bole of a tree. Thus, even in a relatively open stand, cover could appear relatively high, due to the relationship between viewing geometry and tree proximity. Figure 3.9 demonstrates one such example, where mean cover is increased almost entirely due to the presence of a single tree bole. Our use of a 25-photo, multi-angle viewing grid was explicitly aimed at reducing these effects. And, in fact, the calculation of standard deviation between individual photo cover estimates allowed us to quantify the effects of this viewing geometry-based structural complexity on lidar-understory density model fit. As can be seen in Figure 3.10, as

.

structural complexity increases, the ability to accurately characterize understory density using lidar decreases.

3.7 Conclusions

Lidar is an incredibly powerful remote sensing dataset capable of assessing a wide range of vegetation structural conditions; however, it is not without its limitations. In this study, we inquired into several important considerations that studies aimed at quantifying understory structure in forested environments must take into account. Specifically, we highlight that lidar NRD is far superior to ORD in terms of its modeling capacity. This is a particularly impactful result, as no one has yet quantitatively compared the two, and yet each is widely used throughout the lidar literature. We also provide robust, quantitative backing to the oft-cited but scarcely-quantified effects of pulse density, overstory vegetation density, and canopy height on the ability to characterize forest understory vegetation density.

Although every attempt was made to maximize the variety of conditions sampled in our study, continued study is needed in a broader range of vegetation conditions – especially overstory conditions – to expand the spatial applicability of the results we obtained from our study area in Monroe Mountain, UT. In addition, while the use of cover boards as ground reference data for lidar-based quantification of understory vegetation density is promising, more research is required to determine methodological optimality (e.g. plot layout, board material/color/dimensions).

.

Table 3.1. Spectral variables used in stepwise logistic regression to classify board vs. non-board on cover board photos.

Variable	Abbreviation	Calculation
Red	R	8-bit R pixel mean
Green	G	8-bit G pixel mean
Blue	B	8-bit B pixel mean
Normalized red	R_{norm}	R / (R + G + B)
Normalized green	G_{norm}	G / (R + G + B)
Normalized blue	B_{norm}	B / (R + G + B)
Magenta	M	(R + B) / 2
Cyan	C	(B + G) / 2
Yellow	Y	(G + R) / 2
Normalized magenta	M_{norm}	M / (M + C + Y)
Normalized cyan	C_{norm}	C / (M + C + Y)
Normalized yellow	Y_{norm}	Y / (M + C + Y)
Normalized difference red-green	NDRG	(R – G) / (R + G)
Normalized difference green-blue	NDGB	(G – B) / (G + B)
Normalized difference blue-red	NDBR	(B – R) / (B + R)
Normalized difference magenta-cyan	NDMC	(M – C) / (M + C)
Normalized difference cyan-yellow	NDCY	(C – Y) / (C + Y)
Normalized difference yellow-magenta	NDYM	(Y – M) / (Y + M)

.

Table 3.2. Stepwise logistic regression model results for cover board photo classification. Null deviance = 6131.12 on 4799 degrees of freedom. Residual deviance = 658.92 on 4791 degrees of freedom.

Model Parameter	Coefficient	Standard Error	z value	p
Intercept	-0.015	38.00	-3.907	< 0.001
R	0.039	0.009	4.456	< 0.001
G	-0.077	0.015	-5.127	< 0.001
B	0.052	0.016	3.323	< 0.001
R_{norm}	423.9	113.6	3.730	< 0.001
NDGB	8.678	4.980	1.743	0.081
NDBR	57.57	24.56	2.344	0.019
NDMC	-237.0	58.06	-4.082	< 0.001
NDYM	-62.63	16.24	-3.856	< 0.001

.

Table 3.3. Cover board photo classification accuracy assessment.

		Reference data		Accuracy		
		Board	*Non-board*	*User*	*Producer*	*Overall*
Classified data	*Board*	95	0	100.0%	95.0%	97.5%
	Non-board	5	100	95.2%	100.0%	

.

Table 3.4. Results of multiple regression analysis between bootstrapped R^2 values and pulse density, overstory density, and canopy height ($R^2 = 0.104$, $p < 0.001$).

Model Parameter	Coefficient	Standardized Coefficient	Standard Error	t value	p
Intercept	0.029	0.476	0.054	0.525	0.6
Pulse density	0.050	0.024	0.003	17.64	< 0.001
Overstory density	-0.489	-0.018	0.048	-10.15	< 0.001
Canopy height	-0.017	-0.017	0.002	-9.281	< 0.001

.

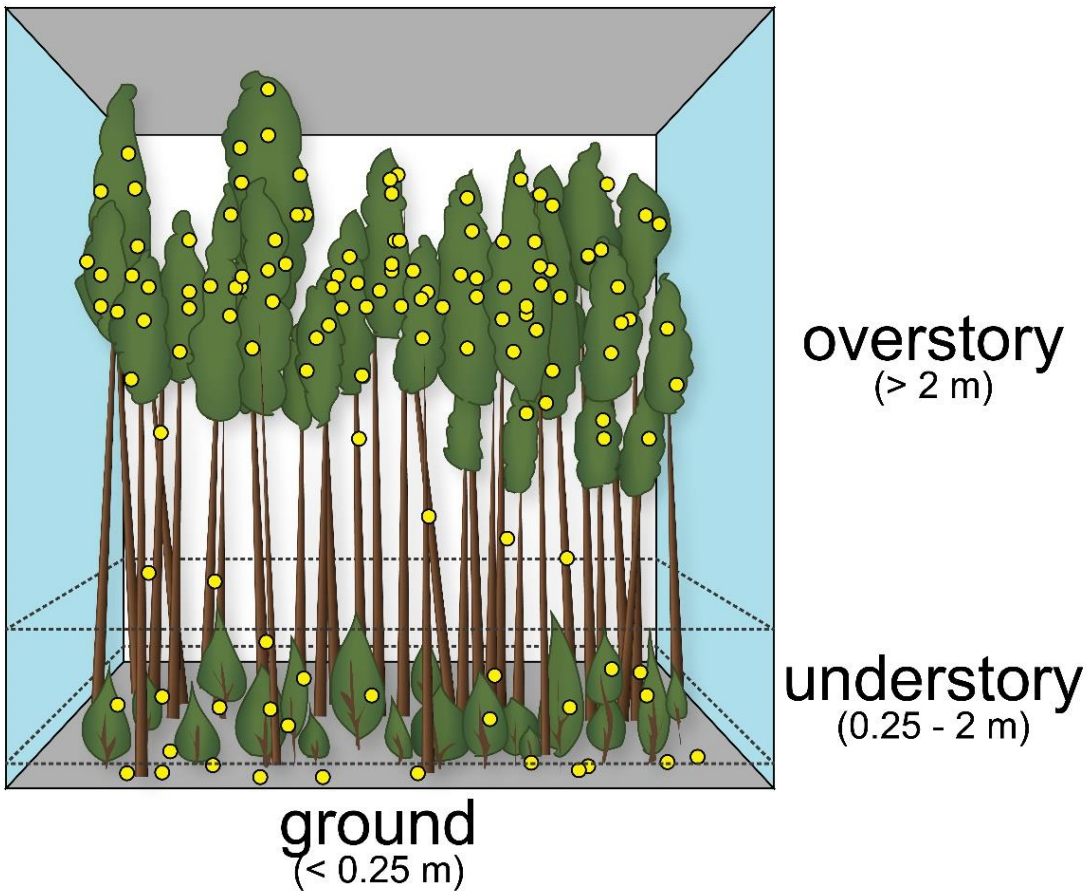

Figure 3.1. Three-dimensional lidar point cloud example of a multi-aged lodgepole pine (*Pinus contorta*) forest stand containing both a dense overstory and understory. The yellow circles represent simulated lidar point returns. The dotted lines distinguish between vertical strata representing ground returns (< 0.25 m), understory returns (0.25 – 2 m), and overstory returns (> 2 m).

.

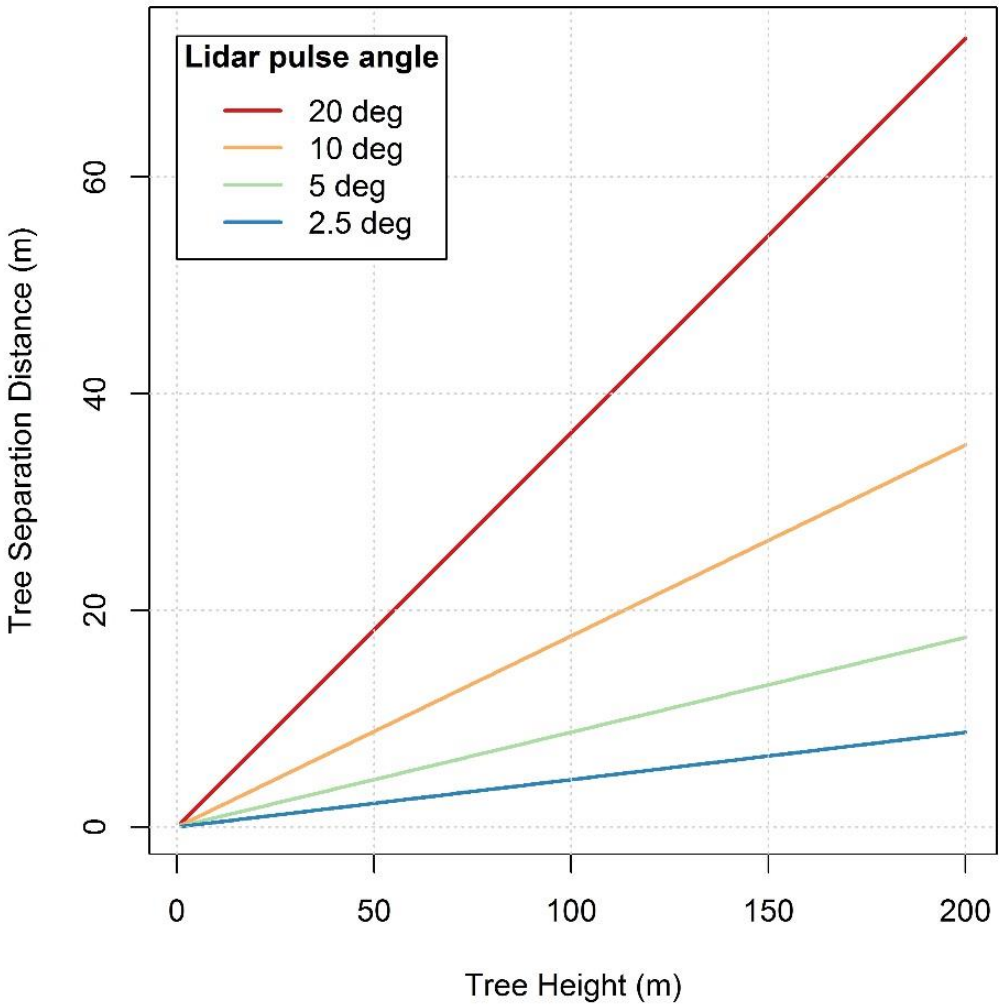

Figure 3.2. The relationship between tree height and theoretical tree separation distance under which individual lidar pulses could interact with multiple trees at various scan angles.

.

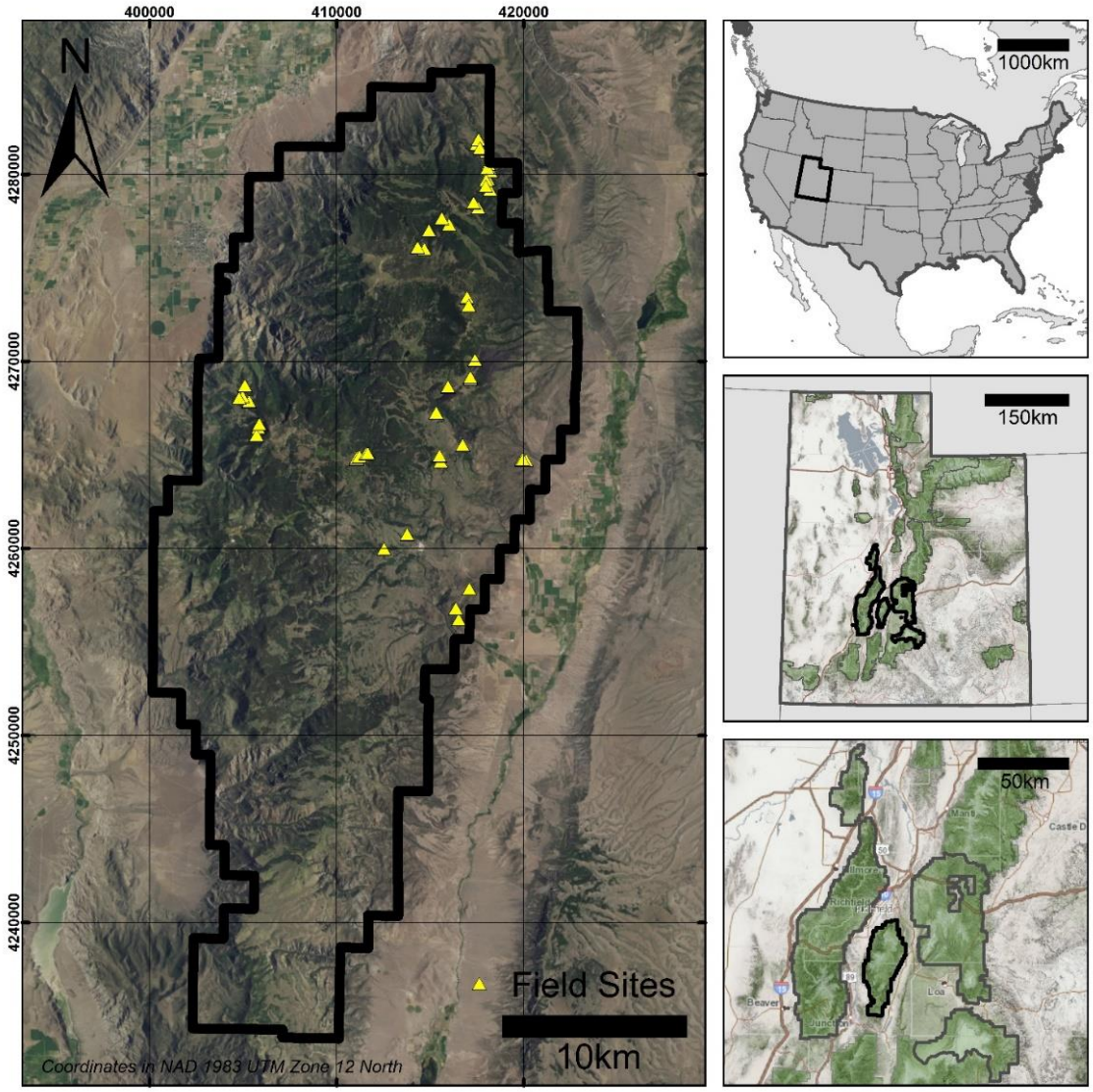

Figure 3.3. Study area map. Monroe Mountain area of Fishlake National Forest outlined in black.

.

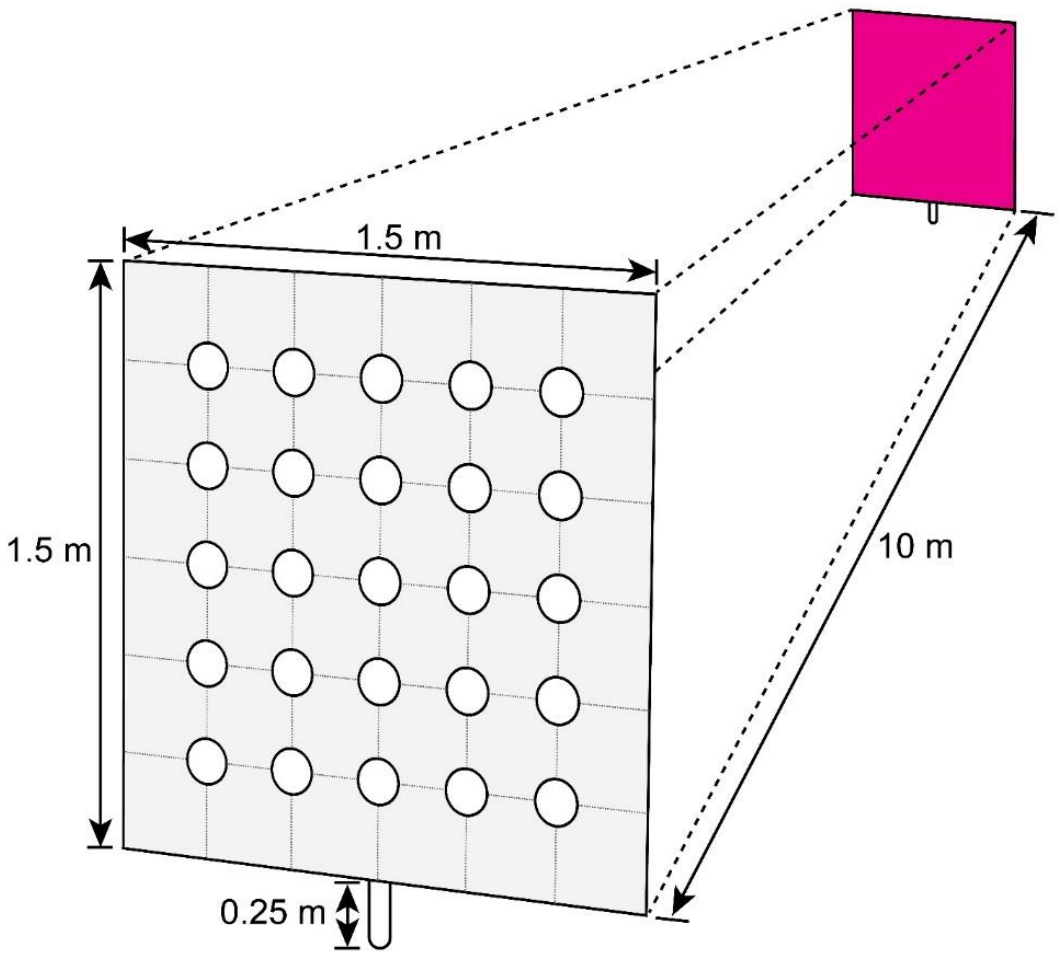

Figure 3.4. Cover board photo setup.

.

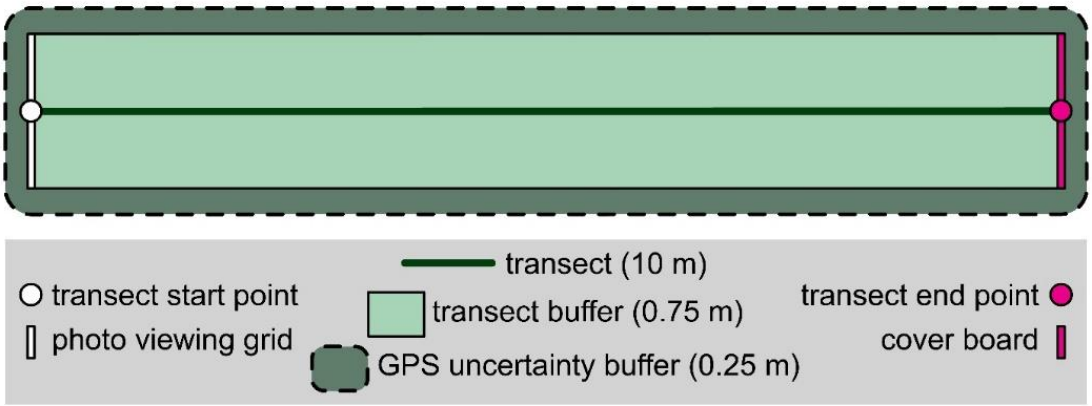

Figure 3.5. Transect layout.

.

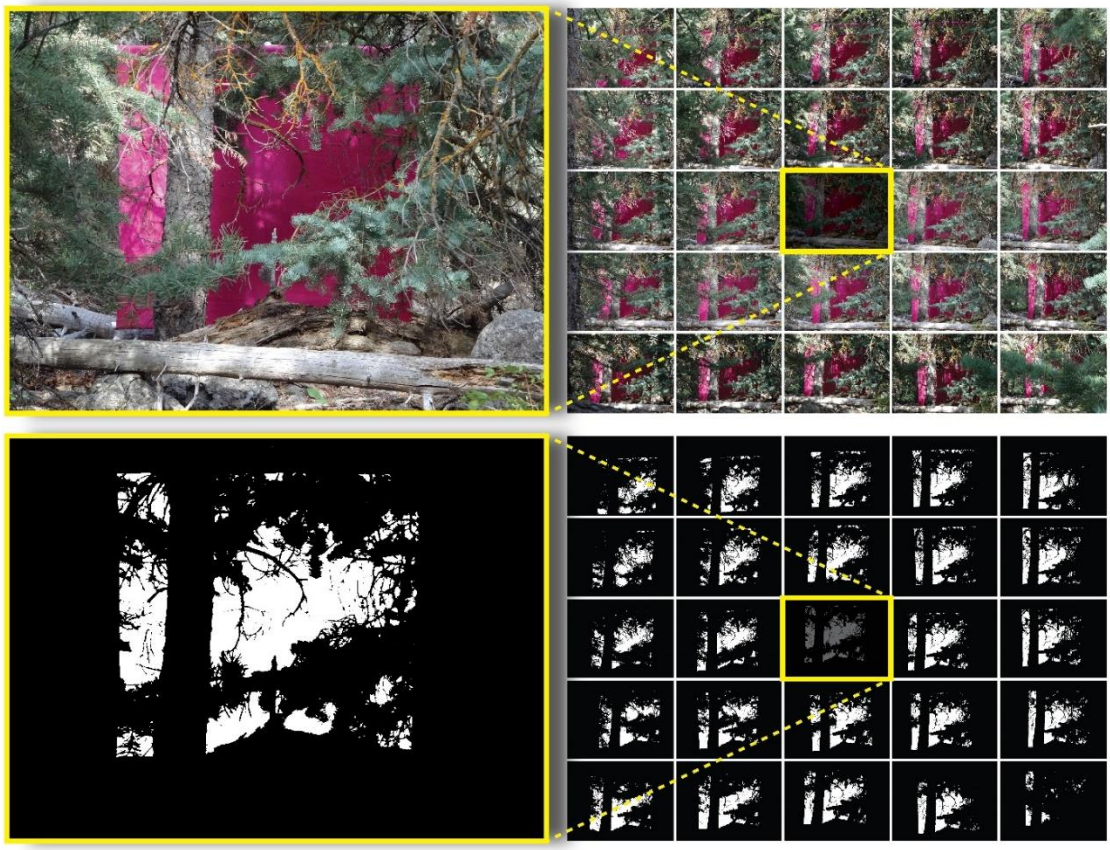

Figure 3.6. Cover board photo classification example results. In the lower two panels, white indicates pixels classified as “board” and black indicates pixels classified as “non-board”.

.

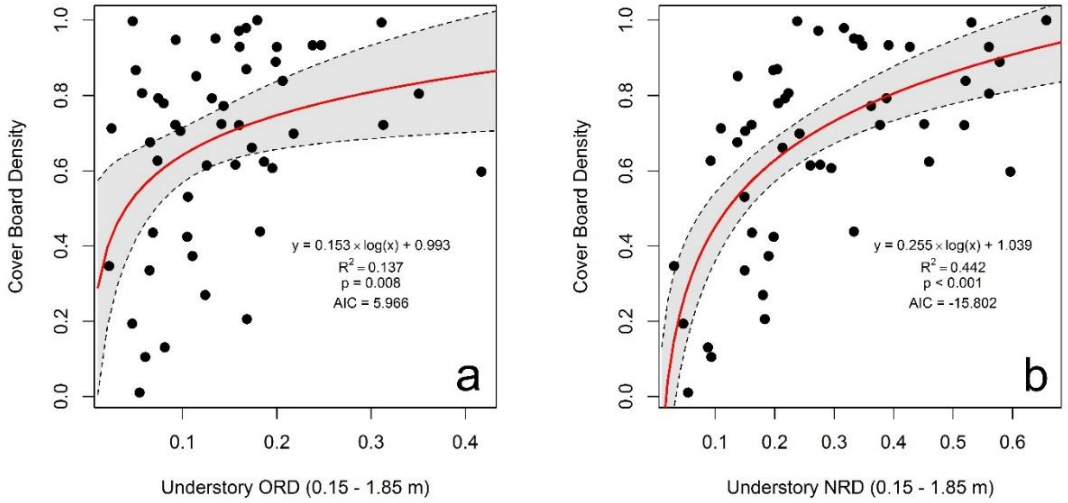

Figure 3.7. Comparison between ordinary least squares regression models predicting cover board density using lidar-based understory overall relative point density (ORD) (a) and normalized relative point density (NRD) (b).

.

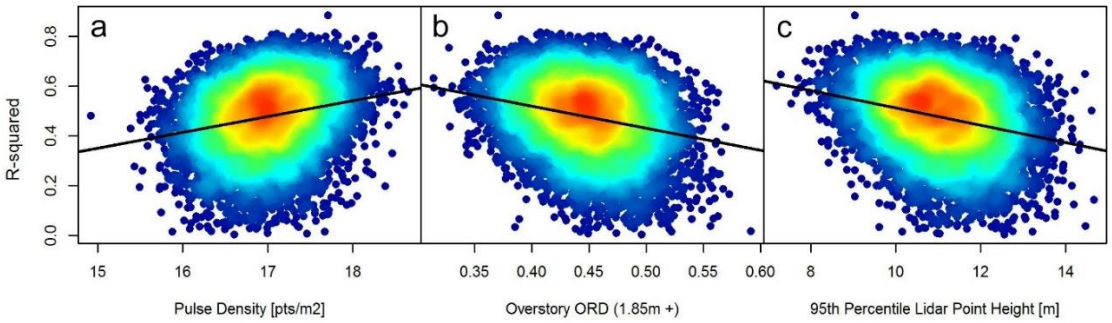

Figure 3.8. The bootstrapped effect of lidar pulse density (a), overstory canopy density (as approximated by lidar overall relative point density of all points higher than 1.85 m) (b), and canopy height (as approximated by 95th percentile of lidar point return height) (c) on the ability of lidar to model understory cover (as approximated by the amount of variance in cover board cover explained by lidar understory normalized relative point density).

.

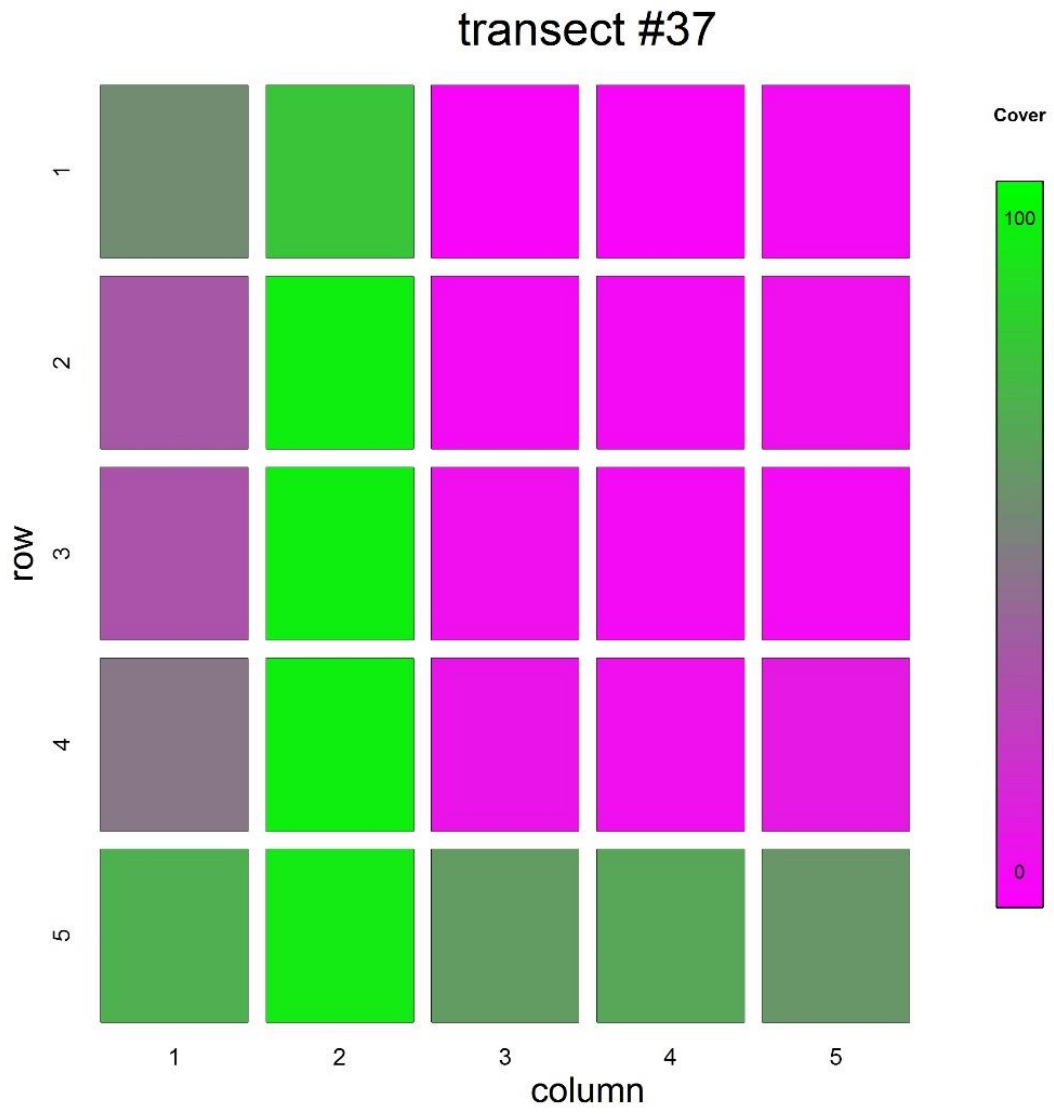

Figure 3.9. Photo-by-photo cover estimates for an example transect that demonstrate the effect that a single tree can have on overall, transect-level cover estimates.

.

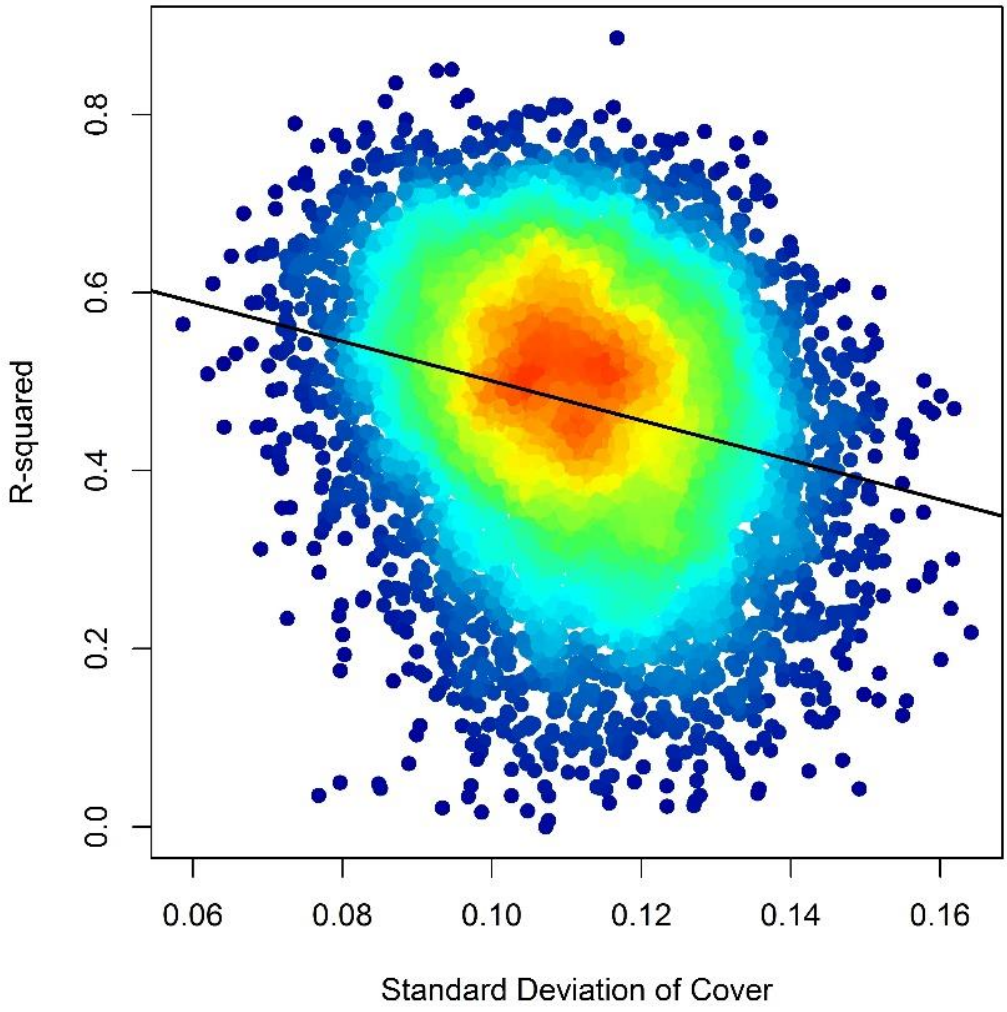

Figure 3.10. The effect of understory complexity, as approximated by the standard deviation of cover derived from individual photo cover estimates, on the ability to characterize understory density using lidar NRD.

.

3.8 References

Ahmed, O.S., Franklin, S.E., Wulder, M.A., White, J.C., 2015. Characterizing stand-level forest canopy cover and height using Landsat time series, samples of airborne LiDAR, and the Random Forest algorithm. ISPRS Journal of Photogrammetry and Remote Sensing 101, 89–101.

Alexander, C., Moeslund, J.E., Bøcher, P.K., Arge, L., Svenning, J.-C., 2013. Airborne laser scanner (LiDAR) proxies for understory light conditions. Remote Sensing of Environment 134, 152–161.

Anderson, H.E., 1982. Aids to determining fuel models for estimating fire behavior (General Technical Report No. INT-122). USDA Forest Service, Intermountain Forest and Range Experiment Station, Ogden, UT.

Bartemucci, P., Messier, C., Canham, C.D., 2006. Overstory influences on light attenuation patterns and understory plant community diversity and composition in southern boreal forests of Quebec. Canadian Journal of Forest Research 36, 2065–2079.

Ben-Arie, J.R., Hay, G.J., Powers, R.P., Castilla, G., St-Onge, B., 2009. Development of a pit filling algorithm for LiDAR canopy height models. Computers & Geosciences 35, 1940–1949.

Booth, D.T., Cox, S.E., Johnson, D.E., 2005. Detection-threshold calibration and other factors influencing digital measurements of ground cover. Rangeland Ecology & Management 58, 598–604.

Boyd, C.S., Svejcar, T., 2005. A visual obstruction technique for photo monitoring of willow clumps. Rangeland Ecology & Management 58, 434–438.

Brandtberg, T., 2007. Classifying individual tree species under leaf-off and leaf-on conditions using airborne lidar. ISPRS Journal of Photogrammetry and Remote Sensing 61, 325–340.

Bright, B.C., Hudak, A.T., McGaughey, R., Andersen, H.-E., Negrón, J., 2013. Predicting live and dead tree basal area of bark beetle affected forests from discrete-return lidar. Canadian Journal of Remote Sensing 39, S99–S111.

Campbell, M.J., Dennison, P.E., Butler, B.W., 2017a. A LiDAR-based analysis of the effects of slope, vegetation density, and ground surface roughness on travel rates for wildland firefighter escape route mapping. International Journal of Wildland Fire 26, 884-895.

.

Campbell, M.J., Dennison, P.E., Butler, B.W., 2017b. Safe separation distance score: a new metric for evaluating wildland firefighter safety zones using lidar. International Journal of Geographical Information Science 31, 1448–1466.

Carlyle, C.N., Fraser, L.H., Haddow, C.M., Bings, B.A., Harrower, W., 2010. The use of digital photos to assess visual cover for wildlife in rangelands. Journal of Environmental Management 91, 1366–1370.

Chasmer, L., Hopkinson, C., Treitz, P., 2006. Investigating laser pulse penetration through a conifer canopy by integrating airborne and terrestrial lidar. Canadian Journal of Remote Sensing 32, 116–125.

Chen, Q., Gong, P., Baldocchi, D., Tian, Y.Q., 2007. Estimating Basal Area and Stem Volume for Individual Trees from Lidar Data. Photogrammetric Engineering & Remote Sensing 73, 1355–1365.

Clark, M.L., Clark, D.B., Roberts, D.A., 2004. Small-footprint lidar estimation of sub-canopy elevation and tree height in a tropical rain forest landscape. Remote Sensing of Environment 91, 68–89.

Clark, M.L., Roberts, D.A., Ewel, J.J., Clark, D.B., 2011. Estimation of tropical rain forest aboveground biomass with small-footprint lidar and hyperspectral sensors. Remote Sensing of Environment, DESDynI VEG-3D Special Issue 115, 2931–2942.

Collins, W.B., Becker, E.F., 2001. Estimation of horizontal cover. Journal of Range Management 54, 67–70.

Dalponte, M., Bruzzone, L., Gianelle, D., 2011. A system for the estimation of single-tree stem diameter and volume using multireturn LIDAR Data. IEEE Transactions on Geoscience and Remote Sensing 49, 2479–2490.

Drake, J.B., Dubayah, R.O., Clark, D.B., Knox, R.G., Blair, J.B., Hofton, M.A., Chazdon, R.L., Weishampel, J.F., Prince, S., 2002. Estimation of tropical forest structural characteristics using large-footprint lidar. Remote Sensing of Environment, Recent Advances in Remote Sensing of Biophysical Variables 79, 305–319.

Duebbert, H.F., Lokemoen, J.T., 1976. Duck nesting in fields of undisturbed grass-legume cover. The Journal of Wildlife Management 40, 39–49.

Eskelson, B.N.I., Madsen, L., Hagar, J.C., Temesgen, H., 2011. Estimating riparian understory vegetation cover with beta regression and copula models. Forest Science 57, 212–221.

.

Estornell, J., Ruiz, L.A., Velázquez-Martí, B., Fernández-Sarría, A., 2011. Estimation of shrub biomass by airborne LiDAR data in small forest stands. Forest Ecology and Management 262, 1697–1703.

Evans, J.S., Hudak, A.T., Faux, R., Smith, A.M.S., 2009. Discrete return lidar in natural resources: Recommendations for project planning, data processing, and deliverables. Remote Sensing 1, 776–794.

Falkowski, M.J., Hudak, A.T., Crookston, N.L., Gessler, P.E., Uebler, E.H., Smith, A.M.S., 2010. Landscape-scale parameterization of a tree-level forest growth model: a k-nearest neighbor imputation approach incorporating LiDAR data. Canadian Journal of Forest Research 40, 184–199.

Falkowski, M.J., Smith, A.M.S., Gessler, P.E., Hudak, A.T., Vierling, L.A., Evans, J.S., 2008. The influence of conifer forest canopy cover on the accuracy of two individual tree measurement algorithms using lidar data. Canadian Journal of Remote Sensing 34, S338–S350.

Goodwin, N.R., Coops, N.C., Bater, C., Gergel, S.E., 2007. Assessment of sub-canopy structure in a complex coniferous forest, in: Proceedings of the ISPR Workshop "Laser Scanning 2007 and SilviLaser 2007", Espoo, September 12–14, 2007, Finland. pp. 169–172.

Griffith, B., Youtie, B.A., 1988. Two devices for estimating foliage density and deer hiding cover. Wildlife Society Bulletin (1973-2006) 16, 206–210.

Higgins, K.F., Jenkins, K.J., Clambey, G.K., Uresk, D.W., Naugle, D., Norland, J., Barker, W.T., 2005. Vegetation sampling and measurement, in: Techniques for Wildlife Investigations and Management. The Wildlife Society, Bethesda, MD, pp. 524–553.

Hijmans, R.J., Etten, J. van, Cheng, J., Mattiuzzi, M., Sumner, M., Greenberg, J.A., Lamigueiro, O.P., Bevan, A., Racine, E.B., Shortridge, A., 2016. raster: Geographic Data Analysis and Modeling.

Hill, R.A., Broughton, R.K., 2009. Mapping the understory of deciduous woodland from leaf-on and leaf-off airborne LiDAR data: A case study in lowland Britain. ISPRS Journal of Photogrammetry and Remote Sensing 64, 223–233.

Holmgren, J., Nilsson, M., Olsson, H., 2003. Simulating the effects of lidar scanning angle for estimation of mean tree height and canopy closure. Canadian Journal of Remote Sensing 29, 623–632.

Hopkinson, C., Chasmer, L., Lim, K., Treitz, P., Creed, I., 2006. Towards a universal lidar canopy height indicator. Canadian Journal of Remote Sensing 32, 139–152.

.

Hudak, A.T., Crookston, N.L., Evans, J.S., Falkowski, M.J., Smith, A.M.., Gessler, P.E., Morgan, P., 2006. Regression modeling and mapping of coniferous forest basal area and tree density from discrete-return lidar and multispectral satellite data. Canadian Journal of Remote Sensing 32, 126–138.

Hudak, A.T., Crookston, N.L., Evans, J.S., Hall, D.E., Falkowski, M.J., 2008. Nearest neighbor imputation of species-level, plot-scale forest structure attributes from LiDAR data. Remote Sensing of Environment, Earth Observations for Terrestrial Biodiversity and Ecosystems Special Issue 112, 2232–2245.

Isenburg, M., 2015. LAStools. rapidlasso GmbH, Gilching, Germany.

Jones, R.E., 1968. A board to measure cover used by prairie grouse. The Journal of Wildlife Management 32, 28–31.

Jorgensen, C.F., Stutzman, R.J., Anderson, L.C., E. Decker, S., Powell, L.A., Schacht, W.H., Fontaine, J.J., 2013. Choosing a DIVA: A comparison of emerging digital imagery vegetation analysis techniques. Applied Vegetation Science 16, 552–560.

Keane, R.E., 2014. Wildland Fuel Fundamentals and Applications. Springer.

Kerns, B.K., Ohmann, J.L., 2004. Evaluation and prediction of shrub cover in coastal Oregon forests (USA). Ecological Indicators 4, 83–98.

Khosravipour, A., Skidmore, A.K., Wang, T., Isenburg, M., Khoshelham, K., 2015. Effect of slope on treetop detection using a LiDAR Canopy Height Model. ISPRS Journal of Photogrammetry and Remote Sensing 104, 44–52.

Korhonen, L., Korpela, I., Heiskanen, J., Maltamo, M., 2011. Airborne discrete-return LIDAR data in the estimation of vertical canopy cover, angular canopy closure and leaf area index. Remote Sensing of Environment 115, 1065–1080.

Korpela, I., Hovi, A., Morsdorf, F., 2012. Understory trees in airborne LiDAR data — Selective mapping due to transmission losses and echo-triggering mechanisms. Remote Sensing of Environment 119, 92–104.

Korpela, I., Ørka, H., Maltamo, M., Tokola, T., Hyyppä, J., Tokola, M., Maltamo, T., 2010. Tree species classification using airborne LiDAR - Effects of stand and tree parameters, downsizing of training set, intensity normalization, and sensor type. Silva Fennica 44, 319–339.

Kramer, H.A., Collins, B.M., Lake, F.K., Jakubowski, M.K., Stephens, S.L., Kelly, M., 2016. Estimating ladder fuels: A new approach combining field photography with LiDAR. Remote Sensing 8, 766.

.

Latifi, H., Nothdurft, A., Koch, B., 2010. Non-parametric prediction and mapping of standing timber volume and biomass in a temperate forest: application of multiple optical/LiDAR-derived predictors. Forestry (Lond) 83, 395–407.

Lefsky, M.A., Harding, D., Cohen, W.B., Parker, G., Shugart, H.H., 1999. Surface lidar remote sensing of basal area and biomass in deciduous forests of eastern Maryland, USA. Remote Sensing of Environment 67, 83–98.

Limb, R.F., Hickman, K.R., Engle, D.M., Norland, J.E., Fuhlendorf, S.D., 2007. Digital photography: Reduced investigator variation in visual obstruction measurements for Southern Tallgrass Prairie. Rangeland Ecology & Management 60, 548–552.

Lone, K., Loe, L.E., Gobakken, T., Linnell, J.D.C., Odden, J., Remmen, J., Mysterud, A., 2014. Living and dying in a multi-predator landscape of fear: Roe deer are squeezed by contrasting pattern of predation risk imposed by lynx and humans. Oikos 123, 641–651.

Maltamo, M., Mustonen, K., Hyyppä, J., Pitkänen, J., Yu, X., 2004. The accuracy of estimating individual tree variables with airborne laser scanning in a boreal nature reserve. Canadian Journal of Forest Research 34, 1791–1801.

Maltamo, M., Packalén, P., Yu, X., Eerikäinen, K., Hyyppä, J., Pitkänen, J., 2005. Identifying and quantifying structural characteristics of heterogeneous boreal forests using laser scanner data. Forest Ecology and Management 216, 41–50.

Marsden, S.J., Fielding, A.H., Mead, C., Hussin, M.Z., 2002. A technique for measuring the density and complexity of understory vegetation in tropical forests. Forest Ecology and Management 165, 117–123.

Martinuzzi, S., Vierling, L.A., Gould, W.A., Falkowski, M.J., Evans, J.S., Hudak, A.T., Vierling, K.T., 2009. Mapping snags and understory shrubs for a LiDAR-based assessment of wildlife habitat suitability. Remote Sensing of Environment 113, 2533–2546.

Meng, X., Currit, N., Zhao, K., 2010. Ground filtering algorithms for airborne LiDAR data: A review of critical issues. Remote Sensing 2, 833–860.

Minasny, B., McBratney, A.B., 2006. A conditioned Latin hypercube method for sampling in the presence of ancillary information. Computers & Geosciences 32, 1378–1388.

Morrison, L.W., 2016. Observer error in vegetation surveys: a review. Journal of Plant Ecology 9, 367–379.

.

Morsdorf, F., Mårell, A., Koetz, B., Cassagne, N., Pimont, F., Rigolot, E., Allgöwer, B., 2010. Discrimination of vegetation strata in a multi-layered Mediterranean forest ecosystem using height and intensity information derived from airborne laser scanning. Remote Sensing of Environment 114, 1403–1415.

Musil, D.D., Reese, K.P., Connelly, J.W., 1994 Nesting and summer habitat use by translocated sage grouse (Centrocercus urophasianus) in Central Idaho. The Great Basin Naturalist 54, 228–233.

Mutlu, M., Popescu, S.C., Stripling, C., Spencer, T., 2008. Mapping surface fuel models using lidar and multispectral data fusion for fire behavior. Remote Sensing of Environment 112, 274–285.

Næsset, E., 2002. Predicting forest stand characteristics with airborne scanning laser using a practical two-stage procedure and field data. Remote Sensing of Environment 80, 88–99.

Nijland, W., Nielsen, S.E., Coops, N.C., Wulder, M.A., Stenhouse, G.B., 2014. Fine-spatial scale predictions of understory species using climate- and LiDAR-derived terrain and canopy metrics. Journal of Applied Remote Sensing 8, 083572.

Nudds, T.D., 1977. Quantifying the vegetative structure of wildlife cover. Wildlife Society Bulletin (1973-2006) 5, 113–117.

Penner, M., Pitt, D.G., Woods, M.E., 2013. Parametric vs. nonparametric LiDAR models for operational forest inventory in boreal Ontario. Canadian Journal of Remote Sensing 39, 426–443.

Pesonen, A., Maltamo, M., Eerikäinen, K., Packalèn, P., 2008. Airborne laser scanning-based prediction of coarse woody debris volumes in a conservation area. Forest Ecology and Management 255, 3288–3296.

Popescu, S.C., Wynne, R.H., Nelson, R.F., 2002. Estimating plot-level tree heights with lidar: local filtering with a canopy-height based variable window size. Computers and Electronics in Agriculture 37, 71–95.

R Core Team, 2016. R: A language and environment for statistical computing. R Foundation for Statistical Computing, Vienna, Austria.

Reutebuch, S.E., McGaughey, R.J., Andersen, H.-E., Carson, W.W., 2003. Accuracy of a high-resolution lidar terrain model under a conifer forest canopy. Canadian Journal of Remote Sensing 29, 527–535.

.

Riaño, D., Meier, E., Allgower, B., Chuvieco, E., Ustin, S.L., 2003. Modeling airborne laser scanning data for the spatial generation of critical forest parameters in fire behavior modeling. Remote Sensing of Environment 86, 177–186.

Riaño, D., Valladares, F., Condés, S., Chuvieco, E., 2004. Estimation of leaf area index and covered ground from airborne laser scanner (Lidar) in two contrasting forests. Agricultural and Forest Meteorology 124, 269–275.

Richardson, J.J., Moskal, L.M., 2011. Strengths and limitations of assessing forest density and spatial configuration with aerial LiDAR. Remote Sensing of Environment 115, 2640–2651.

Richardson, J.J., Moskal, L.M., Kim, S.-H., 2009. Modeling approaches to estimate effective leaf area index from aerial discrete-return LIDAR. Agricultural and Forest Meteorology 149, 1152–1160.

Robel, R.J., Briggs, J.N., Dayton, A.D., Hulbert, L.C., 1970. Relationships between visual obstruction measurements and weight of grassland vegetation. Journal of Range Management 23, 295–297.

Roudier, P., 2017. clhs: Conditioned Latin hypercube sampling.

Sage, R., Hollins, K., L Gregory, C., Woodburn, M., Carroll, J., 2004. Impact of roe deer Capreolus capreolus browsing on understory vegetation in small farm woodlands. Wildlife Biology 10, 115–120.

Seielstad, C.A., Queen, L.P., 2003. Using airborne laser altimetry to determine fuel models for estimating fire behavior. Journal of Forestry 101, 10–15.

Singh, K.K., Davis, A.J., Meentemeyer, R.K., 2015. Detecting understory plant invasion in urban forests using LiDAR. International Journal of Applied Earth Observation and Geoinformation 38, 267–279.

Skowronski, N., Clark, K., Nelson, R., Hom, J., Patterson, M., 2007. Remotely sensed measurements of forest structure and fuel loads in the Pinelands of New Jersey. Remote Sensing of Environment, The Application of Remote Sensing to Fire Research in the Eastern United States 108, 123–129.

Smith, A.M.S., Falkowski, M.J., Hudak, A.T., Evans, J.S., Robinson, A.P., Steele, C.M., 2009. A cross-comparison of field, spectral, and lidar estimates of forest canopy cover. Canadian Journal of Remote Sensing 35, 447–459.

Stephens, S.L., 1998. Evaluation of the effects of silvicultural and fuels treatments on potential fire behavior in Sierra Nevada mixed-conifer forests. Forest Ecology and Management 105, 21–35.

.

Su, J.G., Bork, E.W., 2007. Characterization of diverse plant communities in Aspen Parkland rangeland using LiDAR data. Applied Vegetation Science 10, 407–416.

Su, J.G., Bork, E.W., 2006. Influence of Vegetation, Slope, and Lidar Sampling Angle on DEM Accuracy. Photogrammetric Engineering & Remote Sensing 72, 1265–1274.

Suchar, V.A., Crookston, N.L., 2010. Understory cover and biomass indices predictions for forest ecosystems of the Northwestern United States. Ecological Indicators 10, 602–609.

Takahashi, T., Yamamoto, K., Miyachi, Y., Senda, Y., Tsuzuku, M., 2006. The penetration rate of laser pulses transmitted from a small-footprint airborne LiDAR: a case study in closed canopy, middle-aged pure sugi (Cryptomeria japonica D. Don) and hinoki cypress (Chamaecyparis obtusa Sieb. et Zucc.) stands in Japan. Journal of Forest Research 11, 117–123.

Tang, H., Brolly, M., Zhao, F., Strahler, A.H., Schaaf, C.L., Ganguly, S., Zhang, G., Dubayah, R., 2014. Deriving and validating Leaf Area Index (LAI) at multiple spatial scales through lidar remote sensing: A case study in Sierra National Forest, CA. Remote Sensing of Environment 143, 131–141.

USDA Forest Service, 2017. Monroe Mountain Aspen Ecosystems Restoration Project [WWW Document]. URL https://usfs.maps.arcgis.com/apps/MapJournal/index.html?appid=6c17eb611f7a4578b5e28681ca684432 (accessed 10.11.17).

USDA Forest Service, 2014. First order lidar metrics: A supporting document for lidar deliverables.

Vaglio Laurin, G., Puletti, N., Chen, Q., Corona, P., Papale, D., Valentini, R., 2016. Above ground biomass and tree species richness estimation with airborne lidar in tropical Ghana forests. International Journal of Applied Earth Observation and Geoinformation 52, 371–379.

Wing, B.M., Ritchie, M.W., Boston, K., Cohen, W.B., Gitelman, A., Olsen, M.J., 2012. Prediction of understory vegetation cover with airborne lidar in an interior ponderosa pine forest. Remote Sensing of Environment 124, 730–741.

Winnard, A.L., Di Stefano, J., Coulson, G., 2013. Habitat use of a critically-endangered species in a predator-free but degraded reserve in Australia. Wildlife Biology 19, 429–438.

.

Wulder, M.A., Coops, N.C., Hudak, A.T., Morsdorf, F., Nelson, R., Newnham, G., Vastaranta, M., 2013. Status and prospects for LiDAR remote sensing of forested ecosystems. Canadian Journal of Remote Sensing 39, S1–S5.

.

CONCLUSIONS

Throughout over a century of wildland firefighting in the US, there have been many important milestones and evolutions in wildland firefighter safety. One of the first major advances was the required establishment of safety zones in response to 11 firefighter fatalities on the Inaja fire in 1957 (Butler, 2014). Since then, a host of safety initiatives, protocols, and tools have been developed. Major safety initiatives included the required passage of a fitness test prior to engaging in wildland firefighting in 1975 (Sharkey, 1998), Project Aquarius, which aimed to study the physiology and effects of wildland firefighting (Budd et al., 1997), the TriData study, a broad-scale survey of firefighting personnel geared towards understanding the major obstacles to safety in wildland firefighting (TriData, 1996), and the establishment of the International Association of Wildland Fire, whose Safety Summit conferences bring together fire science and management in order to share ideas for improving wildland firefighter safety. Major safety protocols include the Lookouts, Communications, Escape routes and Safety zones (LCES) protocol (Gleason, 1991), the 10 Standard Fire Orders (Ziegler, 2007), and the 18 Watch Out Situations (Morse, 2004). Major safety tools include personal protective equipment such as fire-resistant Nomex uniforms (Braun et al., 1980) and fire shelters (Putnam, 1996), fire modeling applications such as FARSITE (Finney, 2004), FlamMap (Finney, 2006), and BehavePlus (Andrews et al., 2005), and fire safety applications such as WUIVAC (Cova et al., 2005; Dennison et al., 2007).

The research presented in this dissertation represents a potentially significant step forward in a direction that has, as yet, remained largely unexplored in the scientific and applied literature: the application of remote sensing and geospatial technology to the evaluation of safety zones (SZ) and escape routes (ER). SZ and ER are two of the most important safety measures that firefighters can employ to mitigate potentially hazardous situations. Although guidelines exist for the suitability assessment of both, the implementation thereof still requires a degree of subjectivity inherent to interpreting ground-level conditions. The use of lidar remote sensing, in particular, can provide firefighters with high spatial resolution models of those landscape conditions that are most directly relevant to SZ and ER suitability, including terrain and vegetation structure. The methods that I have developed for the lidar-based identification and evaluation of potential SZ and ER can provide firefighters with objective, quantitative information in advance of firefighting, not to replace, but to assist in the selection of SZ and ER on the ground.

In Chapter 1, I presented a new metric for identifying and evaluating SZ and an algorithm for calculating this metric on a broad spatial scale using lidar. Existing SZ safe separation distance guidelines are based solely on the effects of radiant heat (Butler and Cohen, 1998). However, more recent research has suggested that the additional effects of convective heat can significantly increase safe separation distance, particularly when upslope and/or downwind of flames (Butler, 2015, 2014; Parsons et al., 2014). Chapter 1 represents the first attempt at incorporating these effects into the mapping and suitability assessment of SZ. The proposed metric, the Safe Separation Distance Score (SSDS), is a single value that can be computed for all potential SZ in a given area, incorporating

.

vegetation height within and surrounding the SZ, the geometry of the SZ, and the number of firefighting personnel and assets present. This enables firefighters to use the resultant maps of SSDS to determine when a given SZ will be suitable according to local slope and wind conditions to improve the efficiency and effectiveness of the SZ designation process.

In Chapter 2, I presented the results of an experiment geared towards improving our understanding of the degree to which landscape conditions affect travel rates when moving along an escape route in wildland environments. Specifically, I tested three landscape variables – slope, understory vegetation density, and ground surface roughness – each of which can be mapped using lidar. The effects of slope have been previously explored by several authors (Butler et al., 2000; Davey et al., 1994; Tobler, 1993), and a select few have examined the effects of broad, categorical vegetation and ground surface types (Alexander et al., 2005; Soule and Goldman, 1972), but my work represents the first experimental characterization of the more scalable and broadly-applicable measures of vegetation density and ground surface roughness on travel rates. The results suggest that all three conditions negatively affect travel rates, with vegetation density having the strongest effect. Knowing the specific, quantitative effects that each of these variables possessed, I was able to generate maps of relative travel impedance from lidar. These travel impedance surfaces could then be combined and used in conjunction with a geospatial route-finding algorithm in order to identify the maximally efficient route between any two locations in a wildland environment. This approach could provide firefighters with an objective, experimentally-backed and quantitatively robust method for identifying an escape route between the fire line and a safety zone. This work

.

represents the first-ever attempt at the geospatial optimization of wildland firefighter escape routes on a broad spatial scale using lidar remote sensing.

In Chapter 3, I explored the process of quantifying understory vegetation density using lidar. Given the importance of this landscape condition in predicting wildland travel rates, it is essential to develop a sound understanding of the strengths and limitations of its quantification. There are several key variables that can affect the quality of a lidar-based assessment of understory vegetation structure, including the methods selected for field reference data collection, the lidar metrics used as model predictors, the pulse density of the lidar data, and overstory vegetation conditions, such as canopy density and height. My study contains one of the first applications of vegetation cover boards as training data for lidar-based modeling of understory vegetation, and the first such application that employed an automated cover board photo classification technique – a technique that shows much promise for future implementation. Throughout the literature, there have been many lidar metrics used as model predictors for imputing vegetation structure, but two vertically-stratified, point density-based metrics have dominated: overall relative point density (ORD) and normalized relative point density (NRD). Though their conceptual bases, underlying assumptions, and equations are quite similar, my study was the first to compare and reveal their significant differences in relative predictive power, with NRD far out-performing ORD. I also determined that with increasing pulse density, decreasing overstory vegetation density, and decreasing canopy height, the ability to accurately characterize understory vegetation density increases. The results of this study broadly provide a foundation upon which future studies of understory vegetation structure can be built, and perhaps most importantly, highlight the conditions

.

that will control the relative effectiveness of lidar-based wildland firefighter escape route mapping in different environments.

Taken together, the studies presented in this dissertation highlight much promise for the use of lidar in wildland firefighter safety applications. The ability to identify, evaluate, and map SZ and ER in advance of firefighting using objective measures of existing landscape conditions stands to greatly improve the implementation of LCES, ideally reducing the risk of injury and fatality among firefighters. Using the SZ evaluation procedure I have introduced, it may be feasible to produce a nationwide map of existing potential SZ in the relatively near future. Such a map could be provided to fire management agencies, or an interagency groups such as the National Wildfire Coordinating Group and National Interagency Fire Center and be distributed to fire crews on the ground to assist in fire safety planning. The map could act as either a basis of quantitative suitability comparison of existing SZ, if there are a number of potential SZ in a given area, or highlight a lack of SZ in a given area, prompting fire crews to create a SZ manually or rely on previously-burnt, "black" areas for safety. Similarly, generating nationwide maps of existing landscape conditions, such as terrain slope, vegetation density, and ground surface roughness in advance of firefighting would allow for the rapid computation maximally efficient ER, given the relative travel impedance results gleaned from this research. Although lidar data processing on broad scales remains fairly cumbersome at present, route-finding algorithms require comparably less computing power, potentially enabling such computation to occur on a smartphone or GPS unit on the fire line, provided that landscape conditions can be mapped in ahead of time. Thus, even in the complex firefighting environment, where situational awareness and visibility

.

can be greatly reduced, following a pre-defined route mapped onto the display of a handheld device may provide firefighters with an unparalleled ability to navigate to safety.

The broad-scale implementation of the SZ and ER mapping and evaluation techniques introduced in these studies, however, are not without critical limitations. I explicitly tested the effects of some of these limitations, particularly with respect to ER mapping, in Chapter 3. The most significant obstacle to broad-scale implementation is the current lack of nationwide lidar. This obstacle will likely be resolved in the near future with the implementation of the USGS 3D Elevation Program, which aims to collect high-quality lidar data throughout the entire US (Snyder, 2012; Sugarbaker et al., 2014). That said, although nationwide lidar would be a boon to research in the field of wildland firefighter safety and well beyond, a single snapshot in time will not provide sufficient temporal relevancy for analyzing conditions that are prone to short-term changes, such as vegetation structure. Particularly in fire-prone areas throughout the western US, it would be highly advantageous to have lidar data collected at a fairly high temporal resolution – at least once every 5 years or so. It is even conceivable that, with the increasing availability and decreased cost of unmanned aerial vehicle and lidar technology, combined with an ever-increasing capacity for rapidly and efficiently processing complex datasets, SZ and ER mapping can eventually be accomplished in real time.

These limitations, although important, do not detract from the work that I have presented here. Developing these methods in advance of data availability allows us to refine my understanding of the complex interactions between humans, fire, and the surrounding landscape. One of the major risks in engaging in wildland firefighter safety

.

research, particularly when attempting to evaluate critical safety measures such as SZ and ER, is that errors in the analytical methodology and/or theoretical framework could put firefighters in danger. Accordingly, there is still much work to be done to build upon the foundational research that I have presented here. With respect to the mapping of SZ, one of the key variables not addressed in my algorithm is mapping of fuel type and conditions within and surrounding the SZ. My model accounts for vegetation height in these areas, but does not distinguish between, for example, short shrubby vegetation and short herbaceous vegetation within the safety zone, which could result in significantly different rates of fire spread and intensities. Likewise, in the area surrounding a safety zone, an analysis of fuel loading and/or bulk density, each of which can be estimated using lidar (e.g. Andersen et al., 2005; Erdody and Moskal, 2010; Mutlu et al., 2008; Riaño et al., 2004a), may have a significant effect on safe separation distance. Though our understanding of the very precise effects these variables have on radiant and convective heat transfer is still developing, at the very least an assessment of, for example, an SZ with “high fuel load” versus “low fuel load” surrounding vegetation could provide valuable insight into its relative safety.

In terms of ER mapping, there are a host of variables that affect travel rates that I was simply unable to account for due to limitations in experimental logistics. For example, a key variable that has been shown to have significant effects on wildland firefighter travel efficiency is load carriage (Alexander et al., 2005; Ruby et al., 2003). In addition to necessitating more physical exertion, carrying a large, heavy pack through dense vegetation, for example, may have an interacting effect, due to the increased bulk, and the decrease in agility. Thus, future experiments should incorporate a pack versus no

.

pack variable when assessing travel rates. In addition, regardless of the travel efficiency, if an ER were to send firefighters into an area where their viewshed was dramatically reduced (e.g. a gully), this would reduce their situational awareness, and potentially increase their risk of injury or fatality. Given that lidar provides a detailed three-dimensional account of both terrain and aboveground vegetation structure, the incorporation of a viewshed analysis to highlight landscape visibility along the ER could provide a quantitative measure of ER situational awareness.

Lastly, for both SZ and ER mapping, it would be highly advantageous to incorporate the results of these mapping algorithms with those of a fire behavior model. For example, a SZ with a high SSDS value (suitable in a wide range of conditions) that is in the path of predicted fire spread may prove to be of less value than a SZ with a lower SSDS value in an area that the fire is not anticipated to reach. Likewise, an ER of maximal travel efficiency that travels through an area within the predicted fire spread is of comparably little utility to a less efficient route that travels through an area where fire is unlikely to spread. Accordingly, future research should attempt to provide a more holistic and realistic account of the wildland fire environment as a whole when assessing SZ and ER suitability.

References

Alexander, M.E., Baxter, G.J., Dakin, G.R., 2005. Travel rates of Alberta wildland firefighters using escape routes, in: Butler, B.W., Alexander, M. E. (Eds.), Human Factors - 10 Years Later. Presented at the Eighth International Wildland Fire Safety Summit, International Association of Wildland Fire, Missoula, MT.

Andersen, H.-E., McGaughey, R.J., Reutebuch, S.E., 2005. Estimating forest canopy fuel parameters using LIDAR data. Remote Sensing of Environment 94, 441–449.

.

Braun, E., Cobble, V.B., Krasny, J.F., Peacock, R.D., 1980. Measurement of the protective value of apparel fabrics in a fire environment. Journal of Consumer Product Flammability 7, 15–25.

Budd, G.M., Brotherhood, J.R., Hendrie, A.L., Jeffery, S.E., Beasley, F.A., Costin, B.P., Zhien, W., Baker, M.M., Cheney, N.P., Dawson, M.P., 1997. Project aquarius 1. stress, strain, and productivity in men suppressing Australian summer bushfires with hand tools: Background, objectives, and methods. International Journal of Wildland Fire 7, 69–76.

Butler, B.W., 2015. Firefighter safety zones [WWW Document]. Fire, Fuel, and Smoke Science Program, Rocky Mountain Research Station. URL https://www.firelab.org/project/firefighter-safety-zones (accessed 10.21.17).

Butler, B.W., 2014. Wildland firefighter safety zones: A review of past science and summary of future needs. International Journal of Wildland Fire 23, 295–308.

Butler, B.W., Cohen, J.D., 1998. Firefighter safety zones: A theoretical model based on radiative heating. International Journal of Wildland Fire 8, 73–77.

Butler, B.W., Cohen, J.D., Putnam, T., Bartlette, R.A., Bradshaw, L.S., 2000. A method for evaluating the effectiveness of firefighter escape routes. 4th International Wildland Fire Safety Summit 10–12.

Cova, T.J., Dennison, P.E., Kim, T.H., Moritz, M.A., 2005. Setting wildfire evacuation trigger points using fire spread modeling and GIS. Transactions in GIS 9, 603–617.

Davey, R.C., Hayes, M., Norman, J.M., 1994. Running uphill: An experimental result and its applications. The Journal of the Operational Research Society 45, 25–29.

Dennison, P.E., Cova, T.J., Mortiz, M.A., 2007. WUIVAC: A wildland-urban interface evacuation trigger model applied in strategic wildfire scenarios. Natural Hazards 41, 181–199.

Erdody, T.L., Moskal, L.M., 2010. Fusion of LiDAR and imagery for estimating forest canopy fuels. Remote Sensing of Environment 114, 725–737.

Finney, M.A., 2006. An overview of FlamMap fire modeling capabilities, in: Fuels management -- How to measure success: Conference proceedings. USDA Forest Service, Rocky Mountain Research Station, Portland, OR, pp. 213–220.

Finney, M.A., 2004. FARSITE: Fire area simulator: Model development and evaluation (Research Paper No. RMRS-RP-4). USDA Forest Service, Rocky Mountain Research Station Ogden, UT.

.

Gleason, P., 1991. Lookouts, communications, escape routes, and safety zones [WWW Document]. Wildland Fire Leadership. URL https://www.fireleadership.gov/toolbox/documents/lces_gleason.html (accessed 2.17.17).

Morse, G.A., 2004. A trend analysis of fireline "watch out" situations in seven fire-suppression fatality accidents. Fire Management Today 66.

Mutlu, M., Popescu, S.C., Stripling, C., Spencer, T., 2008. Mapping surface fuel models using lidar and multispectral data fusion for fire behavior. Remote Sensing of Environment 112, 274–285.

Parsons, R., Butler, B., Mell, W. "Ruddy," 2014. Safety zones and convective heat: numerical simulation of potential burn injury from heat sources influenced by slopes and winds. Imprensa da Universidade de Coimbra, Coimbra.

Putnam, T., 1996. Your fire shelter: Beyond the basics. National Interagency Fire Center.

Riaño, D., Chuvieco, E., Condés, S., González-Matesanz, J., Ustin, S.L., 2004. Generation of crown bulk density for Pinus sylvestris L. from lidar. Remote Sensing of Environment 92, 345–352.

Ruby, B.C., Iii, G.W.L., Armstrong, D.W., Gaskill, S.E., 2003. Wildland firefighter load carriage: Fffects on transit time and physiological responses during simulated escape to safety zone. International Journal of Wildland Fire 12, 111–116.

Sharkey, B., 1998. Work capacity tests for wildland firefighters: Test administrator's guide (No. 9851–2810–MTDC), Technology and Development Program. USDA Forest Service, Missoula, MT.

Snyder, G.I., 2012. The 3D elevation program: Summary of program direction (USGS Numbered Series No. 2012–3089), Fact Sheet. U.S. Geological Survey, Reston, VA.

Soule, R.G., Goldman, R.F., 1972. Terrain coefficients for energy cost prediction. Journal of Applied Physiology 32, 706–708.

Sugarbaker, L.J., Constance, E.W., Heidemann, H.K., Jason, A.L., Lukas, V., Saghy, D.L., Stoker, J.M., 2014. The 3D elevation program initiative: A call for action (USGS Numbered Series No. 1399), Circular. U.S. Geological Survey, Reston, VA.

Tobler, W.R., 1993. Three presentations on geographical analysis and modeling (No. 93–1). National Center for Geographic Information and Analysis, University of California at Santa Barbara.

.

TriData, 1996. Wildland firefighter safety awareness study: Phase I - Identifying the organizational culture, leadership, human factors, and other issues impacting firefighter safety.

Ziegler, J.A., 2007. The story behind an organizational list: A genealogy of wildland firefighters' 10 standard fire orders. Communication Monographs 74, 415–442.

.